

New Color Patterning Techniques for OLED Displays

by

Yoshitaka Kajiyama

A thesis
presented to the University of Waterloo
in fulfillment of the
thesis requirement for the degree of
Doctor of Philosophy
in
Electrical and Computer Engineering

Waterloo, Ontario, Canada, 2015

©Yoshitaka Kajiyama 2015

Author's Declaration

I hereby declare that I am the sole author of this thesis. This is a true copy of the thesis, including any required final revisions, as accepted by my examiners.

I understand that my thesis may be made electronically available to the public.

Abstract

Organic light emitting devices (OLEDs) are light emitting devices consisting of a stack of organic semiconductors sandwiched by electrodes. Since the first report of a high-efficiency device by Tang and Van Slyke in 1987, OLEDs have attracted considerable attention, particularly for use in flat panel displays. OLEDs provide these products improved power consumption, contrast, response speed, viewing angle, and compatibility with flexible displays. The performance of OLEDs has improved considerably, especially in terms of stability and efficiency, so they can now meet the requirements for some display products. However, the commercialization of OLED displays remains limited and is hampered primarily by manufacturing issues. These issues include low manufacturing yield, high fabrication cost, and low display quality. Manufacturing issues are largely attributed to difficulties with the color patterning process, the fabrication process by which arrays of red, green and blue (RGB) OLEDs can be made side-by-side on one substrate in order to obtain a full-color display. Currently, RGB color patterning is done by sequential vacuum deposition of red, green and blue materials through a pre-patterned shadow mask, which is typically made of a thin metal sheet. This technique is widely known as fine metal mask (FMM) technology. However, this technique has several inherent limitations, including mask deformation, difficulties in mask-to-substrate overlay alignment, and ability to make masks with micrometer level dimensional accuracy. These limitations reduce the manufacturing yield, display resolution, and display aperture ratio (the ratio of the emissive area to the total surface area of a display). Despite the fact that several approaches for addressing these limitations in OLED displays have been proposed, there is still no commercially viable solution.

In this thesis, two novel color patterning techniques for OLED displays are proposed. One approach utilizes laser-patterned polyimide (PI) sheets as shadow masks. This technique takes advantage of the good processability of PI by direct laser ablation, which makes it possible to cut through it to create slits with very high dimensional accuracies. In addition, because this is a dry process, the laser-patterning of the PI sheets can be done after the sheets are already stretched and mounted on the metal holder. This avoids post-patterning deformation of the masks by the stretching step. The use of laser also makes it possible to pattern the PI sheets after they have already been mounted on the thin film transistor (TFT) backplane substrates and thus, in a variant of this technique, allows for the shadow mask to be created *in-situ*. This *in-situ* shadow mask patterning technique can be expected to offer further accuracy advantages, since the slits are created by laser over the desired TFT locations directly, and thus eliminates the need for a subsequent mechanical alignment step. This approach can be particularly useful for RGB OLED patterning on flexible substrates where the poor mechanical and dimensional stability of substrates pose additional challenges for aligning shadow masks accurately.

The other color patterning approach proposed here is based on the diffusion of a luminescent material from a donor substrate into the organic host material layer of the OLED that is pre-coated on the backplane substrate. The RGB color patterning in this case can be done without the use of shadow masks, so this approach offers significant advantages. The use of a pre-patterned micro stamp as the donor substrate allows the physical contact between the two substrates to be selectively limited to

certain areas, which in turn allows limiting this diffusion to only certain areas of the OLED substrate. Such selective diffusion can also alternatively be done through local heating via electric currents, using electrodes in the OLED backplane for this purpose. This eliminates the need for patterned stamps and mechanical alignment.

In this work, these two techniques are introduced and tested with the purpose of assessing their potential for RGB patterning. As part of this investigation, the effect of using these techniques on OLED performance is also studied. Finally, a first proof-of-concept utilization of the techniques for producing RGB OLEDs fabricated side-by-side on one substrate is demonstrated.

Acknowledgments

I would like to show my greatest appreciation to my supervisor Professor Hany Aziz for his constructive comments and warm encouragement during my research. Without his guidance and persistent help, this thesis would not have been possible. I cannot express enough my feelings of appreciation for everything he did throughout my academic work at the University of Waterloo.

I would like to acknowledge my advisory committee, Professor Dayan Ban, Professor Yuning Li and Professor William Wong. I would particularly like to thank Professor Ian Hill, Professor of Dalhousie University, who accepted my invitation to be my external examiner.

I am in debt to Mr. Richard Barber, Lab manager of Giga to Nano (G2N), for his helpful technical assistance in the lab.

I am grateful for the contributions made by Mr. Kevin Joseph and Ms. Amanda Victorious who helped with my experiments as a co-op student.

My special thanks to my colleagues, Dr. Hossein Siboni, Dr. Qi Wang, Mr. Michael Zhang, Mr. Thomas Borel, Dr. Graeme Williams, Mr. Sibi Sutti, and Mr. Tyler Davidson-Hall for giving insightful comments and suggestions during our regular discussions.

I want to thank my father who gave me the support and encouragement.

Also, special thanks to my wife for her constant support, kindness and love.

Finally, I thank the Natural Sciences and Engineering Research Council of Canada (NSERC) for the financial support during my research.

Table of Contents

List of Figures	ix
List of Tables	xiii
List of Abbreviations	xiv
Chapter 1 Introduction and Background	1
1.1 Thesis organization	3
1.2 Organic light emitting diodes - Introduction.....	4
1.2.1 Working principle of OLEDs.....	4
1.2.2 Basic structure of OLEDs	5
1.2.3 SMOLEDs vs PLEDs.....	7
1.3 OLED displays.....	8
1.3.1 Standard architecture and working principle of OLED displays	8
1.3.2 RGB OLEDs fabrication technique using fine metal masks.....	15
1.3.3 Limitation of current small molecule OLED display fabrication technology.....	16
1.3.4 Alternative color patterning techniques	18
1.4 Current status of OLEDs and OLED displays	20
1.4.1 Current status of OLEDs in display technology.....	20
1.4.2 Current status of OLED display	22
Chapter 2 New Color Patterning Techniques for OLED Displays: Introduction and Research Objectives	25
2.1 Introduction to the proposed techniques	25
2.1.1 Technique 1: Color patterning using laser-patterned PI sheets.....	26
2.1.2 Technique 2: Color patterning via diffusion of a luminescent material.....	28
2.2 Research objectives.....	29
2.3 General Methodology	30
Chapter 3 Experimental Procedure	32
3.1 Substrate preparation and OLED device fabrication	32
3.2 Device characterization.....	33

Chapter 4 Technique 1: Color Patterning Using a Laser-Patterned PI shadow mask.....	35
4.1 Color patterning using PI shadow masks patterned <i>ex-situ</i> off substrate.....	36
4.1.1 Assessing and investigating the capability of the laser-pattered PI sheet as a shadow mask	36
4.1.2 Device Performance: examining the effect of contact of an organic layer with a PI sheet.....	39
4.1.3 Demonstrating RGB OLEDs with small feature sizes (<25 μm) fabricated side-by-side on one substrate	42
4.1.4 Conclusions.....	45
4.2 <i>In-situ</i> Shadow Mask Patterning Technique	45
4.2.1 Device Performance : Investigating the effect of laser patterning of PI sheets <i>in-situ</i> on an electrode .	46
4.2.2 Device Performance (II): Investigating the effect of laser patterning of a PI sheet <i>in-situ</i> on an electrode with a protective layer	48
4.2.3 Demonstrating RGB OLEDs with very small feature sizes (<25 μm) fabricated side-by-side on one substrate	52
4.2.4 Conclusions.....	54
Chapter 5 Technique 2: Color Patterning via Diffusion of a Luminescent Material	56
5.1 Assessing the effectiveness of physical contact between a donor and acceptor substrate to achieve sufficiently high doping levels via diffusion.....	57
5.2 Examining electroluminescence characteristics of devices fabricated using this technique.....	65
5.3 Demonstrating RGB color patterning by selective diffusion of a luminescent material.....	70
5.4 Assessing solvent vapor exposure as a method to accelerate solid state diffusion	73
5.5 Assessing semiconducting diffusion barrier as a method to block undesirable diffusion.....	82
5.5.1 Assessing the effectiveness of using a $\text{MoO}_3\text{:HTM}$ film in reducing inter-diffusion of luminescent materials.....	84
5.5.2 Investigating capability of the diffusion barrier for controlling a dopant concentration	87
5.5.3 Demonstrating the ability of the diffusion barrier to produce OLEDs with highly controlled device structure and performance.....	91
5.6 Theoretical analysis of dopant concentration profile	96

5.6.1 Determining the Diffusion Coefficient	97
5.6.2 Determining the Mass Transfer Coefficient.....	101
5.6.3 Estimating the Transient Dopant Concentration Profile	103
5.7 Conclusions.....	104
Chapter 6 Summary and Future Work	106
6.1 Technique 1: Color patterning using the laser-patterned PI shadow masks.....	106
6.2 Technique 2: Color patterning via diffusion of a luminescent material.....	107
Bibliography	110
Appendix 1 Selective Diffusion Using Laser Local Heating	117
Appendix 2 Absorption Spectrum of NPB Doped with DCJTB.....	120
Appendix 3 ITO Temperature vs Bias Voltage.....	121

List of Figures

Figure 1.1 Chemical structure of the common OLED materials a) Alq ₃ b) N,N'-bis(1-naphthyl)-N,N'-diphenyl-1,10-biphenyl-4,40-diamine (NPB).....	5
Figure 1.2 Structure of the standard Alq ₃ /NPB bilayer OLED device.....	5
Figure 1.3 Schematic presentation for the energy diagram of the field-applied bilayer device.....	6
Figure 1.4. Cross section view of a) bottom emitting device and b) top emitting device.....	6
Figure 1.5 Chemical structure of the common PLED materials: a) poly(phenylenevinylene) (PPV) and b) poly(fluorene) (PF).	8
Figure 1.6 RGB approaches for OLED displays: a) side-by-side RGB OLEDs, b) white OLEDs plus CFs, and c) blue OLEDs with CCMs.	11
Figure 1.7 Schematic presentation for matrix driving of a PMOLED.....	13
Figure 1.8 Cross section view of OLEDs fabricated on a TFT substrate.....	14
Figure 1.9 Typical OLED display circuit with two TFTs and one capacitor. V_{supply} is the voltage of the power supply.....	15
Figure 1.10. Schematic presentation for the conventional color patterning technique using FMMs.....	16
Figure 1.11 Magnified view of an AMOLED with the PenTile layout.	18
Figure 1.12. Schematic presentation for the transfer of an organic layer stack by laser exposure of LITI process.....	19
Figure 2.1 Comparison between the conventional patterning technique using FMMs and the patterning technique using laser-patterned PI sheet shadow masks.	27
Figure 2.2 General scheme for RGB OLED display fabrication using the <i>in-situ</i> shadow mask patterning technique.	27
Figure 2.3 General scheme for RGB OLED display fabrication using pre-patterned micro stamp as the donor substrate.	28
Figure 2.4 General scheme for the selective diffusion of a luminescent material through local heating via electric currents. Details of the process steps are shown in Section 5.3.	29
Figure 3.1. Photograph of the inside of the vacuum chamber.....	33
Figure 3.2. Typical architecture of the standard bottom emitting OLEDs.....	33
Figure 4.1. Schematic presentation for the laser system.	38
Figure 4.2. (a) 3D AFM image and (b) cross section view of an Alq ₃ layer (~140nm thick) deposited through a laser patterned PI shadow mask with 25 μm wide slits.....	39
Figure 4.3 Procedure for the experiment on effects of contact of an organic layer with PI.....	40
Figure 4.4 (a) J-V and L-V characteristics and (b) normalized EL intensity and driving voltage under constant current density of 20 mA/cm ² for devices in which the organic layers are put in contact with PI sheets for 50 hours and control devices.....	41
Figure 4.5. EL images of (a) unencapsulated devices in which the organic layers are put in contact with PI sheets for 50 hours and (b) control devices which are kept in a dry nitrogen condition.....	41
Figure 4.6. Procedure for RGB OLED fabrication using a pre-patterned PI sheet.....	43
Figure 4.7. EL images of OLEDs fabricated by the procedure in Fig.4.6.	44

Figure 4.8 Schematic presentation for OLED device fabrication on the electrode where the PI sheet is patterned by laser ablation.	47
.....	
Figure 4.9 The electrode where the PI sheet is patterned (a) and EL of the fabricated device (b).	48
Figure 4.10 Schematic presentation for the ITO coated glass substrate where the SiNx layer is patterned. ..	49
Figure 4.11 Schematic presentation for the patterning of the sub-pixel size OLED device using the <i>in-situ</i> shadow mask patterning technique.	50
Figure 4.12 Microscopic images of (a) patterned PI sheet over the sub-pixel, (b) deposited materials on the electrode, and (c) EL of the patterned device.	51
Figure 4.13 J-V characteristics of the fabricated device.	51
Figure 4.14 Procedure for RGB OLED fabrication using a PI sheet patterned <i>in-situ</i> on the substrate.	53
Figure 4.15 EL images of OLEDs fabricated by the procedure in Fig.4.14.	54
Figure 5.1. A schematic diagram illustrating the steps of the procedure followed for introducing luminescent dopant from a donor substrate to an acceptor substrate.	59
Figure 5.2. UV-Vis absorption spectra of the acceptor host films after contact with the donor substrate for 30min (a), 60min (b), 90min (c) and 105min (d). The dotted traces represent spectra collected from the non-contacted areas for reference.	61
Figure 5.3 (a) UV-Vis absorption spectra of the acceptor host films after contact with the donor substrate for the various times after subtracting the background absorption by NPB and the substrate. (b) The corresponding absorbance at 510 nm vs contact time (bottom axis). The absorbance of 5 nm NPB films doped with various DCJTb concentrations at the same wavelength after subtracting absorption from NPB and substrate background are shown for comparison (top axis).	61
Figure 5.4 UV-Vis absorption spectra of the acceptor host films ((a) CBP, (b) NPB, (c) TBADN and (d) Alq ₃) after contact with the donor substrate for 60 min at (1) 60°C, (2) 80°C, (3)100°C and (4) 120°C. The dotted traces represent spectra collected from the non-contacted areas for reference.	64
Figure 5.5 Absorbance of the acceptor films (CBP, NPB, TBADN and Alq ₃) at the DCJTb peak absorption peak wavelength of 510 nm after contact with the donor substrate for 60min at various temperature from 60°C to 120°C. The absorbance of the corresponding control films is subtracted.....	65
Figure 5.6. A schematic diagram illustrating the steps of the procedure followed for fabricating OLEDs. (ii) and (iii) illustrate the steps of introducing the dopant via diffusion.	66
Figure 5.7. Red, green and blue colored solid lines: EL spectra of the devices fabricated following the procedure in Fig. 5.6 for various contact times. Black lines: EL spectra of reference devices with 0, 2, 4, 8 and 100% DCJTb fabricated by conventional co-deposition. Corresponding CIE coordinates of these devices are also included.....	69
Figure 5.8. Red, green and blue colored solid lines: J-V and L-V characteristics of devices fabricated following the procedure in Fig. 5.6. Black lines: those of reference devices with 2, 4, 8 and 100% DCJTb concentration.....	70
Figure 5.9 A schematic diagram illustrating the steps of the procedure followed for fabricating red, green and blue OLEDs. (ii) and (iv) show the Joule heating steps used to induce the diffusion for introducing the red and green dopants selectively in devices x and y, respectively.....	72

Figure 5.10 (a) EL images and (b) EL spectra of the devices fabricated following the procedure in Fig. 5.9. Corresponding CIE coordinates of these devices are also included.....	73
Figure 5.11 Schematic presentation for the experimental setup for exposing the sample to solvent vapor. ..	75
Figure 5.12 A schematic diagram illustrating the steps of the procedure followed for fabricating OLEDs. (ii) illustrate the steps of exposing the sample to solvent vapor.	75
Figure 5.13 PL spectra of the NPB/DCJTB bilayer stack before and after the acetone vapor exposure. The spectra are collected under 360nm excitation.	77
Figure 5.14 PL images of the NPB/DCJTB bilayer stack before (a) and after (b) the acetone vapor exposure.	77
Figure 5.15 J-V and L-V characteristics of the devices whose HTL (NPB (a) and TcTa (b)) is exposed to toluene vapor. The inset is the J-L characteristics.	78
Figure 5.16 J-V and L-V characteristics of the devices where the HTL/dopant bilayer ((a) NPB/DCJTB and (b) NPB/C545T) are exposed to toluene vapor. The inset is the J-L characteristics. The dotted lines represent those of the corresponding control devices.	79
Figure 5.17 EL spectrum of the devices where the HTL/dopant bilayer (NPB/DCJTB (red) and NPB/C545T (blue)) is exposed to toluene vapor. The dotted lines represent those of the corresponding control devices.....	80
Figure 5.18 J-V and L-V characteristics of the devices where the HTL:dopant bilayer ((a) NPB:DCJTB and (b) NPB:C545T) is exposed to toluene vapor. The inset is the J-L characteristics. The dotted lines represent those of the corresponding control devices.	81
Figure 5.19 EL spectrum of the devices where their HTL:dopant bilayer (NPB:DCJTB (red) and NPB:C545T (blue)) is exposed to toluene vapor. The dotted lines represent those of the corresponding control devices.	81
Figure 5.20 Scheme for the diffusion-based doping method without (a), and with (b) the diffusion barrier.	84
Figure 5.21 (a) and (d) the structure of the organic layer stacks without and with the diffusion barrier film, respectively; (b) and (e) spectra collected every 10 minutes from the organic stacks; and (e) and (f) PL images of the stacks before and after heating.	86
Figure 5.22 (a) and (d) the structure of the organic layer stacks without and with the diffusion barrier film, respectively; (b) and (e) spectra collected from the organic stacks before and after solvent vapor exposure; and (e) and (f) PL images of the stacks before and after solvent vapor exposure.	87
Figure 5.23 Schematic presentation for the device structure of (a) device A and (b) device B.....	89
Figure 5.24 EL spectra from the devices (with 15nm NPB (a) and 10nm NPB (b)) with the neat DCJTB layer collected periodically while at 100 °C. The dotted lines represent the EL spectra of the corresponding control devices.	90
Figure 5.25 Current efficiencies collected every few minutes from the devices with the neat DCJTB layer during the heating step for the device with the 15nm host NPB layer (the blue solid line); and the device with the 10nm host NPB layer (the red solid line). The dotted lines represent the current efficiency of the corresponding control devices.	91
Figure 5.26 A schematic diagram illustrating the steps of the procedure followed for the diffused-dopant OLEDs. (i)-(iii) illustrates the steps of introducing the dopant via diffusion and (iv) illustrates the subsequent heating step used for making the DCJTB concentration uniform across the layer.	93

Figure 5.27 Schematic presentation for the device structure of (a) the dopant-diffused device and (b) the control device. The concentration of DCJTB in NPB is supposed to be graded as shown in the figure since DCJTB is transferred to the host through physical contact. The structure with the graded DCJTB concentration appears in the step (iii) of Fig. 5.26.....	93
Figure 5.28 EL spectra collected every few minutes from the “diffused-dopant” devices during the heating step (of Fig.5.26 (iv)) for the device with the 15nm host NPB layer (a); and the device with the 10nm host NPB layer (b). The dotted lines represent the EL spectra of the corresponding control devices. ...	95
Figure 5.29 Current efficiencies collected every few minutes from the “diffused-dopant” devices during the heating step (of Fig.5.26 (iv)) for the device with the 15 nm host NPB layer (the blue solid line); and the device with the 10 nm host NPB layer (the red solid line). The dotted lines represent the current efficiency of the corresponding control devices.	96
Figure 5.30 Schematic representation for the theoretical model. Adjacent NPB and DCJTB layers are sandwiched by impermeable layers in this model.....	99
Figure 5.31 The actual device structure for the model in Fig. 5.30.	99
Figure 5.32 The change in the uniformity of dopant concentration ($U(t)$) with time for various diffusion coefficients (right axis). The experimental result of the change in luminescent efficiency due to heating with time is also shown (left axis).	100
Figure 5.33 The transient dopant concentration distribution across the NPB layer.....	101
Figure 5.34 Schematic representation for the actual experiment considered in this model.	102
Figure 5.35 Schematic representation for the theoretical model based on the actual experiment in Fig. 5.34. DCJTB molecules are transferred to the host NPB film via diffusion by physical contact in this model.	102
Figure 5.36 The total amount of the dopant in the host film with time for various mass transfer coefficients. The total amount is shown as the relative amount to the amount of DCJTB in 5nm NPB doped with 4% DCJTB by volume.	103
Figure 5.37 The transient dopant profile of the “diffused-dopant” device.	104
Figure 0.1 General scheme for the selective diffusion of a luminescent material through local heating via laser.....	117
Figure 0.2 A schematic diagram illustrating the steps of the procedure followed for fabricating OLEDs selectively doped via diffusion by local laser heating.....	118
Figure 0.3 EL image of the OLED fabricated through the procedure in Fig. 0.2	119
Figure 0.4 The absorption spectra of 5nm of NPB films doped with various DCJTB concentrations (0-16%)	
Figure 0.5 Temperature vs bias voltage of the ITO strip	

List of Tables

Table 1.1 Summary of an OLED television business to date.....	22
Table 1.2 Comparison between OLED display and LCD.	24
Table 4.1 Percentage of dark spot area of the total emitting area and average dark spot diameter of the devices in which the organic layers are put in contact with PI sheets for 50 hours and control devices.	42
Table 5.1 Complete device structures. (Solvent) indicates the solvent vapor exposure step.....	76

List of Abbreviations

AMOLED:	Active Matrix OLED
AFM:	Atomic Force Microscope
CT:	Charge Transfer
CCFL:	Cold Cathode Fluorescent Lamp
CCM:	Color Conversion Medium
CF:	Color Filters
EDM:	Electric Discharge Machining
EL:	Electroluminescence
EBL:	Electron Beam Lithography
EIL:	Electron Injection Layer
ETL:	Electron Transport Layer
EML:	Emission Layer
FMM:	Fine Metal Mask
HOMO:	Highest Occupied Molecule Orbital
HIL:	Hole Injection Layer
HTL:	Hole Transport Layer
HTM	Hole Transport Material
LED:	Light Emitting Diode
LC:	Liquid Crystal
LIPS:	Laser Induced Pattern-wise Sublimation
LITI:	Laser Induced Thermal Imaging
LTHC:	Light To Heat Conversion
LTPS:	Low Temperature Polysilicon
LUMO:	Lowest Unoccupied Molecule Orbital
Nd:YAG:	Neodymium-doped Yttrium Aluminum Garnet
PECVD	Plasma-Enhanced Chemical Deposition

PMOLED:	Passive-matrix OLED
PDA	Personal Digital Assistance
PL:	Photoluminescence
PLED:	polymer OLED
ppi:	pixel per inch
RIST:	Radiation Induced Sublimation Transfer
RIE:	Reactive Ion Etching
SMOLED:	Small Molecules OLED
T _g :	Glass transition temperature
TFT:	Thin Film Transistor
TCE:	Transparent Conductive Electrode
V _d :	Driving voltage

Chemical Names

Alq ₃ :	Tris-(8-hydroxyquinoline) aluminum
DCJTb:	4-(dicyanomethylene)-2-t-butyl-6-(1,1,7,7-tetramethyljulolidyl-9-enyl)-4H-pyran
LiF:	lithium fluoride
MEH:PPV	poly[2-methoxy-5-(2-ethylhexyloxy)-1,4-phenylenevinylene]
MoO ₃ :	molybdenum trioxide
NPB:	N,N'-bis(1-naphthyl)-N,N'-diphenyl-1,10-biphenyl-4,4'-diamine
PF:	poly(fluorene)
PI:	polyimide
PPV:	poly(phenylenevinylene)
SiN _x :	silicon nitride
TBADN:	2-tert-butyl-9,10-di(naphth-2-yl)anthracene
TcTa:	4,4',4''-tri(N-carbazolyl) triphenylamine
TPBi:	1,3,5-tris(N-phenylbenzimidazole-2-yl)benzene

Chapter 1

Introduction and Background

Since the invention of the first high-efficiency organic light emitting device (OLED) by Tang and Van Slyke in 1987 using a bilayer structure and tris-(8-hydroxyquinoline) aluminum (Alq₃)^[1], a great amount of research has been conducted in this area. From the early period on this research, the application of OLEDs to flat panel displays (FPDs) has attracted tremendous attention due to the unique advantages of OLEDs, which are suitable for FPDs, including their higher contrast, lower power consumption relative to liquid crystal displays (LCDs) and mechanical flexibility^{[2][3][4][5]}. Although device performance of OLEDs such as efficiency and stability was limited in the early stage, OLEDs have now met performance requirements for some commercialized FPD products as a result of intensive research and efforts. As such, OLED displays are now emerging as an alternative to LCDs^{[5][6][7]}.

Nevertheless, the current mainstream technology in use in FPDs is still LCDs^[8]. The commercialization of OLED displays is hampered primarily by manufacturing issues. These include low manufacturing yield, high fabrication cost, and low display quality. These manufacturing issues are largely attributed to difficulties with the color patterning process; i.e. the fabrication process by which red, green and blue (RGB) OLEDs can be made side-by-side in order to obtain a full-color display. Currently, RGB color patterning is done by sequential vacuum deposition of red, green and blue materials through a pre-patterned shadow mask, typically made of a thin metal sheet in what is widely known as fine metal mask (FMM) technology^{[4][9][10]}. However, this technique has several inherent limitations. These include mask deformation, difficulties in mask-to-substrate overlay alignment, and ability to make masks with micrometer level dimensional accuracy. These limitations reduce the manufacturing yield, display resolution, and display aperture ratio (the ratio of the emissive area to the total surface area of a display).

In this work, two novel alternative color patterning techniques are proposed. In one of these proposed techniques, polyimide (PI) sheets patterned by direct laser ablation are utilized as contact

shadow masks instead of the conventional FMMs^{[11][12][13]}. This color patterning technique is referred to as “laser-patterned PI mask technique” in this thesis. Because of the good processability of PI sheets by direct laser ablation, which enables them to be cut through to create slits with very high dimensional accuracies^{[14][15]}, high precision pixel patterning can be achieved by using laser-patterned PI masks. Furthermore, by utilizing a dry patterning process (i.e. laser ablation), it is possible to pattern them *in-situ* on the OLED backplane. In this work, the patterning technique where shadow masks are patterned *in-situ* on the substrate is referred to as “*in-situ* shadow mask patterning technique”. The *in-situ* shadow mask patterning technique has an additional advantage to achieve precise patterning even on flexible substrates where precise patterning is more challenging due to poor mechanical stability of the flexible substrates. Successful demonstration of RGB OLEDs with small feature sizes (~25 μm) fabricated through these two techniques is presented in this work. The results show that these techniques have a significant potential for enabling the fabrication of high resolution OLED displays.

In addition to the laser-patterned PI mask technique, color patterning via diffusion of a luminescent material is also proposed, which is referred as a “diffusion-based technique” in this thesis. In this technique, emission color is not patterned by using shadow masks but by selective doping of a luminescent material via physical contact of a host layer with a donor layer. This being a maskless approach, patterning accuracy is not susceptible to issues such as the poor mechanical stability of masks or shadow effects. Furthermore, by utilizing local anode Joule heating for selectively inducing doping, it becomes possible to avoid the need for mechanical registration or alignment. The first demonstration of RGB color patterning of small molecule OLEDs by the diffusion-based technique is presented. Additionally, related techniques, including diffusion enhancement by solvent vapor exposure and the use of a semiconducting diffusion barrier to enhance the technical advantage and reliability of this technique, are also provided.

The main focus of this work is to conduct the first proof-of-concept investigation of these techniques and to test their technical feasibility. The feasibility study on the laser-patterned PI mask technique includes assessment of the capability of the laser-patterned PI sheet as a shadow mask, investigation on the effect of direct contact of organic materials with PI on device performance, and

demonstration of RGB OLEDs with small feature sizes ($<25\ \mu\text{m}$) fabricated side-by-side on one substrate. In addition to these studies, the effect of carrying out the mask patterning *in-situ* on the substrates on device performance is investigated. As an end goal of this study, RGB OLEDs fabricated through the *in-situ* shadow mask patterning technique are also demonstrated. For the diffusion-based technique, doping levels of a luminescent material achieved via physical contact between donor and acceptor layers are first examined, followed by investigations of its effects on device performance. RGB OLEDs are then fabricated by the selective diffusion technique to demonstrate its technical feasibility. In addition, diffusion enhancement by solvent vapor exposure and the use of a semiconducting diffusion barrier are also discussed as approaches for enhancing technical advantage and reliability of this technique. Finally, concentration profiles of the luminescent material doped via diffusion is theoretically estimated.

1.1 Thesis organization

In the first introductory chapter, basic information on OLED devices such as a standard structure and operational principle is provided. The standard architecture, advantages, and fabrication techniques of OLED displays are then described. The remaining issues of the current OLED display manufacturing and suggested solutions such as alternate color patterning techniques are then presented. Finally, the current status of OLEDs in display technology and OLED display businesses are briefly reviewed.

In chapter 2, the proposed new color patterning techniques are introduced, and specific objectives of a series of studies on these techniques are summarized. This is followed by a brief description of general experimental procedures in chapter 3. The experimental results and discussions for these studies are presented in the following two chapters. Studies on the color patterning technique using laser-patterned PI sheets are presented in chapter 4. Studies on the technique via diffusion of a luminescent material are presented in chapter 5.

Chapter 4 is divided into two sections where *ex-situ* shadow mask patterning and *in-situ* shadow mask patterning approaches are described in parallel. Each section consists of a series of subsections

describing specific experiments with introduction, experimental procedure, and discussion. Chapter 5 consists of six sections. Sections 5.1, 5.2 and 5.3 describe the primary studies for the diffusion-based technique including examination of doping levels of a luminescent material, investigation of effects on device performance, and demonstration of RGB OLEDs. Sections 5.4 and 5.5 present related techniques including diffusion enhancement by solvent vapor exposure and the use of semiconducting diffusion barriers. In addition, theoretical analysis of dopant concentration profiles is presented in Section 5.6.

Finally, summary of research results and conclusions of this work are provided in chapter 6.

1.2 Organic light emitting diodes - Introduction

1.2.1 Working principle of OLEDs

In general, organic semiconductors are organic materials made of molecules characterized by having a high density of carbon-carbon double bonds (Fig.1.1). In these double bonds, π molecular orbitals are created due to the overlap of 2p orbitals. Since π electrons are delocalized, electrons are able to move freely within the molecule, which contributes to the carrier transport property of organic electronics materials. In the case of highly conjugated molecules where multiple double carbon bonds are contained, continuous energy bands are formed due to presence of overlapping π -orbitals of a collection of atoms. The highest energy occupied molecular orbital and the lowest energy unoccupied molecular orbital are named highest occupied molecule orbital (HOMO) and lowest unoccupied molecule orbital (LUMO), respectively. Under the influence of an electric field, electrons in the LUMO level and holes in the HOMO level transport by hopping from one molecule to the next over an energy barrier between them. This carrier transport mechanism is called hopping transport, and is the dominant carrier transport mechanism in organic amorphous semiconductors. In addition to the carrier transport property, electron-photon interactions are able to occur in the visible range of the electromagnetic spectrum, since the typical band gap between bonding and anti-bonding orbitals of π molecular orbitals is 1.5-3.5 eV. Due to these optoelectrical properties, organic electric materials are useful in practical applications such as light emitting diodes and solar cells.

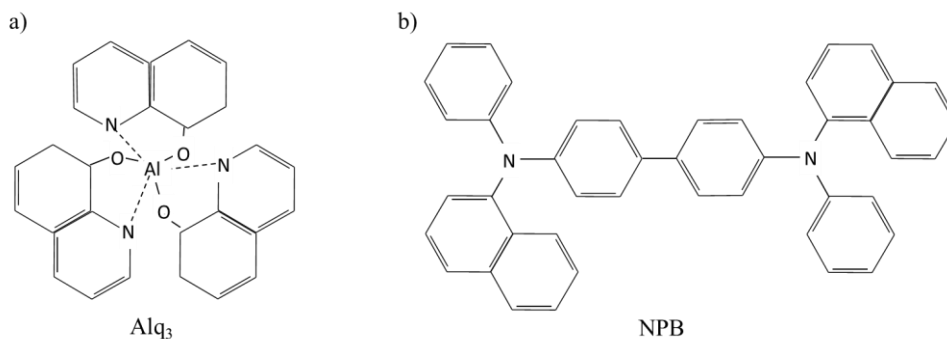


Figure 1.1 Chemical structure of the common OLED materials a) Alq₃ b) N,N'-bis(1-naphthyl)-N,N'-diphenyl-1,10-biphenyl-4,4'-diamine (NPB).

1.2.2 Basic structure of OLEDs

Figure 1.2 presents the typical structure of a N,N'-bis(1-naphthyl)-N,N'-diphenyl-1,10-biphenyl-4,4'-diamine (NPB)/Alq₃ bilayer OLED device. As shown in the figure, the standard bilayer device consists of heterojunction of two thin layers of OLED materials, a hole transport layer (HTL) and an electron transport layer (ETL), sandwiched by cathode and anode. In this device, NPB and Alq₃ serve as a HTL and ETL, respectively. Transparent conductive electrode (TCE) such as indium tin oxide (ITO) is commonly used as an anode for light extraction. Figure 1.3 depicts carrier transport and recombination phenomenon in the bilayer device. When voltage is applied between the anode and cathode, electrons and holes are injected from the cathode and the anode, respectively. The injected carriers transport to the opposite direction, and when electrons and holes meet each other, recombination occurs. As a result, energy of the excited electrons is released as light, which is extracted from the TCE.

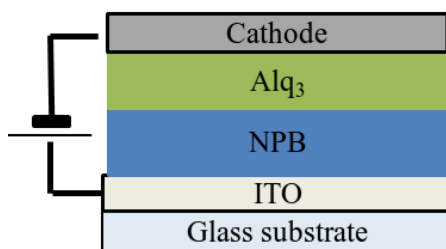


Figure 1.2 Structure of the standard Alq₃/NPB bilayer OLED device.

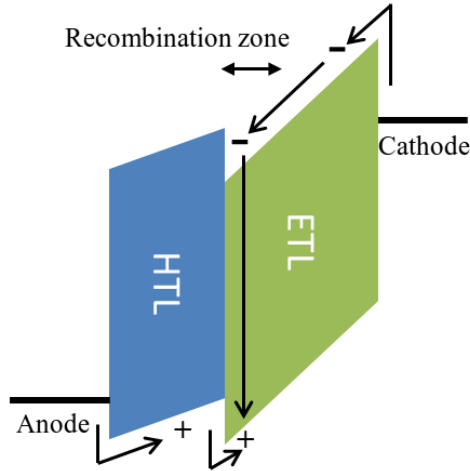


Figure 1.3 Schematic presentation for the energy diagram of the field-applied bilayer device.

The device architecture shown in Figure 1.2 is called bottom emitting architecture, since light is extracted through the bottom TCE or the glass substrate side. This architecture is widely used in lab experiments due to its relatively simple fabrication. However, the bottom emitting structure is not suitable for application in displays, since the opaque component of the driving circuits presented under the OLED pixels limits the aperture ratio of displays (Fig. 1.4(a)). Therefore, the top emitting architecture is preferred. In this architecture, light is extracted from the top TCE and deposited on the top of organic layers (Fig. 1.4 (b)). Since depositing ITO on organic layers causes damage to the underlying organic layers, a thin film of metal such as Al and Ag (~15 nm) are typically used as the TCE in this case. Higher aperture ratio can be achieved in this architecture, and thus, pixel sizes can be larger, resulting in reduced driving voltage given a luminescence, and longer device lifetime.

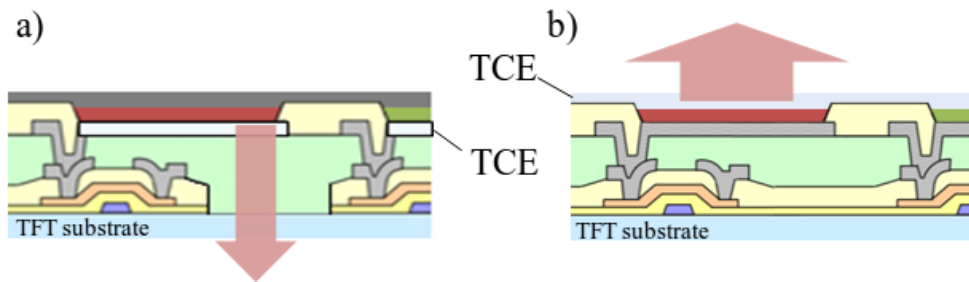


Figure 1.4. Cross section view of a) bottom emitting device and b) top emitting device.

1.2.3 SMOLEDs vs PLEDs

Organic semiconductor materials used in OLEDs can be categorized into two types: small molecule materials and polymer materials. Although there is no clear definition to differentiate them, polymer materials can be in general characterized by long chains of repetitive individual molecules and its large molecular weight while other materials with small molecular weight can be categorized as small molecules. The chemical structure of typical small molecule and polymeric OLED materials are shown in Figure 1.1 and Figure 1.5, respectively. In general, small molecule OLEDs (SMOLEDs) and polymer OLEDs (PLEDs) are processed through different methods, which provide each with different advantages and disadvantages. PLEDs are generally processed through a wet process. This is because large polymer molecules with long chains cannot be deposited through vacuum evaporation, since main-chains of polymer molecules are broken before evaporation. Polymer OLED materials therefore have been developed to be soluble by chemical engineering such as introduction of alkyl or alkoxy substituents for compatibility with wet processes.

In contrast, SMOLEDs are generally processed by means of vacuum evaporation since small molecule materials can be evaporated without affecting molecular structures in vacuum condition. Furthermore, unlike polymer OLED materials, wet processes cannot generally be used with many OLED small molecule materials because their chemical structure makes them generally insoluble in common solvents. Chemical structure modification, such as the incorporation of bulky substituents, is required to achieve solubility since small molecule materials with planar and symmetric structure tend to be prevented from dissolution due to their close molecular stacking.

The advantage of wet processing is its compatibility with cost efficient mass production processes such as inkjet printing and blade coating. These methods do not require vacuum conditions, so the amount of material needed is lower than would be the case in vacuum evaporation. Therefore, the fabrication cost of PLEDs can be potentially much lower than that of SMOLEDs. In contrast, the primary advantage of vacuum evaporation process is that optimization of device structure is relatively easy. While multilayer deposition is generally difficult in wet processing due to inter-layer mixing,

more complex device structures can be readily formed using vacuum evaporation. Also, precise thickness control and high film uniformity are relatively easily achieved in vacuum evaporation. Because of an optimized device structure, SMOLEDs generally have much higher device performance including efficiency and stability in comparison with PLEDs.

In summary, due to the difference in the process methods, SMOLEDs are advantageous in terms of device performance while PLEDs are advantageous in term of fabrication cost in mass production. Currently, OLED display products mainly use SMOLEDs since the performance of PLEDs still does not meet requirements for display products^{[16][17]}.

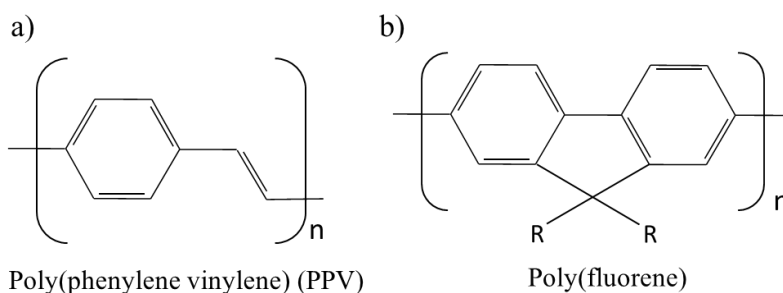


Figure 1.5 Chemical structure of the common PLED materials: a) poly(phenylenevinylene) (PPV) and b) poly(fluorene) (PF).

1.3 OLED displays

1.3.1 Standard architecture and working principle of OLED displays

RGB pixel structure for color generation

Visual images of full color displays are created by a number of individual picture elements that are called pixels. Each pixel consists of red, green and blue (RGB) primary color sub-pixels that generate a useful range of color for visual images. In OLED displays, several RGB pixilation approaches, such as (a) side-by-side RGB OLEDs, (b) white OLEDs plus color filters (CFs), and (c) blue OLEDs with

fluorescent color conversion materials (CCMs), have been suggested^{[41][9]} (Fig.1.6). The details of these approaches are briefly described here.

- **a) Side-by-side RGB OLEDs**

The RGB approach using side-by-side RGB OLEDs is conceptually very simple. In this approach, one pixel consists of independent red, green, and blue OLEDs, similar to traditional cathode ray tube displays (Fig.1.6 (a)). Since the light emitted from the emitting devices is directly seen without any additional layers such as CFs, this approach is superior in terms of utilization efficiency of light. However, this structure requires either separate growth or post-deposition patterning for arrays of RGB OLEDs. Separate growth of thin films is conventionally done using FMMs, but patterning accuracy of this method is limited due to inherent limitations of the shadow mask approach. Details of the issues arising by using this approach are discussed in the following section. Also, although a post-deposition patterning approach of OLEDs has great potential to achieve high resolution OLED patterning, conventional photolithographic techniques cannot be applied, because small molecule OLEDs are generally not compatible with solution processes. In summary, while this approach is desirable in terms of efficiency, there are difficulties in fabricating independent RGB OLEDs side-by-side.

- **b) White OLEDs plus color filters**

A display architecture which uses white OLEDs plus CFs has been emerging in accordance with development of white OLEDs. The first white OLEDs that have demonstrated reasonable efficiency, 0.83 lm/W, were created by blending different color dopants into a host organic layer by Kido et al. in 1994^[18]. As a result of development of materials and refinement of structures, the efficiency of white OLEDs has now reached to 90 lm/W at 1000 cd/m² with 100,000 hours long life time, which meets requirements for practical application to displays^[19]. In these highly efficient white OLEDs, multilayer structures with different emitting layers arranged in stacks is generally used to obtain white emission. In display applications, white OLEDs serve as a back light of displays, and RGB colors are produced by using CFs like LCDs (Fig.1.6 (b)). Therefore, the difficulty of sub-pixel to sub-pixel color patterning of OLEDs is eliminated in this method, contributing to relatively higher yield rate and lower fabrication

cost in comparison with the side-by-side RGB approach. However, the efficiency of this architecture is much less than that of the side-by-side RGB architecture, since light is absorbed (~70%) by the color filters in this case. This also results in shorter lifetime of OLEDs, since the OLED must be driven by higher current for obtaining required RGB pixel brightness.

- **c) Blue OLED with color conversion medium**

This approach uses down conversion of blue light from an array of blue OLEDs to produce RGB pixels by means of converging the blue emission of the OLEDs into red and green emission using CCMs (Fig.1.6 (c)). The blue OLED is deposited on the entire substrate, and pre-patterned film of red and green fluorescent materials are positioned on the substrate. The blue light emitted from the underlying blue OLEDs is absorbed from the fluorescent materials, and the energy is re-emitted as either red or green light. Although the efficiency is limited by quantum yield of the fluorescent materials, and is less than that achieved by the side-by-side RGB approach, higher efficiency can be expected in comparison with the color filter method. Another disadvantage of this approach is unintentional color conversion in neighboring sub-pixels, which is caused by light waveguided to the neighbor sub-pixels in a glass substrate. Manipulation of a glass substrate is thus required to avoid this.

In summary, the side-by-side RGB approach is the best in term of a utilization efficiency of light while the other approaches are advantageous in producing RGB colors. Ideally, the side-by-side RGB approach should be employed for OLED displays because the high light utilization efficiency contributes to lower power consumption and, more importantly, longer lifetime of OLEDs. In fact, most commercialized small-to-medium size AMOLED displays employ the side-by-side RGB method, even though display quality and manufacturing yield tend to be low. For large size displays, the white OLED plus CFs approach is employed because fabricating RGB OLEDs side-by-side on large size substrates is much more difficult than that on small size substrates. However, the advantage of the use of OLEDs is lost when the color filters are used. This results in unsuccessful commercialization of television size OLED displays due to competition with LCDs that use the same color generation approach using CFs.

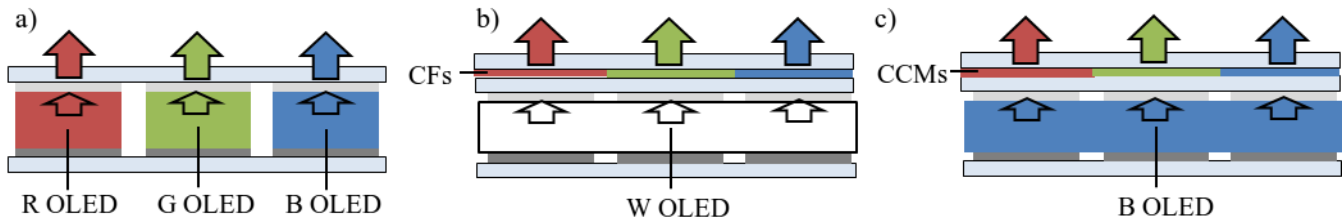


Figure 1.6 RGB approaches for OLED displays: a) side-by-side RGB OLEDs, b) white OLEDs plus CFs, and c) blue OLEDs with CCMs.

Brightness control

LCDs have several inherent limitations such as contrast, viewing angle and response speed. These limitations mainly originate from their brightness control method. In LCDs, the RGB emissions are generated by the RGB color filters backlit by white emission from cold cathode fluorescent lamp (CCFL) or light emitting diodes (LEDs). The brightness of each sub-pixel is controlled by changing voltage applied to a liquid crystal (LC) layer that is sandwiched by polarizing filters. The axes of transmission of the polarizing filters are perpendicular to each other, so no light can pass through the layer stack without the LC layer. The LC layer allows controlling the polarization state of light by changing its molecular orientation, and so the amount of light passing the layer stack can be controlled. Since LC molecular orientation is aligned by applying voltage, the brightness of sub-pixels can be controlled by changing the voltage applied to the LC layer. The brightness control method in LCD tends to limit display performance such as contrast, viewing angle and response speed due to light leaking and slow response speed of molecules to voltage.

In contrast, the brightness controlling system is much simpler in the case of OLED displays. Since OLEDs are self-emitting devices, the brightness of each sub-pixel can be controlled simply by varying the amount of current following through the corresponding emitting devices. OLED displays are therefore current-driven, while LCD displays are voltage-driven. The simple system of OLED displays

using self-emitting devices allows them to be thinner and lighter and provide higher color contrast and higher response speed over LCD displays.

Addressing method

Though OLED displays and LCDs employ different driving methods, the two common addressing methods used in LCDs can be also used in OLED displays^{[4][10]}. These two addressing methods are known as passive-matrix system and active-matrix system. Passive-matrix OLED (PMOLED) displays consist of a matrix of row and column electrodes, where OLEDs are fabricated in the intersections of these electrodes (Fig.1.7). The OLED at each intersection forms a sub-pixel of a display. At the periphery of the matrix, integrated circuits are attached to both row and column electrodes to provide voltage to the sub-pixels that are to be illuminated. A video image can be created by sequentially scanning each row while the column voltages are applied in parallel. The scanning is done at a time frame of T , meaning voltage is applied to each row during a period of T/N , where N stands for the number of row lines. In the active-matrix system, therefore, the emission period for each sub-pixel becomes shorter as display resolution is higher. As a result, higher brightness is required at higher resolutions to produce the desired luminous effect, which results in shorter lifetime of devices. For this reason, PMOLED displays are mainly used only for display products that do not require high display resolution.

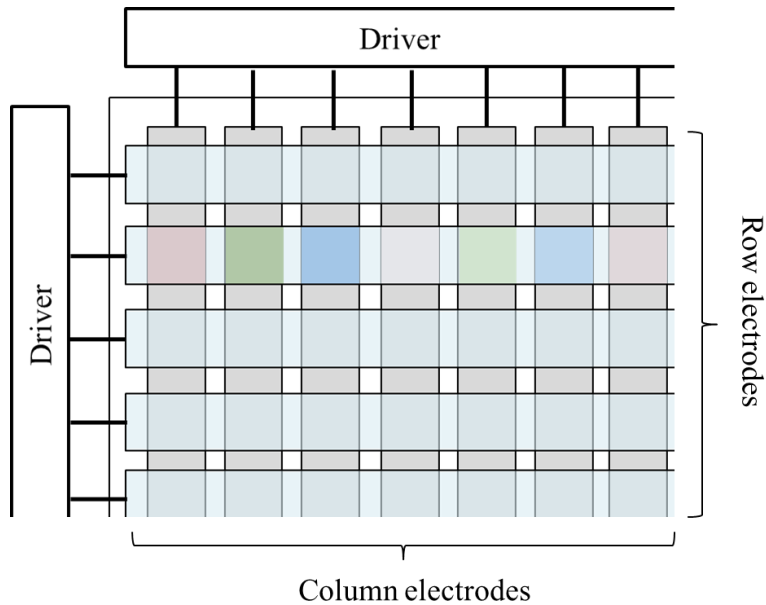


Figure 1.7 Schematic presentation for matrix driving of a PMOLED

For display products with high resolution, active matrix system is generally used. Because of strong demand for high performance devices such as smart phones, FPDs currently mainly use AMOLED displays. In an active matrix system, each sub-pixel is located in the intersections of a matrix with row and column electrodes, like in a passive matrix system. However, each pixel consists not only of an OLED but also of a circuitry comprising of thin film transistors (TFTs) and a capacitor to drive it (Fig.1.8)^[10]. The TFTs are fabricated on a glass substrate through deposition of metal electrode, amorphous silicon and insulator which are patterned by photolithographic methods. The glass substrate with TFTs is called a TFT substrate or backplane substrate. With reference to the associated TFT terminals, the row and column electrodes are often called gate and source electrodes in active matrix system. Figure 1.9 presents the typical OLED display circuit with two TFTs and one capacitor. This circuit is called 2T1C, which stands for the number of TFTs and capacitor. As can be seen, the gate of one of these TFTs (T_1) is directly connected to the gate (row) electrode, and thus, when voltage is applied to one gate electrode, all the TFTs along the gate electrode are turned on. In this state, the voltage applied to the source (column) electrode is imposed to the gate of the other TFT (T_2). Assuming T_2 is operating in its saturation regime, the current flowing to the OLED is proportional to the value of

the voltage applied to the source electrode, and thus the luminance of the OLED is controlled. Due to the switching using TFTs, each pixel is independently controlled without affecting neighbor devices, contributing to higher contrast in comparison with the passive matrix system. Additionally, unlike passive matrix system, the current flowing to the emitting device is kept constant during whole time frame because of the applied voltage stored by the capacitor. Hence, high resolution and large size can be achieved without compromising device lifetime in the active matrix system. Due to these advantages, AMOLED is currently the mainstream system for OLED displays in spite of the complicated system and high fabrication cost of the TFT backplane^{[4][5]}.

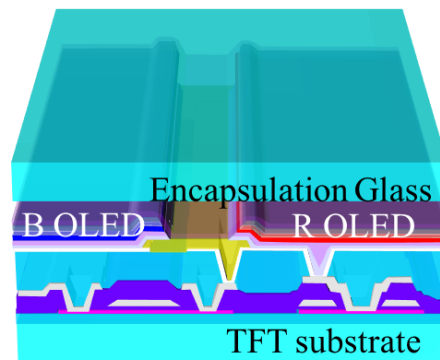


Figure 1.8 Cross section view of OLEDs fabricated on a TFT substrate.

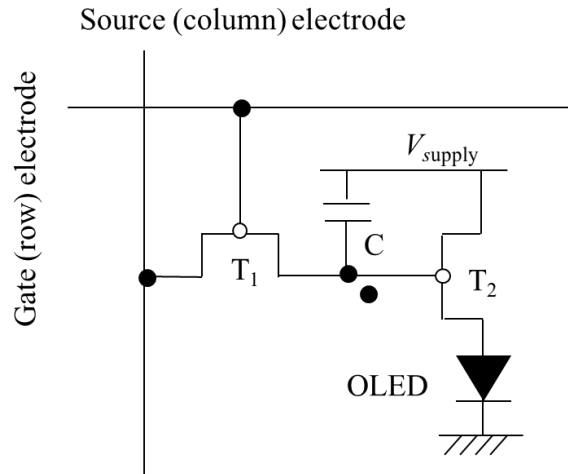


Figure 1.9 Typical OLED display circuit with two TFTs and one capacitor. V_{supply} is the voltage of the power supply.

1.3.2 RGB OLEDs fabrication technique using fine metal masks

As stated in the previous section, the side-by-side RGB approach is ideal for OLED displays and currently employed for most commercialized OLED display products. Fabricating RGB OLEDs side-by-side is conventionally done by using FMMs (Fig.1.10)^{[4][5]}. FMMs are made of thin metal sheets where slits are pre-patterned with a pixel pitch (distance between sub-pixels of the same color). The thickness of FMMs is usually made as thin as possible to minimize undesirable shadow effects. For example, 30 μm thick FMMs are typically used for fabricating AMOLED displays with the resolution of over 200 ppi (pixels per inch). FMMs for OLED display fabrication are conventionally patterned by a wet process such as chemical etching or electrodeposition. Direct patterning techniques such as electric discharge machining (EDM) and laser cutting can also be used, but feature sizes achieved by these techniques is limited to $\sim 50 \mu\text{m}$ due to rough sidewalls and non-uniform lines^[20]. Therefore, these techniques can be applied only to the FMMs for lower resolution displays.

In fabricating RGB OLEDs side-by-side, the slits patterned on FMMs with a pixel pitch are aligned to one of the three color sub-pixels. OLED materials are then deposited on the sub-pixel electrode through these slits. Once deposition for one color OLED is completed, the shadow mask is shifted to the

next color sub-pixel and the same process will be repeated for the other colors. Because multilayer stack structures with fine thickness control and fine film quality is possible in thermal evaporation of small molecules, high performance RGB OLEDs with optimized structure are relatively easily fabricated with this approach.

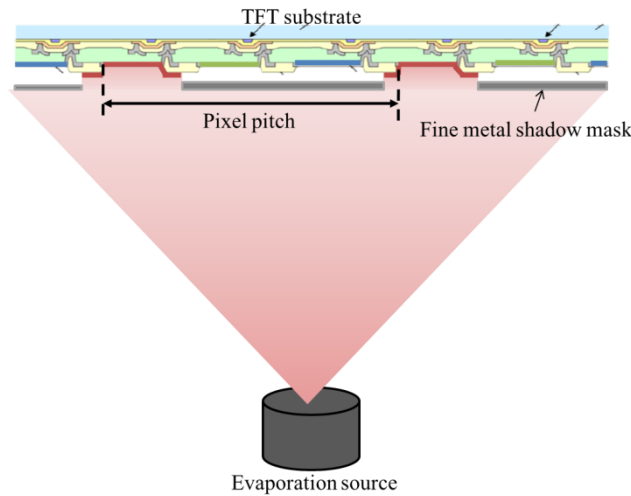


Figure 1.10. Schematic presentation for the conventional color patterning technique using FMMs.

1.3.3 Limitation of current small molecule OLED display fabrication technology

Fabricating RGB OLEDs side-by-side using FMMs has several inherent limitations which cause technical challenges in manufacturing OLED displays, however. One of these limitations is difficulty in making masks with micrometer level dimensional accuracy^{[5][21][22]}. Conventionally, FMMs are patterned by a wet process such as chemical etching or electrodeposition. However, the patterning accuracy of metals achieved by these methods is limited, leading to non-uniform slit width varying by $\pm 10 \mu\text{m}$. For smaller feature sizes less than $20 \mu\text{m}$, dry processes such as reactive ion etching (RIE) and electron beam lithography (EBL) are required, but these techniques are not suitable for OLED display fabrication due to limitation in scalability and high fabrication cost^[20].

Another issue for these techniques is deformation of masks upon their alignment over TFT substrates. Because these masks have to be made as thin as possible (typical FMM thickness: $\sim 30 \mu\text{m}$)

in order to reduce shadow effects and because these masks are strained by a stretcher upon mounting them on TFT substrates, these masks are easily deformed, resulting in misalignment of the masks over the substrates.

Other issues include mechanical alignment inaccuracy between the masks and substrates, and shadow effects due to the thickness of FMMs. Because of inaccurate pixel patterning caused by these issues, pixel pitch tends to be large and aperture ratio tends to be low. Furthermore, the unreliability of the color patterning method also leads to low manufacturing yield, high fabrication cost, and low display quality.

In this context, several alternate color patterning techniques have been suggested for more reliable color patterning process. These alternate approaches include contact printing techniques using pre-patterned stamps^{[23][24]}, selective transfer (or sublimation) of organic layers from a donor substrate to the OLED substrate using lasers or other thermal transfer techniques^{[25][26][27]}, and selective diffusion of a luminescent material^{[28][29][30][31]}. Notable approaches are introduced in the following sections in detail. Nevertheless, these techniques remain under development, and there is still no commercially viable solution to this issue.

Finally, it is worth noting that some latest personal digital assistant (PDA) products employ a high quality OLED display with resolution over 300 ppi^[32]. However, this resolution is actually a “pseudo resolution” which is achieved by means of a special pixel matrix scheme, called “PenTile”, along with a rendering technique. The PenTile pixel layout typically consists of small green sub-pixels interleaved with alternating larger red and blue sub-pixels (RGBG) in each unit cell (Fig.1.11). Making good use of high sensitivity of human eyes to green color, this RGBG scheme can create as many pixels per inch as the RGB scheme, with one third fewer sub-pixels than that in the conventional matrix scheme, through the use of sub-pixel rendering^{[33][34]}. However, image quality is significantly compromised in this case, and the issue of low aperture ratio cannot be addressed by this approach.

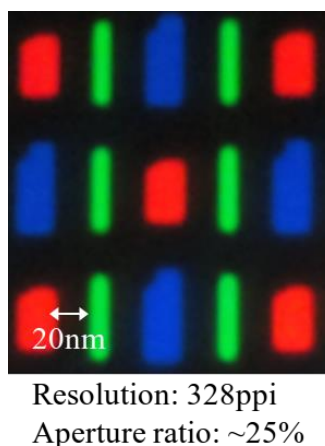


Figure 1.11 Magnified view of an AMOLED with the PenTile layout.

1.3.4 Alternative color patterning techniques

Laser based printing techniques and photolithographic techniques for fabricating RGB small molecule OLEDs side-by-side have been suggested as an alternative to the FMM technique. Both techniques do not require use of shadow masks, so limitations associated with shadow masks can be eliminated. Although these techniques are still under investigation, they have great potential to achieve reliable color patterning in OLED display fabrication.

Laser based printing techniques

There are several color patterning techniques using laser based printing, such as laser induced thermal imaging (LITI)^{[25][26][35]}, radiation induced sublimation transfer (RIST), and laser induced pattern-wise sublimation (LIPS)^[36]. LITI is the first to be proposed and is the most intensively studied among these techniques. LITI employs laser exposure to selectively transfer organic layers that are coated on a donor sheet to an acceptor substrate (Fig.1.12). In this method, thin organic films are first coated on the donor sheet. The pre-coated donor sheet is then laminated to a TFT back plane, and the organic layers on the donor sheet are transferred selectively to the sub-pixel on the TFT backplane by local laser exposure. It has been reported that, through this technique, organic layers can be transferred with uniform thickness and uniform dimensional line edges with reasonable device characteristics

which are on par with those of devices fabricated through standard thermal vacuum deposition [25][26]. Because of the high precision transfer and high positioning accuracy of laser, high patterning accuracy of $\pm 2.5\sim 5\ \mu\text{m}$ can be achieved by this method.

Primary drawbacks of the LITI process are high production cost and adverse effects on device performance. The donor sheet used in this process consists of four layers: the support layer, the light to heat conversion layer (LTHC), the interlayer, and the transfer layer. Production cost of the LITI process tends to be high because the four layer donor sheet is not commercially available and not reusable due to deformation of the sheet. The adverse effects on device performance arise from the thermal transfer process by laser. Since organic materials are heated during laser exposure, morphological changes occur in organic materials with low glass transition temperature (T_g) resulting in poor device performance. Because of this limitation, the variety of materials used in LITI process is limited despite the fact that some high efficiency and long lifetime organic materials have low T_g . Therefore, although several display companies have pursued this technique, it has not been commercially viable.

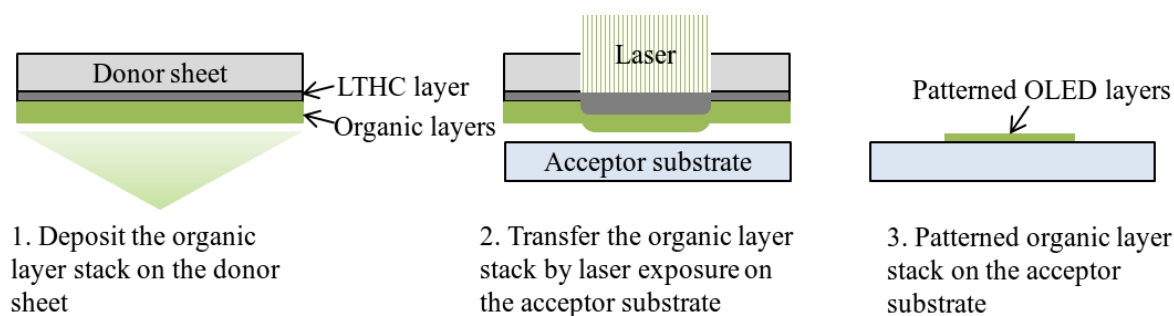


Figure 1.12. Schematic presentation for the transfer of an organic layer stack by laser exposure of LITI process.

Photolithography

In general, photolithographic patterning cannot be applied to OLED color patterning because organic materials are soluble in standard chemicals used in photolithography processes, such as photoresists, developers, and strippers. To avoid this, highly fluorinated chemicals such as

hydrofluoroethers (HFEs) are often used^{[37][38]}. Because they are orthogonal to the majority of non-fluorinated organic electronic materials, solution processes can be performed without dissolving the organic materials. An advanced photolithographic approach is direct photolithographic patterning of OLEDs. In this case, a light emissive polymer with a photoresist-like property, which can be cross-linked to produce an insoluble polymer by exposure to UV light, is used^{[39][40]}. Several photolithographic process steps such as deposition and stripping of resists can be eliminated with this method, which contributes to reducing risks in damaging organic layers. Three color polymer OLEDs patterned through this technique have been successfully demonstrated with reasonable electro-optical characteristics and efficiency. However, the variety of materials which are compatible with this method is limited and further investigation is required for higher device performance.

While photolithographic patterning of OLEDs is initially studied for patterning of polymer OLEDs, application of photolithography to small molecule OLEDs is recently demonstrated^[41]. Although details of this technique have not been disclosed, operating RGB OLEDs patterned with 20 μm subpixel pitch through the photolithographic technique has been demonstrated. However, the first report shows that the device performance drops due to the patterning process. For example, current efficiency decreases to one sixth of that of a control device, and lifetime decreases to half. Although further investigation is required to avoid the adverse effects on devices, this technique has a great potential to obtain full color displays with ultra-high resolution.

1.4 Current status of OLEDs and OLED displays

1.4.1 Current status of OLEDs in display technology

The two main requirements of OLEDs for application to displays are high operational stability and high efficiency. In general, it is accepted that the lifetime of RGB color should be over 50,000h with a reasonable brightness level of at least $1000\text{cd}/\text{m}^2$ for large size OLED displays^{[4][5]}. Considering the low aperture ratio of display panels, the brightness of each red, green, and blue sub-pixel has to maintain brightness of 3500, 7000, and 1500 cd/m^2 , respectively^[5]. For small size displays, such as PDAs

including smart phones and tablets, the lifetime is required to exceed 30,000 h with an initial brightness of approximately 200-300 cd/m² [4].

Although the first bilayer OLEDs demonstrated by Tang and Van Slyke demonstrate just 1.5 lm/W luminous efficiency and maximum 1000 cd/m² brightness^[1], significant improvement has been made over the past 20 years in device stability and efficiency with the discovery of new materials and better understanding of degradation mechanisms.

The significant advancement in terms of efficiency made on OLEDs is attributed to the discovery of phosphorescent OLED materials^{[7][42][42]}. The first generation OLED material, which is used in the first bilayer OLEDs, is a fluorescent material. Because photons are emitted only with the recombination of singlet excitons in fluorescent materials, theoretical quantum yield of fluorescent material based OLEDs is limited to 25%. In contrast, in phosphorescent materials such as tris[2-phenylpyridinato-C₂,N]iridium(III) (Ir(ppy)₃), all excitons including triplet excitons can emit photons due to the presence of heavy atoms such as iridium or platinum, which increases spin-orbit coupling and allows radiative triplet transitions^{[7][43]}. Therefore, 100% theoretical quantum yield is possible in phosphorescent OLEDs. The discovery and development of the phosphorescent materials have made dramatic improvement in the efficiency of OLEDs.

In parallel to work on achieving high efficiency, intensive studies have been conducted for understanding degradation mechanisms and improving stability^{[44][45]}. In the early stage of study on degradation phenomena, extrinsic degradation mechanisms such as dark spot formation or catastrophic failure are investigated^{[46][47][48][49]}. Since extrinsic degradation is caused by external factors such as defects in organic layers and electrodes or exposure to water and oxygen, it has been found that this kind of degradation can be readily circumvented by adequate fabrication control and encapsulation^{[50][51]}. However, though stability of OLEDs has been improved due to development of these techniques to avoid extrinsic degradation, intrinsic degradation, which occurs under operation without an external factor, is a more challenging problem to solve. Intrinsic degradation of OLEDs is still intensively investigated for further improvement in device stability^{[44][45][52][53][54]}.

As a result of these developments, the current OLEDs demonstrate long lifetime with reasonable efficiency and brightness, which meet the requirements for some commercialized small size active matrix OLED (AMOLED) displays^[5]. In fact, PDAs using small size AMOLED displays have already been in the market for several years. For large size displays, however, the required lifetime of blue phosphorescent OLEDs has not yet been reached. Further investigations are expected for commercialization of large size AMOLED displays.

1.4.2 Current status of OLED display

Company	Sony	Samsung	LG
OLED TV business to date	- 2008 First commercialized OLED TV [11", 960*540, \$2,500]	- 2013 Commercialized 55" OLED TV [55", Full HD, \$9,999]	- 2013 First commercialized 55" OLED TV [55", Full HD, \$15,000]
	- 2014 Announce being withdrawn from OLED TV businesses	- 2014 Announce no OLED TVs will be released in 2015	- 2014 [55", Full HD, \$6,999] -2015 [65", 4KUHD, \$9,999] [77", 4KUHD, \$25,000]
Current status	Withdrawn	Resume as needed	Increasing investment
Color patterning method	RGB by FMM & LITI	RGB by FMMs	White OLEDs plus CFs

Table 1.1 Summary of an OLED television business to date.

The first commercialized OLED television was launched by Sony in 2008 with 11" screen size and 960 by 540 resolution. In 2013, new OLED televisions were released from two companies, Samsung Electronics and LG Electronics with a larger screen size of 55" and higher resolution of 1920 by 1080 (Table 1.1). However, the commercialization of OLED displays still remains limited. For example, the latest report says the shipment of OLED televisions in 2014 is still limited to 7,7000 units (or ~0.003%

of the total television shipment in 2014)^[55]. Also, there is now only one OLED television panel supplier in 2015 after Sony and Samsung Electronics decided to focus on LCDs because of the low profitability of the OLED television business.

In comparison with large television size displays, OLED displays are relatively prevalent in small and medium sizes. The shipment share of OLED displays in small to medium size displays started increasing since 2010 when Samsung Mobile Display launched the first AMOLED smartphone: 4.4% in 2010 and 8.4% in 2012^[56]. The impact on smartphones is particularly significant, and in 2013, AMOLED displays had a 35% share of mobile phone display revenues^[57]. Nevertheless, it is expected that the growth of OLED displays will stop mainly due to competition with the high performance low temperature polysilicon (LTPS) LCDs^{[56][57]}.

As discussed in previous sections, the commercialization of OLED displays is hampered primarily by immature manufacturing processes, which leads low manufacturing yield, high fabrication cost, and low display quality. In fact, the fabrication cost of OLED televisions is 8-10 times higher than that of amorphous silicon LCDs depending on process methods^[58]. In particular, fabrication cost of side-by-side RGB OLED televisions is 25% higher than that of the televisions with white OLEDs with CFs. The OLED television business is therefore still not profitable due to the high fabrication cost, which caused display companies to step away from the OLED television business. Also, the resolution and fill factor (the ratio of the emissive area to the total surface area of a display) of OLED displays tends to be low in small to medium size displays. While the resolution and fill factor of recent LCD smartphones exceeds 300 ppi and 60%, respectively, those of AMOLED smartphones via the standard side-by-side RGB sub-pixel matrix scheme have been limited to ~200 ppi and ~40%, respectively^[32] (Table 1.2).

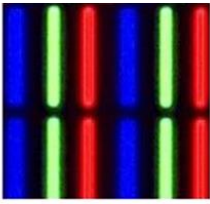
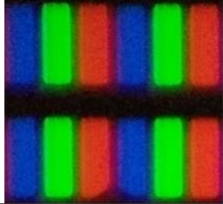
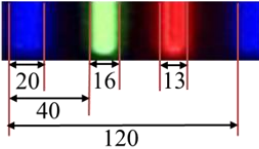
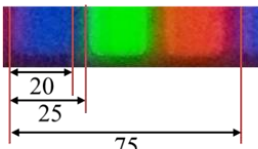
	OLED display	LCD
Pixel layout		
Pixel pitch		
Sub-pixel pitch		
Sub-pixel width (um)		
Fill factor	~40%	~60%
Resolution	~210 ppi	~330 ppi

Table 1.2 Comparison between OLED display and LCD.

Chapter 2

New Color Patterning Techniques for OLED Displays: Introduction and Research

Objectives

As stated in the previous chapter, OLED display manufacturing issues are largely attributed to the limitations of the FMM technology. Several color patterning techniques have been proposed, but there are still no commercially feasible alternatives since these techniques often raise production costs and compromise device performance. In this work, two new OLED color patterning techniques are proposed as alternatives. The first technique (Technique 1) involves color patterning using laser-patterned PI shadow masks. The second technique (Technique 2) involves color patterning via diffusion of a luminescent material. In this chapter, these techniques are introduced, and the objectives and general methodology of the experimental investigations of these techniques are presented.

2.1 Introduction to the proposed techniques

The new color patterning techniques include: Technique 1, color patterning using laser-patterned PI shadow masks; and Technique 2, color patterning via diffusion of a luminescent material. In Technique 1, PI sheets that are patterned by laser ablation are utilized as shadow masks. The PI sheets are patterned either *ex-situ* off substrates or *in-situ* on substrate. The latter technique is specifically named *in-situ* shadow mask patterning technique. Technique 2 is based on the diffusion of a luminescent material from a donor substrate into the organic host material layer of the OLED that is pre-coated on an acceptor substrate. This is a sort of a maskless color patterning technique which does not require use of shadow masks.

2.1.1 Technique 1: Color patterning using laser-patterned PI sheets

As discussed in the previous section, the causes of inaccurate color patterning in the conventional technique using FMMs include the limited accuracy of the FMM patterning techniques, post-patterning deformation of FMMs due to stretching upon mounting them on the metal frame, and shadow effects due to the thickness of FMMs ($\sim 30 \mu\text{m}$). The proposed patterning technique using laser-patterned PI shadow masks have a potential to overcome all three of these issues^[13]. First, precise patterning of masks can be achieved much more easily using PI sheets compared to using metal sheets. It is well known that PI can be patterned by direct laser ablation with very high dimensional accuracy, as indicated by the fact that even sub 100 nm patterning is possible by laser ablation, while the patterning accuracy of a thin metal ($\sim 30 \mu\text{m}$) by a wet process is limited to $\pm 10 \mu\text{m}$ ^{[14][15]}. Second, post-patterning deformation of masks by stretching can be limited in this technique since PI sheets can be patterned after they are already stretched and mounted on the metal holder, while FMMs are deformed due to stretching as depicted in Figure 2.1. Finally, since thin PI sheets ($\sim 7.5 \mu\text{m}$) are commercially available and can be mounted directly on the TFT substrate as a contact shadow mask, shadow effects can be significantly reduced compared to those in FMMs. These advantages of using laser-patterned PI shadow masks enable us to precisely pattern pixels on TFT substrates, thus achieving high pixel density and high aperture ratio.

Furthermore, taking advantage of the simple laser dry mask patterning process, it is possible to create masks after PI sheets are mounted on the TFT backplane substrate as depicted in Figure 2.2^[13]. This technique is named the *in-situ* shadow mask patterning technique since PI shadow masks are patterned *in-situ* on the substrates. This *in-situ* shadow mask patterning technique can be expected to offer further accuracy advantages, since the slits are created by laser over the desired TFT locations directly and thus eliminates the need for a subsequent mechanical alignment step. This approach is particularly useful for pixel patterning on flexible substrates where the poor mechanical and dimensional stability of substrates pose additional challenges for aligning shadow masks accurately.

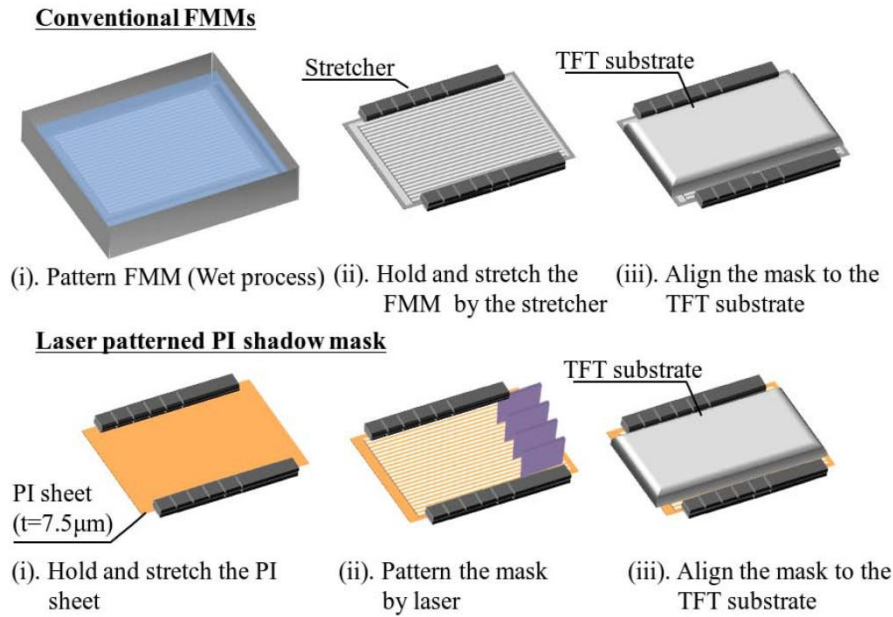


Figure 2.1 Comparison between the conventional patterning technique using FMMs and the patterning technique using laser-patterned PI sheet shadow masks.

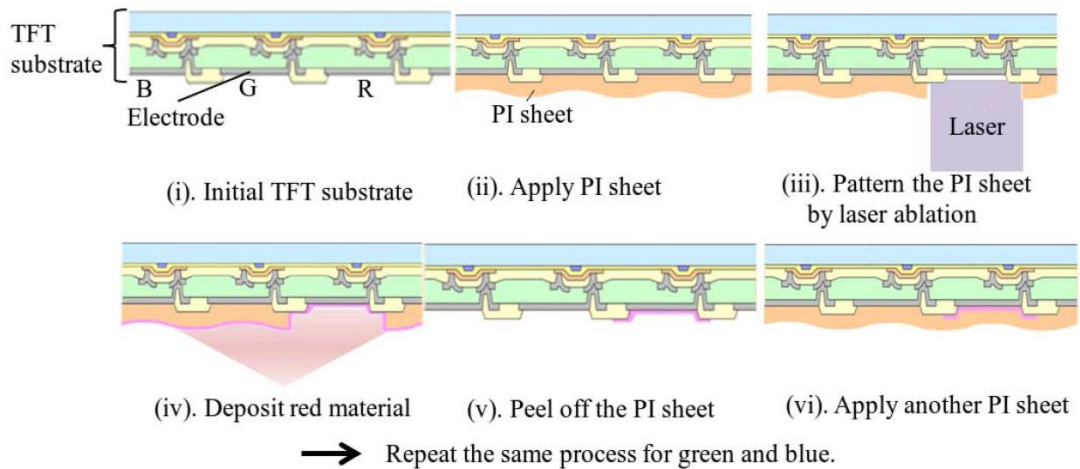


Figure 2.2 General scheme for RGB OLED display fabrication using the *in-situ* shadow mask patterning technique.

2.1.2 Technique 2: Color patterning via diffusion of a luminescent material

In addition to the laser-patterned PI mask technique, another technique that utilizes diffusion as a way to introduce luminescent materials in order to achieve RGB colors is proposed. This technique is based on the diffusion of a luminescent material from a donor substrate into the organic host material layer of the OLED that is pre-coated on the backplane substrate. The use of a pre-patterned micro stamp as the donor substrate allows the physical contact between the two substrates to be selectively limited to certain areas. This in turn limits this diffusion to only certain areas of the OLED substrate (Fig. 2.3). This maskless color patterning method offers a significant advantage in term of patterning accuracy since limitations arising from using FMMS can be eliminated. Furthermore, such selective diffusion can also instead be done through local heating via electric currents, utilizing electrodes in the OLED backplane for this purpose, which eliminates the need for patterned stamps and mechanical alignment (Fig. 2.4). It is also possible to utilize local laser heating for selective diffusion. This technique is described in Appendix 1 in detail.

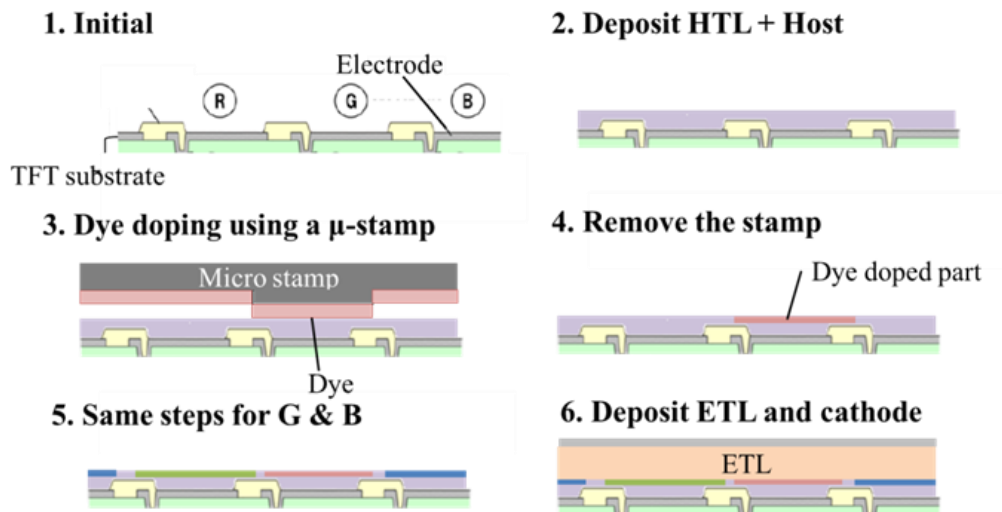


Figure 2.3 General scheme for RGB OLED display fabrication using pre-patterned micro stamp as the donor substrate.

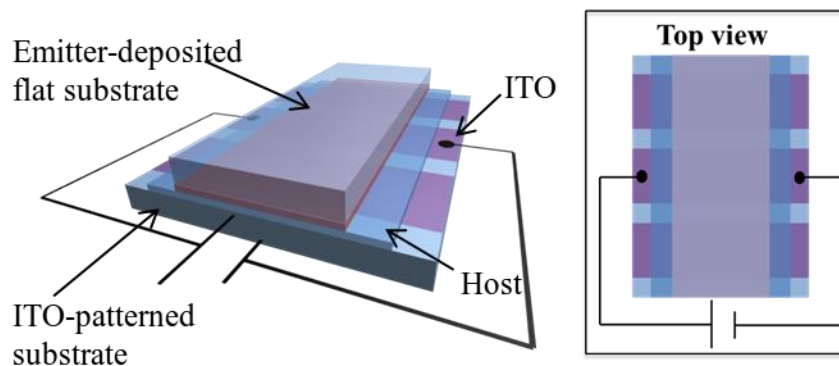


Figure 2.4 General scheme for the selective diffusion of a luminescent material through local heating via electric currents. Details of the process steps are shown in Section 5.3.

2.2 Research objectives

The main objective of this work is to provide an initial experimental assessment of these techniques for RGB color patterning of small molecule OLEDs. Toward this main over-arching objective, the specific objectives of the experimental investigations are as follows:

I) Technique 1: Color patterning using laser-patterned PI masks

1. Assessing and investigating the capacity of the laser-patterned PI sheet as a shadow mask
2. Examining the effect of contact of organic layer with a PI sheet on device performance
3. Demonstrating RGB OLEDs with very small feature sizes ($<25\ \mu\text{m}$) fabricated side-by-side on one substrate using the laser-patterned PI mask technique
4. Investigating the effect of laser ablation of PI sheets *in-situ* on an electrode on device performance
5. Investigating the effect of laser ablation of PI sheet *in-situ* on an electrode with a protective layer on device performance
6. Demonstrating RGB OLEDs with very small feature sizes ($<25\ \mu\text{m}$) fabricated side-by-side on one substrate using the *in-situ* shadow mask patterning technique

II) Technique 2: Color patterning via diffusion of a luminescent material

1. Assessing the effectiveness of physical contact between a donor and an acceptor substrate in bringing about sufficiently high doping levels via diffusion
2. Examining electroluminescence (EL) characteristics of devices fabricated using this technique
3. Demonstrating RGB color patterning by selective diffusion of a luminescent material
4. Discussing possible issues and solutions for them
5. Theoretically estimating luminescent material concentration profile

2.3 General Methodology

In this work, the investigation is primarily performed experimentally. The experimental study basically follows a part of the actual procedure for the proposed techniques. Such a study therefore helps us discover unexpected issues during the procedure. In addition, successfully demonstrating the use of these techniques can be strong evidence that the approach is technically feasible, and allows for expected and unexpected issues to be properly addressed.

In many of the experiments performed in this work, OLED materials including Alq₃, NPB, 4-(dicyanomethylene)-2-t-butyl-6-(1,1,7,7-tetramethyljulolidyl-9-enyl)-4H-pyran (DCJTB), 2,3,6,7-tetrahydro-1,1,7,7-tetramethyl-1H, H,11H-10-(2-benzothiazolyl)quinolizino[9,9a,1gh]coumarin (C545T) are used as an emission layer(EML)/ETL, HTL, red dopant and green dopant, respectively. All these materials are typical fluorescent materials that are intensively studied in the field of OLEDs. The use of such typical materials is suitable for the first proof-of-concept study of the novel techniques. In addition, though luminescence efficiency of fluorescent materials is generally lower than that of phosphorescent materials, fluorescent materials have higher performance in term of stability. High stability is desirable for the experiments in this study because some experiments need to be performed in the ambient air, which can cause degradation of devices. Another reason for using these materials in this work is price. Because these are very common and mass produced materials, the price is much

lower than that of other materials such as phosphorescent materials. Vacuum deposition, which is conventionally employed for OLED display fabrication, will be used to deposit these materials. Because precise thickness control and high film uniformity are relatively easily achieved by vacuum deposition, this method promises a high level of reliability, enough to reproduce experimental results.

Device performance of OLEDs is typically evaluated in term of efficiency, stability and emission color. Therefore, in order to investigate the effect of the use of the proposed techniques on device performance, current versus voltage (J-V) and luminance versus voltage (L-V) characteristics, EL spectrum, and EL and V_d stability measurement of devices fabricated through these techniques are measured. Emission uniformity and dark spot formation also need to be monitored to investigate effects on devices. In this case, EL images of devices are captured by optical microscope. Capabilities of shadow masks can be evaluated by thickness and dimensional uniformity of films deposited through the mask. Atomic force microscopy (AFM) is used as it has the ability to measure thickness profile with the vertical resolution limit of less than 1nm, which is small enough to measure typical organic layer thicknesses used in OLEDs. Detailed approaches for each experiment are given in each experimental section.

Chapter 3

Experimental Procedure

This chapter describes experimental procedures generally used in this research. To be more specific, procedures for substrate preparation, OLED device fabrication, and typical device characterization methods are shown in this chapter. Detailed approaches for each experiment are provided.

3.1 Substrate preparation and OLED device fabrication

The standard bottom emitting OLED devices are usually grown on ITO pre-coated glass substrates by thermal vacuum deposition. Before material deposition, the ITO coated glass substrate is ultrasonically cleaned in acetone solution and then rubbed with a cotton swab to remove contaminants on the surface. The substrates are again ultrasonically cleaned in isopropyl alcohol (IPA) solution, followed by drying on a hot plate at 100 °C.

After cleaning, the substrates are loaded in the vacuum chamber of a thermal deposition system from EvoVac Deposition System. Figure 3.1 presents the photo of the inside of the chamber. There are several resistance heating evaporation sources on the bottom floor of the chamber, which enable multilayer deposition and co-deposition of several materials. The substrate is placed on a substrate holder located ~30 cm above the evaporation sources, to ensure film thickness uniformity. The base pressure of the chamber is kept below $\sim 5 \times 10^{-6}$ Torr, where organic materials are sublimated at 100-500 °C. Organic materials loaded in the evaporation sources are heated to their sublimation temperature by resistive heating, and sublimed materials are then deposited on the substrate at a nominal deposition rate of 0.2-3 nm/s. The deposition rate is measured by crystal quartz sensors.

Figure 3.2 presents an example of the architecture of standard bottom emitting OLEDs fabricated on an ITO coated glass substrate. In this substrate design, organic layers are deposited on the middle five ITO strips, and a metal cathode bridge is deposited across these middle five strips. When voltage is

applied between the ITO anode and the metal cathode, EL is observed from the bottom of the substrate through the transparent glass substrate.

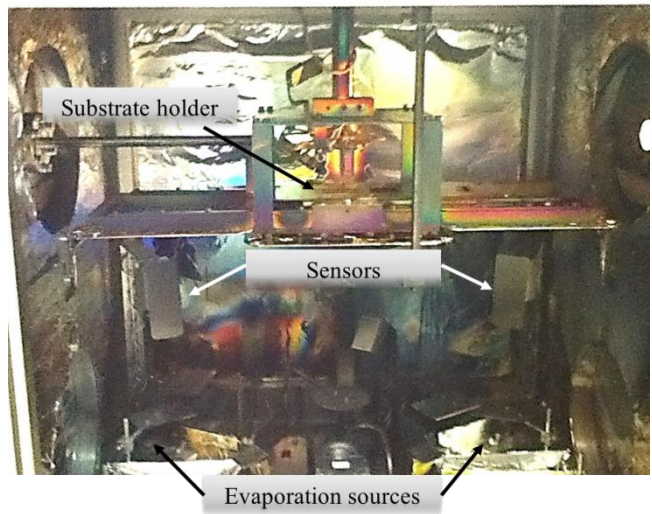


Figure 3.1. Photograph of the inside of the vacuum chamber.

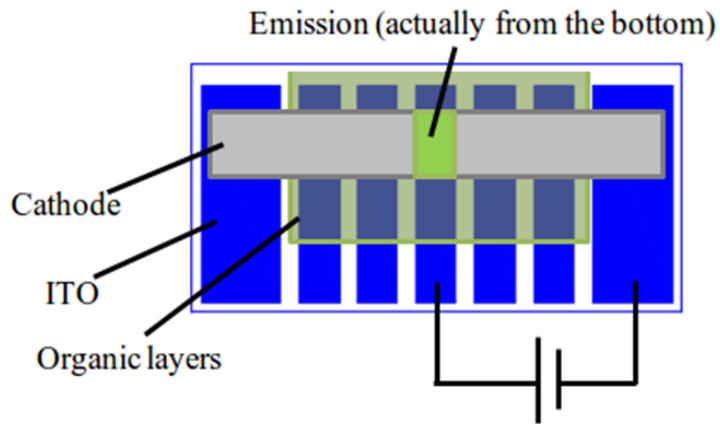


Figure 3.2. Typical architecture of the standard bottom emitting OLEDs.

3.2 Device characterization

Device performance testing includes measurement of PL and EL spectrum, J-V and L-V, and EL and voltage stability. PL spectrum of OLED materials is measured by a spectrophotometer upon certain wavelength light irradiation produced by a monochromator. EL spectrum of devices is measured by a

spectrophotometer at the current density of 20 mA/cm². J-V and L-V characteristics of completed OLED devices are measured by using a photometer and a digital voltmeter. For testing the stability of OLED devices, EL intensity and driving voltage (V_d) of devices driven by an alternating current with a 50% duty cycle are periodically recorded in a dry nitrogen condition.

Chapter 4

Technique 1: Color Patterning Using a Laser-Patterned PI shadow mask

This chapter describes a series of investigations on assessing the technical feasibility and potential of the color patterning technique using laser-patterned PI shadow masks. This chapter is divided into two sections. The first section (Section 4.1) describes investigations of the color patterning using PI shadow masks which are patterned *ex-situ* off substrate. This section consists of three subsections, each of which describes one of the investigations with an introduction, a description of the experimental procedure, and a discussion of its results. Subsection 4.1.1 assesses and investigates the capacity of the laser-patterned PI sheet as a shadow mask. Subsection 4.1.2 examines the effect of contact of an organic layer with a PI sheet on device performance. Subsection 4.1.3 demonstrates RGB OLEDs with very small feature sizes ($<25\ \mu\text{m}$) fabricated side-by-side on one substrate using the patterning technique. The second section (Section 4.2) shows investigations on the variant technique using PI sheets which are patterned *in-situ* on substrates. This section also contains three subsections. Subsection 4.2.1 investigates the effect of laser ablation of PI sheets *in-situ* on an electrode on device performance. Subsection 4.2.2 investigates the effect of laser ablation of PI sheet *in-situ* on an electrode with a protective layer on device performance. Subsection 4.2.3 demonstrates RGB OLEDs with very small feature sizes ($<25\ \mu\text{m}$) fabricated side-by-side on one substrate using the *in-situ* shadow mask patterning technique.

Material in this chapter has been published before. More specifically, material in Subsections 4.1.1, 4.1.2, 4.1.3 and 4.2.3 was published in [Y. Kajiyama, K. Joseph, K. Kajiyama, S. Kudo, and H. Aziz, “Small feature sizes and high aperture ratio organic light-emitting diodes by using laser-patterned polyimide shadow masks,” *Appl. Phys. Lett.*, 104(5), 053303 (2014)], and material in Subsections 4.2.1 and 4.2.2 was published in [Y. Kajiyama, K. Joseph, K. Kajiyama, S. Kudo, and H. Aziz, “Recent progress on the vacuum deposition of OLEDs with feature sizes $\leq 20\ \mu\text{m}$ using a contact shadow mask

patterned *in-situ* by laser ablation,” *Proc. SPIE*, 8829, 882919 (2013)]. Publisher’s permission to reproduce this material in this thesis has been obtained.

4.1 Color patterning using PI shadow masks patterned *ex-situ* off substrate

Several experiments are performed for the purpose of investigating technical feasibility of the laser-patterned PI mask technique. In order to show the capability of the laser-patterned PI sheet as a shadow mask, dimensional uniformity and edge shadow effects of an OLED material deposited through the laser-patterned PI sheet is investigated by AFM. Device performance of OLEDs with PI sheets in direct contact is examined to investigate the effect of direct application of the PI sheets on device performance. Finally, RGB OLEDs are fabricated side-by-side on one substrate using this technique.

4.1.1 Assessing and investigating the capability of the laser-patterned PI sheet as a shadow mask

Introduction

Conventionally, FMMs are patterned by a wet process such as chemical etching or electro deposition. However, poor patterning accuracy of these methods limits dimensional uniformity of masks leading to non-uniform slit width varying by $\pm 10 \mu\text{m}$ ^{[5][21][22]}. As an alternative, use of patterned polymer sheets as contact shadow masks has been suggested^{[59][60]}. These masks are patterned by direct laser ablation of polymer sheets or spin coating of polymer materials on pre-patterned molds, which makes precise patterning of masks possible with $\sim 5 \mu\text{m}$ feature sizes. In addition to the precise mask patterning, limited shadow effects is another advantage of the use of polymer shadow masks. Because these polymer shadow masks can be applied directly on substrates without damaging the underlying metal or organic thin layers, edge shadow effects due to the gap between substrates and shadow masks can be minimized. Because of these advantageous properties of polymer sheets as shadow masks, they are expected to be useful alternatives for FMMs.

In this experiment, in order to assess and confirm these properties of PI sheets as shadow masks, dimensional uniformity and shadow effects of an OLED film deposited through a PI sheet patterned by laser ablation is investigated by AFM.

Experimental Procedure

In order to examine the capability of laser-patterned PI sheets as shadow masks for vacuum deposition of OLED materials, the thickness profile of an organic film deposited on a glass substrate through slits of the laser-patterned PI sheet is investigated by AFM. The laser used for ablation is 266nm neodymium-doped yttrium aluminum garnet (Nd:YAG) solid-state laser from a Callisto VL-C30 Laser System. Figure 4.1 shows the configuration of the laser system including a focusing unit and a scanning stage. The laser light emitted from the laser generator passing through a 0.5×3 mm optical slit is collected by a ×20 magnification UV lens. The collected laser light is then focused on the surface of a 7.5 μm thick PI sheet by using Uranus Auto Focusing Unit with the focused beam size of 25 ×150 μm. 25 μm wide slits can be created on the PI sheet by scanning the laser beam at an energy density and scanning speed of 1 J/cm² and 60 μm/s, respectively. The laser-patterned PI sheet is then applied on a glass substrate, and a 140 nm thin layer of Alq₃ is deposited through the 25 μm wide slits. The deposited Alq₃ film is then analyzed by AFM.

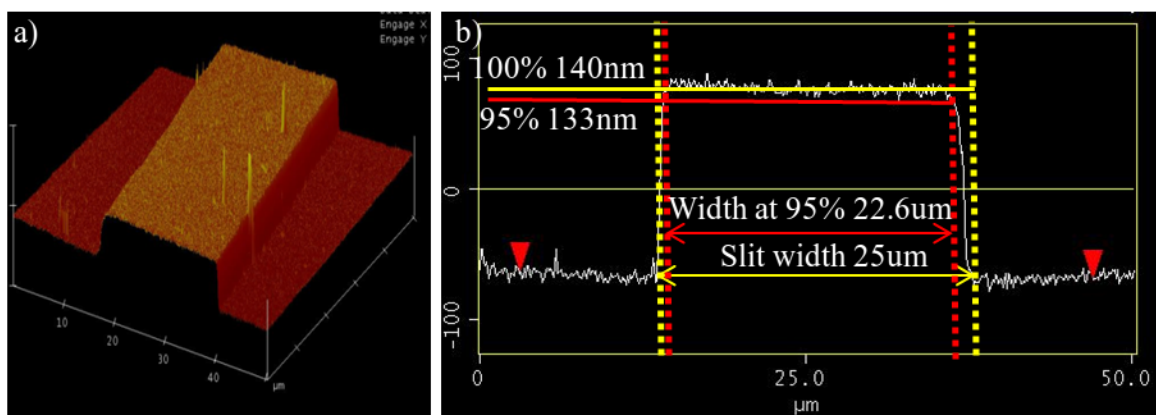


Figure 4.2. (a) 3D AFM image and (b) cross section view of an Alq₃ layer (~140nm thick) deposited through a laser patterned PI shadow mask with 25 μm wide slits.

4.1.2 Device Performance: examining the effect of contact of an organic layer with a PI sheet

Introduction

In the laser-patterned PI mask technique, the patterned PI sheets are directly applied on pre-deposited organic layers. Because the van der Waals bonding force of small molecule OLED materials is very weak, and because the material is susceptible to exposure to aggressive gasses such as moisture or oxygen, there is the possibility that direct contact with the PI sheet could compromise OLED device performance^{[47][48][61][62][63]}. Specifically, one such possible adverse effect is dark spot formation. Dark spots could be formed because of structural defects which can be produced through friction between the PI sheet and organic layers. Dark spots could also form when moisture absorbs in the PI sheet, as exposure to moisture induces morphological change in organic films and/or gas evolution, leading to structural defects in cathode.

Efficiency and stability of devices may also be compromised through direct contact with PI; particles left by the PI sheets and/or byproducts produced through chemical failure due to moisture and oxygen in PI sheets could act as luminescence quenchers and/or charge trapping sites. Tests were

conducted to investigate whether direct contact of organic films could cause these adverse effects, dark spot formation, J-V and L-V characteristics, and device stability of OLED devices.

Experimental Procedure

Figure 4.3 presents the procedure for this experiment. In this experiment, PI sheets are first applied for an extended period of time (50 hours), in a dry N₂ atmosphere, on ITO glass substrates on which NPB(60 nm)/Alq₃(40 nm) bilayer organic stacks were coated. Such long contact times are used to ensure that any adverse effects on the organic layers from physical contact with PI sheets become significant and that they will well surpass what may occur from the much shorter contact times during device fabrication procedure. The PI sheets are then removed, and lithium fluoride (LiF)/Al cathode layers are deposited. For comparison, other devices which were fabricated through the same procedure, including storing for 50 hours in N₂ before depositing the cathodes, without being in contact with PI sheets in this case, are tested to be used as control devices.

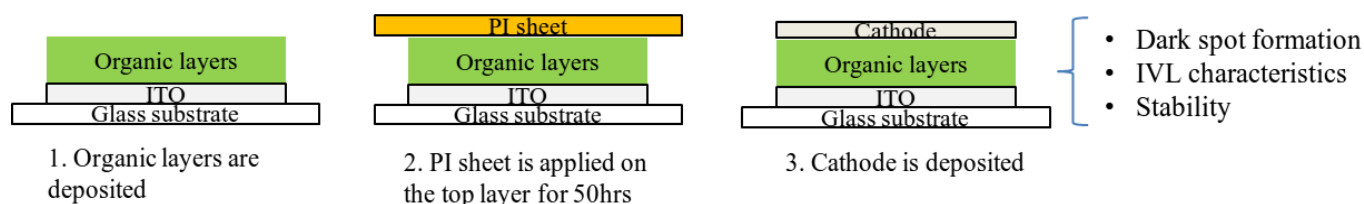


Figure 4.3 Procedure for the experiment on effects of contact of an organic layer with PI.

Results and Discussion

Figure 4.4 presents typical J-V and L-V characteristics and EL stability trends (at a constant current density of 20 mA/cm²) for devices in which the organic layers were put in physical contact with the PI film for 50 hours (denoted by “PI” in the figure labels) and the control devices (denoted by “Control”). Clearly, the contact with PI has no detectable adverse effect on device efficiency or EL stability over a period of 100 hours. Similarly, a comparative analysis of the dark spot growth behavior in the non-encapsulated devices after 50 hours shows no significant differences between the two devices, as can be seen from the EL images (Fig. 4.5) and the corresponding image analysis statistical data (Table

4.1). These results confirm that the contact of the organic materials with PI sheets does not compromise OLED performance.

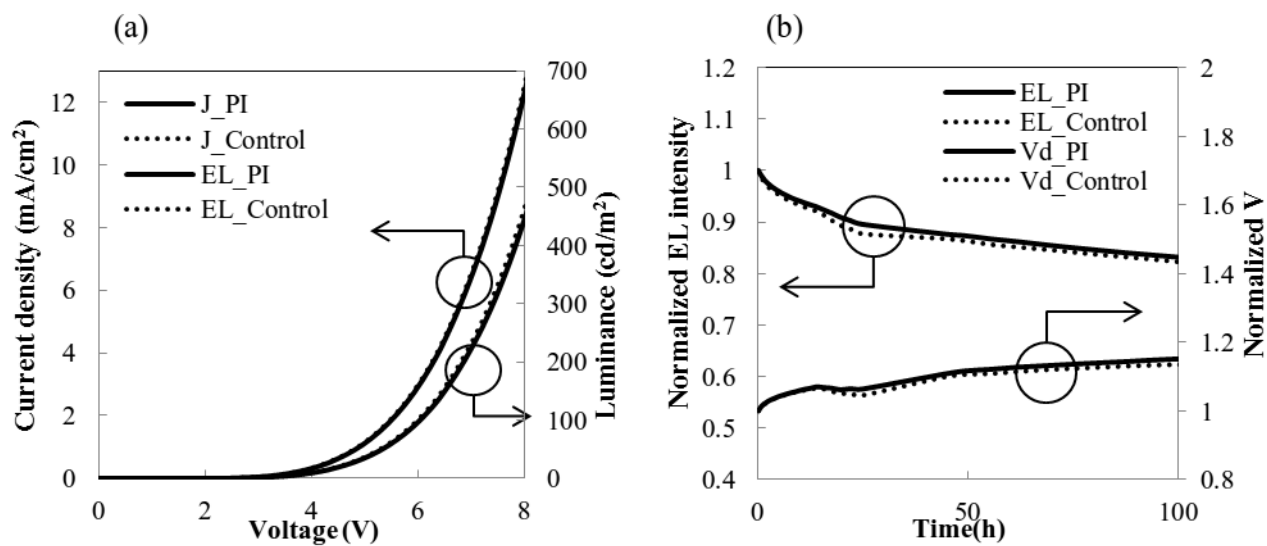


Figure 4.4 (a) J-V and L-V characteristics and (b) normalized EL intensity and driving voltage under constant current density of 20 mA/cm² for devices in which the organic layers are put in contact with PI sheets for 50 hours and control devices.

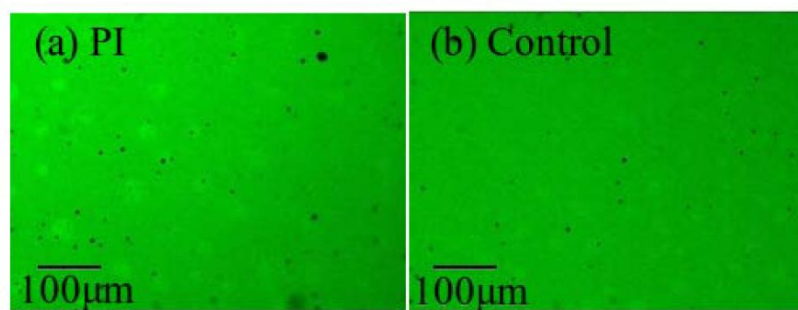


Figure 4.5. EL images of (a) unencapsulated devices in which the organic layers are put in contact with PI sheets for 50 hours and (b) control devices which are kept in a dry nitrogen condition.

	Contact with PI	Control
% of dark area (%)	1.2%	0.97%
Dark spot diameter(μm)	$\sim 5 \mu\text{m}$	$\sim 6 \mu\text{m}$

Table 4.1 Percentage of dark spot area of the total emitting area and average dark spot diameter of the devices in which the organic layers are put in contact with PI sheets for 50 hours and control devices.

4.1.3 Demonstrating RGB OLEDs with small feature sizes ($<25 \mu\text{m}$) fabricated side-by-side on one substrate

Introduction

To further verify the feasibility and potential to achieve high resolution pixel patterning, RGB OLEDs with small feature sizes ($<25 \mu\text{m}$) are fabricated side-by-side on one substrate through this technique. In this demonstration, a PI sheet is first stretched and held on a metal frame, and then patterned by laser ablation. While post-patterning deformation can occur in FMMs due to this stretching step, it does not happen in this technique since the PI sheet is patterned after being held by a metal holder. Considering the limited shadow effects and high dimensional uniformity of the laser-patterned PI sheet, higher accuracy can be expected in color patterning by this method.

Experimental Procedure

In this experiment, a $7.5 \mu\text{m}$ thick PI sheet is first stretched and mounted on a metal frame, and then patterned by laser ablation to create $25 \mu\text{m}$ wide slits in a regular pattern with a pitch of $75 \mu\text{m}$ using 266 nm Nd:YAG laser at an energy density of 1 J/cm^2 as illustrated in Figure 4.6 (i) and (ii) respectively. The patterned film is then used as a shadow mask for depositing red and green OLEDs in sequence on an ITO-coated glass substrate via thermal evaporation in vacuum following the steps illustrated in Figures 4.6 (iii) through (iv). The OLEDs employ molybdenum trioxide (MoO_3) as a hole injection layer (HIL), NPB as a HTL, DCJTB as a red dopant, C545T as a green dopant, 2-tert-butyl-9,10-di(naphth-2-yl)anthracene (TBADN) as a blue EML and host, and Alq_3 as an ETL.

The patterned PI shadow mask is placed directly on the substrate (on which the HIL (~3nm) and HTL (~60 nm) were already pre-deposited). A 5 nm red EML of TBADN doped with 2% DCJTB is then deposited on the pre-deposited layers through the mask. The mask is shifted by 25 μm from the initial position, and a 5 nm green EML of TBADN doped with 2% C545T is deposited. The shadow mask is removed, and a 20 nm blue EML of TBADN is applied, followed by the deposition of a 20 nm Alq₃ and LiF/Al to serve as a common ETL and electron injection layer(EIL)/cathode, respectively.

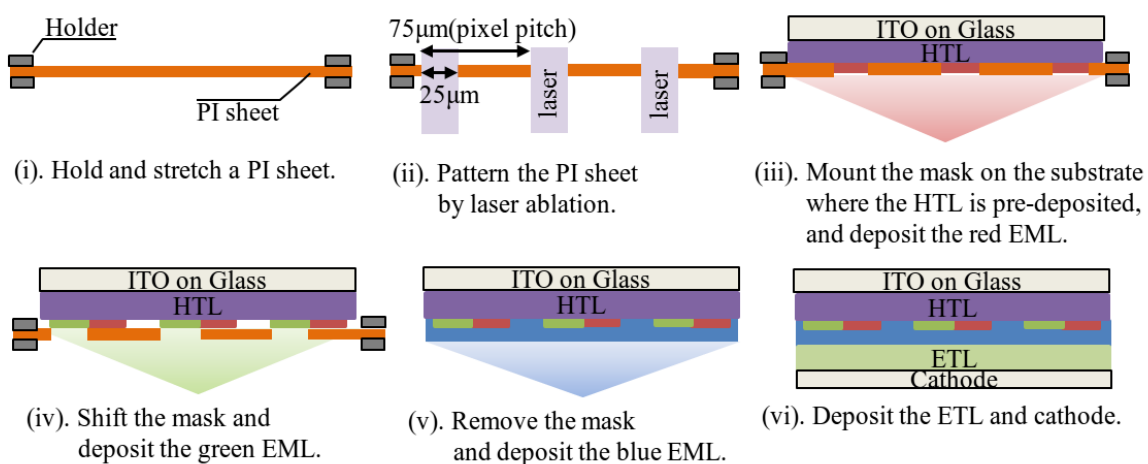


Figure 4.6. Procedure for RGB OLED fabrication using a pre-patterned PI sheet.

Results and discussion

Figure 4.7 shows microscopic EL images of the fabricated devices. As can be seen, red and green 25 μm wide lines with high positional accuracy on a blue background are formed producing a uniform pattern with a 75 μm pitch. As expected, high dimensional uniformity and remarkably straight edges of the patterned lines are achieved, indicating that the laser patterned PI sheet functions as a shadow mask without any significant deformation or edge shadow effects. In addition, as shown in the previous experiment, the high EL uniformity and negligible visible defects from the red lines (the EMLs of which were in physical contact with the PI mask during step (iv) of Figure 4.6), indicate that contact

with the PI sheet does not cause significant damage or degradation in device performance, even when the organic layers are very thin (a ~5 nm EML in this case).

These results demonstrate the strong potential of this technique to fabricate OLEDs with small feature sizes and high dimensional and positional accuracy on substrates. For example, the demonstrated pixel pitch of 75 μm corresponds to a display resolution of over 330 ppi, which indicates that the technique is indeed capable of realizing the fabrication of high resolution OLED displays through simple vacuum deposition processes. It should be also noted that the demonstrated pitch of 75 μm is by no means a limit, and that achieving even smaller pitches should be readily possible given the high positional accuracies and by the fact that making much narrower slits in PI films can be readily achieved via laser ablation^{[14][15]}. In addition, because of the thin PI masks and the ability to place them directly on the substrates without causing damage due to contact, this technique is capable of minimizing edge shadow effects (discussed in more detail below) and thus also the need for large inter-pixel distances, allowing almost 100% aperture ratios.

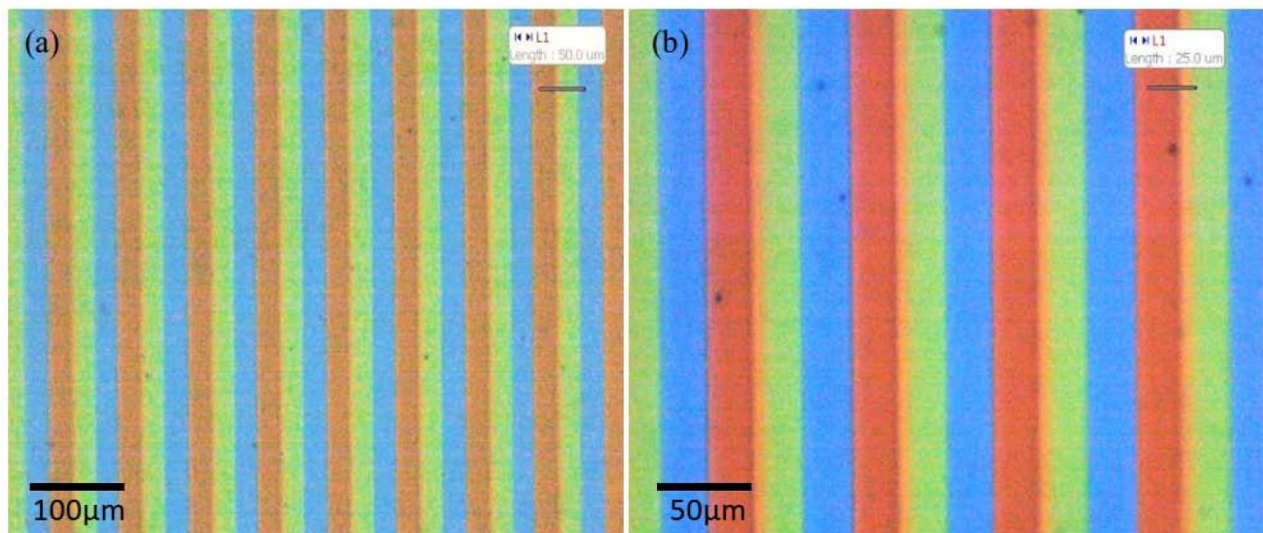


Figure 4.7. EL images of OLEDs fabricated by the procedure in Fig.4.6.

4.1.4 Conclusions

As a part of the feasibility study for the laser-patterned PI mask technique, capability of the plastic film mask as a shadow mask and the effect of contact of organic layers with a PI sheet on device performance have been investigated. The conclusions of this study are summarized as follows:

- ❑ The laser-patterned PI sheets have the strong capability to deposit OLED materials with high line edge uniformity and limited shadow effects without compromising device performance
- ❑ The contact of the organic materials with PI sheets does not compromise OLED performance
- ❑ This technique has the potential to realize OLED displays with high resolution (>330 ppi) and higher aperture ratios (~100%) relative to the current FMM technology

4.2 *In-situ* Shadow Mask Patterning Technique

As a derivative of the patterning technique using laser-patterned PI shadow masks, the *in-situ* shadow mask patterning method is proposed for higher resolution and precise pixel patterning on flexible substrates. Since the slits are created by laser over the desired TFT locations directly in this technique, mechanical alignment of masks can be eliminated, thus higher patterning accuracy can be achieved. This approach can be particularly useful for RGB OLED patterning on flexible substrates where the poor mechanical and dimensional stability of substrates pose additional challenges for aligning shadow masks accurately.

The first two experiments focus on the effect of the laser patterning process on device performance since the *in-situ* laser process on a substrate could cause adverse effects on an electrode. In the first experiment, an OLED device is fabricated on an aluminum electrode where the PI sheet is patterned by laser ablation to investigate the effect of the patterning process on the aluminum electrode. The result of this experiment reveals that the patterning process causes significant contamination to the electrode because of residual contaminants of ablated films. To protect the electrode during laser ablation, a protective layer of PI is introduced beneath the top PI sheet, which will be patterned as a shadow mask

in the second experiment. Using the sacrificial protective layer of another PI sheet, a working OLED device with 16 μm by 130 μm sub-pixel size and with reasonable J-V characteristics has been successfully fabricated by the *in-situ* shadow mask patterning technique. Having verified that the *in-situ* shadow mask patterning step does not have adverse effects on the performance of OLEDs, RGB OLEDs with small feature sizes are fabricated using the *in-situ* shadow mask patterning technique.

4.2.1 Device Performance : Investigating the effect of laser patterning of PI sheets *in-situ* on an electrode

Introduction

Since the PI sheet is patterned by laser ablation *in-situ* on an electrode using the *in-situ* shadow mask patterning technique, there is the possibility that the surface of the electrode can be affected by the laser ablation process. To be specific, the electrodes can be contaminated by the residue of the PI sheet produced in the laser ablation process and/or the electrode surface can be oxidized due to laser exposure, which results in hindering carrier injection. This study, therefore, is conducted to investigate the effect of patterning of PI *in-situ* on substrate on an electrode, and to evaluate the performance of the device.

Experimental Procedure

To investigate the effect of the mask patterning process by laser ablation on the bottom electrode, an OLED device is fabricated on an aluminum electrode where a 12.5 μm thick PI sheet is patterned by laser ablation (Fig. 4.8). In this experiment, the PI sheet mounted on a 300 nm thick aluminum electrode is ablated by means of a 266 nm Nd:YAG laser with a beam size of 25 μm by 150 μm to create an opening on the PI sheet. The ablation process is done in two steps with different laser energy densities to reduce damage to the electrode. The PI sheet is first partially etched using a 0.4 J/cm^2 laser power density, and then the laser intensity is reduced to 0.2 J/cm^2 for the last stage of the ablation process. After the patterning process, the PI sheet is removed, and an OLED device with a transparent cathode is fabricated on the electrode. The device structure used is as follows: Al (300nm)/MoO₃/NPB (60nm)/Alq₃ (40nm)/ 4,7-Diphenyl-1,10-phenanthroline (Bphen) : Cesium carbonate (Cs₂CO₃) (10%,

10nm)/MoO₃ (5nm)/Ag (14nm)/MoO₃ (40nm). The EL of the fabricated device is then observed by optical microscopy.

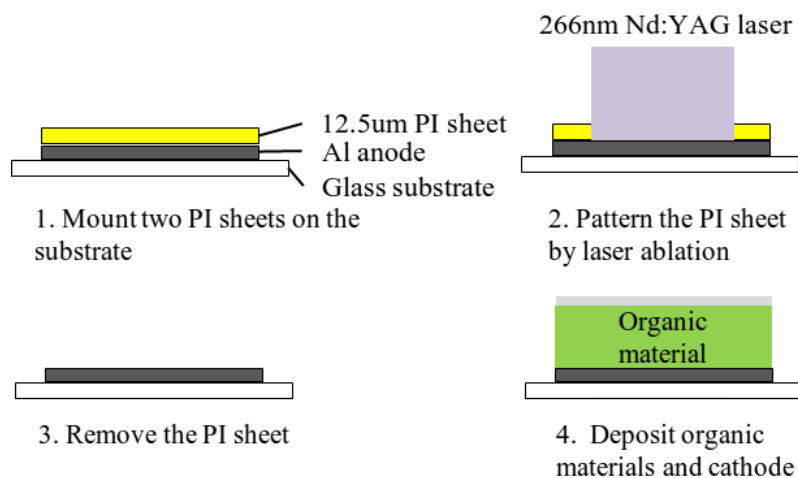


Figure 4.8 Schematic presentation for OLED device fabrication on the electrode where the PI sheet is patterned by laser ablation.

Results and discussion

As can be seen in Figure 4.9 (b), there is a widespread non-emissive section around the laser exposed area in the EL of the device which is fabricated on the electrode where the PI sheet is patterned. This is caused by either decreased electrical contact or decreased carrier injection because of the ablated film left on the electrode. In fact, significant contamination is observed around the laser exposed area on the electrode as shown in the microscopic image of the electrode (Fig. 4.9 (a)). In contrast, it seems that the middle laser exposed area is less affected, as the contaminants from the PI sheet initially left on the electrode are removed by further laser exposure, making the middle area cleaner. From this result, it can be said that although it might be possible to pattern a single sub-pixel with less than 25 μm feature sizes by this technique, it is difficult to achieve three color pixel patterning. The patterning process would significantly affect neighbor sub-pixels because of widespread contaminants from the PI sheet.

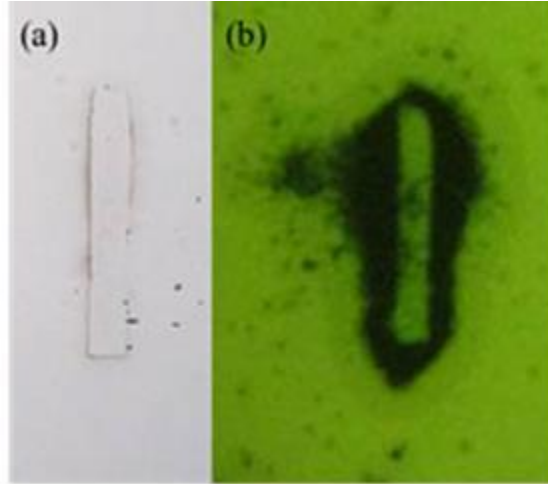


Figure 4.9 The electrode where the PI sheet is patterned (a) and EL of the fabricated device (b).

4.2.2 Device Performance (II): Investigating the effect of laser patterning of a PI sheet *in-situ* on an electrode with a protective layer

Introduction

It has been shown that the laser ablation process causes significant detrimental effects on an electrode. Therefore, a protective layer of a second PI sheet is introduced beneath the top PI sheet, which will be patterned as a shadow mask, protecting the electrode during laser ablation.

Experimental Procedure

In this experiment, a protective layer of another PI sheet is introduced to prevent the electrode from being contaminated with the ablated film during the laser ablation process. To demonstrate the technical feasibility of this modified approach, the standard Alq₃ bilayer OLED device is fabricated on a 16 μm by 130 μm sub-pixel size electrode by the *in-situ* shadow mask patterning technique using the protective layer. The sub-pixel size electrode is the ITO coated glass substrate where silicon nitride (SiN_x) thin film is patterned on the ITO like the actual sub-pixel of the TFT substrate as shown in Figure 4.10. This sub-pixel size electrode is introduced in this experiment for two purposes: to investigate the effect of use of the *in-situ* shadow mask patterning on electrical property or J-V

characteristics of devices, and to investigate how accurately material can be deposited on a desired location. For the sub-pixel size electrode preparation, a 100 nm thick SiN_x thin layer is first deposited on the ITO coated glass substrate via PECVD using silane and ammonium gases. The deposited SiN_x layer is then patterned by using the standard photolithographic technique: photoresist (AZ3312) spin coating at 3000 rpm for 60 seconds and prebaking on a hot plate at 90 °C for 60 seconds, UV exposure through a photo mask for 5 seconds and post-baking at 120 °C for 60 seconds, developed (AZ300MIF) for 30 seconds, wet etching using buffered hydrogen fluoride (BHF) for 10 seconds, and photoresist stripping using acetone.

Figure 4.11 depicts the procedure of the sub-pixel size OLED fabrication using the *in-situ* shadow mask patterning technique. A two sheet stack of 7.5 μm PI sheets are mounted on the sub-pixel size electrode, and only the top PI sheet will be etched by 266 nm Nd:YAG laser at 1 mJ/cm² to create the desired aperture. The beam size of the laser is 25 μm by 150 μm, and the laser head is aligned over the sub-pixel size electrode by the positioning stage. After etching of the top sheet, the lower PI sheet, which acts only as a protective (or “sacrificial”) layer for protecting electrode during the laser ablation step, is removed by being physically pulled out, and the top patterned PI sheet is brought in contact.

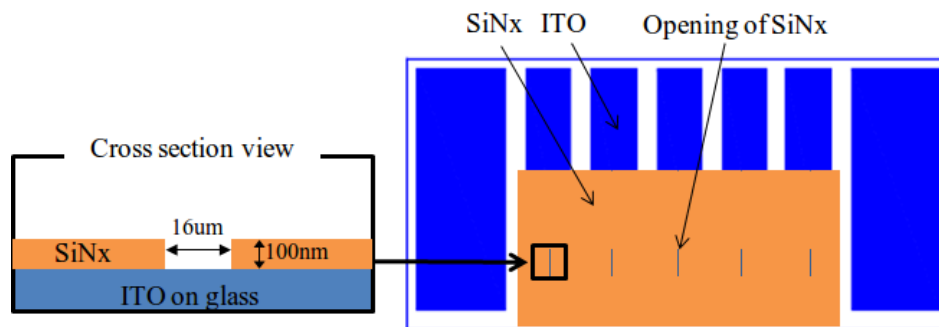


Figure 4.10 Schematic presentation for the ITO coated glass substrate where the SiN_x layer is patterned.

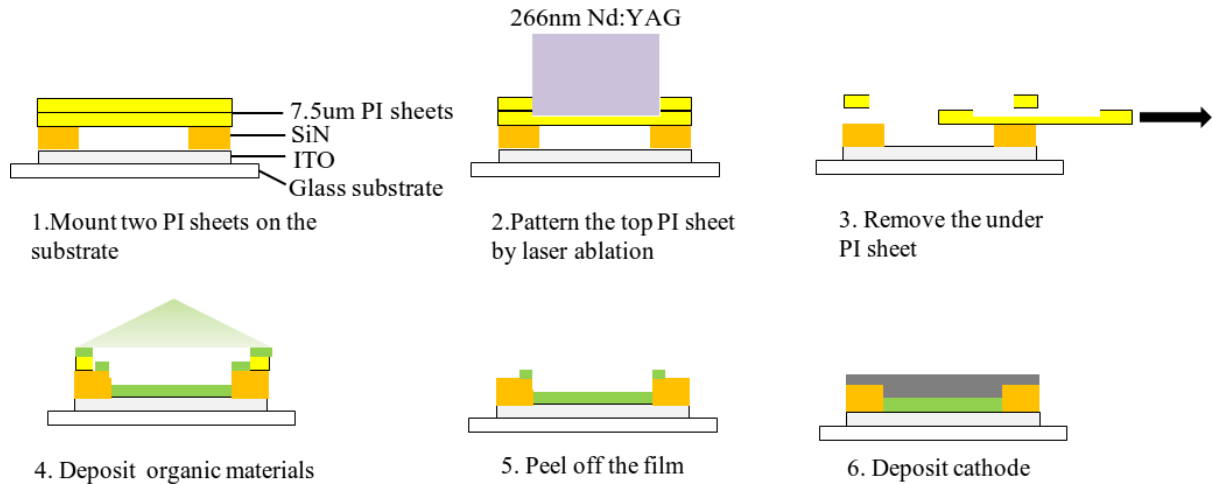


Figure 4.11 Schematic presentation for the patterning of the sub-pixel size OLED device using the *in-situ* shadow mask patterning technique.

Results and discussion

While the electrode is significantly contaminated due to the patterning process in the previous experiment, the patterning of the PI sheet in this experiment is successfully achieved without any contamination of the electrode because of the introduction of the protective layer (Fig. 4.12(b)). The result of this experiment also shows the accuracy of patterning achieved by this technique. As can be seen in Figure 4.12(a), the aperture of the PI film shadow mask is precisely created over the sub-pixel, and OLED materials are deposited with the width of $\sim 25 \mu\text{m}$ on the $16 \mu\text{m}$ wide sub-pixel. In addition, the patterning technique does not compromise device performance as indicated by the uniform EL and the reasonable J-V characteristics, which is on par with that of the device fabricated on the same sub-pixel structure without shadow masks (Fig. 4.12(c)) (Fig. 4.13). Thus, these results show that the *in-situ* shadow mask patterning technique has a great potential to achieve high resolution patterning of OLEDs without compromising device performance.

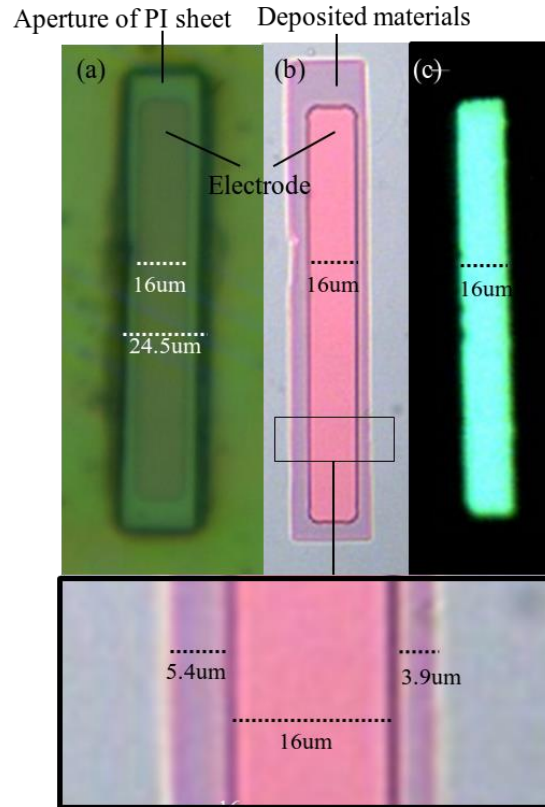


Figure 4.12 Microscopic images of (a) patterned PI sheet over the sub-pixel, (b) deposited materials on the electrode, and (c) EL of the patterned device.

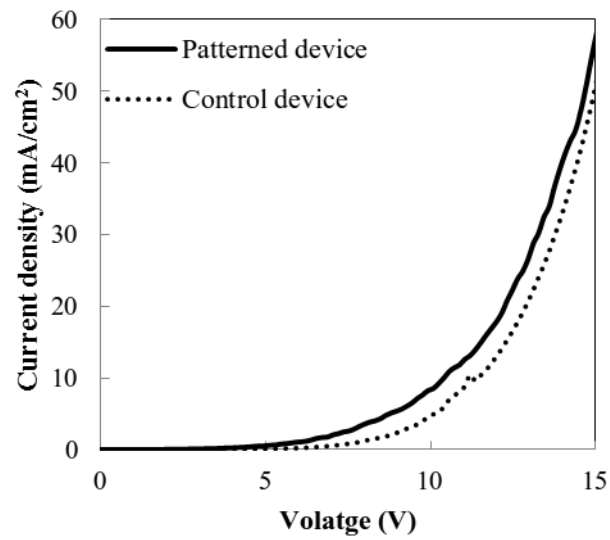


Figure 4.13 J-V characteristics of the fabricated device.

4.2.3 Demonstrating RGB OLEDs with very small feature sizes (<25 μm) fabricated side-by-side on one substrate

Introduction

Having verified that the *in-situ* shadow mask patterning step does not have any adverse effects on performance of OLEDs, RGB OLEDs with small feature sizes are fabricated by using the *in-situ* shadow mask patterning technique as previously demonstrated in RGB OLED fabrication by using the PI shadow masks patterned using laser ablation *ex-situ*.

Experimental Procedure

As the *in-situ* shadow mask patterning technique does not compromise device performance, demonstration of RGB OLEDs fabrication using this technique has been conducted as depicted in Figure 4.14. In this procedure, 25 μm wide green EML lines of TBADN doped with 2% C545T are first deposited on glass substrates pre-coated with ITO, HIL and HTL, again using a pre-patterned PI shadow mask to produce a pattern with 75 μm pitch. A two sheet stack of 7.5 μm PI sheets is placed on the substrate. The top PI sheet is then laser-exposed to create 25 μm wide slits while the bottom PI sheet of the stack serves as a shield to protect the underlying organic layers and the substrate from contamination by the debris from the ablation process. The bottom sheet is removed after the laser ablation step is completed, allowing the now patterned PI sheet to be brought in direct physical contact with the substrate (step (iii) in Fig. 4.14). A red EML of TBADN doped with 2% DCJTb is then deposited through the patterned PI sheet. Finally, the PI sheet shadow mask is removed, and the blue EML, ETL, and cathode layers are deposited.

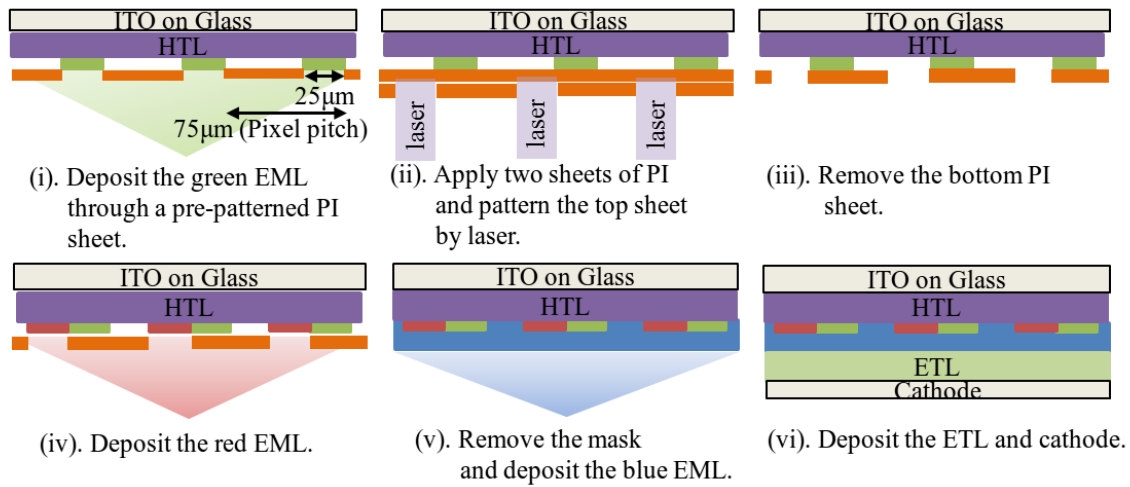


Figure 4.14 Procedure for RGB OLED fabrication using a PI sheet patterned *in-situ* on the substrate.

Results and discussion

Figure 4.15 presents a microscopic EL image of the OLEDs produced by this technique. As can be seen, 25 μm wide red and green emitting lines with good EL uniformity are obtained, and the red emitting lines are positioned accurately next to the green lines, which again demonstrate the ability of this technique to achieve RGB patterning at the level of accuracy required for high resolution displays (i.e. 330 ppi). Furthermore, the laser ablation step for creating the slits in the PI sheet is in this case carried out *in-situ* while the sheet is already mounted on the substrate (and more precisely on the HTL of the red emitting lines, as shown in Figure 4.14 (ii)). Nevertheless, EL from the red emitting lines is clearly uniform. This uniform emission verifies that the *in-situ* laser patterning process does not adversely affect the organic layers or device performance. Here too, EL from the green lines is also clearly uniform, which again shows that placing the PI film on the substrate in direct physical contact with the underlying organic layers does not result in any significant damage to them.

A close examination however reveals that some dark spots appear on the devices. This is perhaps due to ablation debris from some limited unintentional ablation of the bottom protective PI sheet which is left on the back side of the top sheet after the lower sheet is removed. This contamination issue could

be avoided by replacing the bottom protective PI sheet with any other thin sheet which is resistant to laser ablation, such as a thin glass sheet.

As demonstrated in this experiment, the *in-situ* shadow mask patterning technique enables us to pattern OLEDs precisely without compromising device performance. The slits can be created anywhere in the top PI sheet by laser ablation to correspond to locations of certain features on the underlying TFT substrate. This technique has a strong potential to achieve high resolution OLED displays even on flexible substrates.

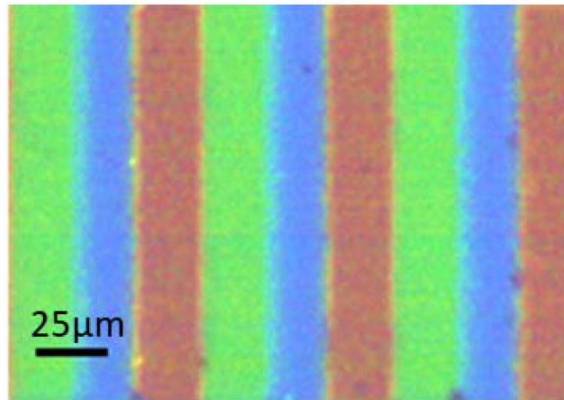


Figure 4.15 EL images of OLEDs fabricated by the procedure in Fig.4.14.

4.2.4 Conclusions

The effect of patterning of PI *in-situ* on an electrode by laser ablation on device performance has been investigated in this chapter. The conclusions of this study are summarized as follows:

- ❑ The mask patterning process by laser ablation *in-situ* on the substrate causes significant contamination of the electrode

- ❑ The contamination can be avoided by introducing the sacrificial protective layer of another PI sheet to protect the electrode during laser ablation, allowing to pattern shadow masks *in-situ* on the substrate without compromising device performance
- ❑ This technique has a strong potential to achieve high performance OLED displays with high resolution (>330 ppi) and high fill factor (~100%) even on flexible substrates

Chapter 5

Technique 2: Color Patterning via Diffusion of a Luminescent Material

This chapter describes a series of investigations to assess technical feasibility and potential of the color patterning technique via diffusion of a luminescent material for full color small molecule OLED displays. The chapter consists of six sections. The first three sections show the main results of this study. Section 5.1 assesses the effectiveness of physical contact between a donor and an acceptor substrate in bringing about sufficiently high doping levels via diffusion. Section 5.2 examines electroluminescence characteristics of devices fabricated using this technique. Section 5.3 demonstrates RGB color patterning by selective diffusion of a luminescent material. Possible issues and solutions are then discussed in the following two sections. Section 5.4 assesses the potential of solvent vapor exposure as a method to accelerate solid state diffusion. Section 5.5 assesses the potential of a semiconducting diffusion barrier as a method to block undesirable diffusion. Finally, Section 5.6 provides a brief theoretical analysis of the concentration profile achieved by the doping method via diffusion.

Material in this chapter has been published before: more specifically, material in Sections 5.1, 5.2, 5.3 and 5.4 was published in [Y. Kajiyama, K. Kajiyama, and H. Aziz, "Maskless RGB color patterning of vacuum-deposited small molecule OLED displays by diffusion of luminescent dopant molecules," *Opt. Express*, 23, 16650-16661 (2015)]. Material in Sections 5.5 was published in [Y. Kajiyama, K. Kajiyama, and H. Aziz, " Diffusion Barriers for Achieving Controlled Concentrations of Luminescent Dopants via Diffusion for Mask-less RGB Color Patterning of Organic Light Emitting Devices," *Opt. Express*, 23, 30783-30792 (2015)]. Publisher's permission to reproduce this material in this thesis has been obtained.

5.1 Assessing the effectiveness of physical contact between a donor and acceptor substrate to achieve sufficiently high doping levels via diffusion

Introduction

The maskless color patterning technique via diffusion of a luminescent material has great potential to be a more reliable alternative to the FMM technique. Nevertheless, this color patterning approach has to date been limited to polymer OLEDs^{[28][29][30][31][64]}. Its utilization for RGB color patterning of small molecule OLEDs, due to their superior electroluminescence performance are currently the mainstream technology for OLED displays, has not been reported. This is perhaps because of several perceived difficulties in extending the approach to small molecule OLEDs. For example, relative to polymers, vacuum-deposited organic small molecule materials form denser thin films, so they can be expected to be less amenable to significant doping by diffusion through a solid state contact. In addition, small molecule materials have lower mechanical yield strength, which makes them more susceptible to damage by physical contact with the donor substrate.

There are some reports on molecular diffusion in small molecule OLEDs. For example, improvement in device performance of bilayer small molecule OLEDs due to thermal annealing around or below the material's T_g has been reported^[65]. The improvement of device performance can be attributed to the mixing of the materials due to molecular diffusion, which results in elimination of heterointerface. Further direct evidence of molecular diffusion has been shown by molecular depth profiling of an annealed NPB/Alq₃ bilayer OLED device using secondary ion mass spectrometry with large argon cluster ion beams^[66].

However, although these results indicate significant molecular diffusion could occur in organic layers, in the proposed diffusion-based techniques, luminescent material molecules need to be diffused into a host layer via physical contact between these two layers. Diffusion via physical contact could be more challenging because of non-uniform contact and less inter-molecule interaction between two layers. Therefore, the present study is performed to investigate whether diffusion of luminescent

material molecules from a donor to an acceptor film on separate substrate placed in physical contact can bring about the doping levels required for achieving the desired color spectra.

Experimental Procedure

The purpose of this study is to confirm physical contact between a luminescent material coated on one substrate and an OLED host material coated on another substrate can allow for doping of the latter by the former to sufficient levels through solid state diffusion. Three variables including contact time, temperature, and material are considered in this investigation. First, dependency on contact time is studied, followed by similar investigations taking temperature and material as variables.

In this test, the amount of luminescent material molecules introduced to the host film by diffusion is estimated by measuring changes in the optical absorbance of the host film after the contact. Figure 5.1 depicts detailed experimental steps. In this experiment, NPB and DCJTb are used as the host and the luminescent dopant, respectively. These materials are vacuum-deposited on different substrates. 20 nm of NPB is deposited on a quartz substrate, which is referred as an “acceptor” substrate, and 20 nm of DCJTb is deposited on a glass substrate, which is referred as a “donor” substrate. After depositing the materials on their respective substrates, the two substrates are placed in physical contact by holding them together using a 5 mm thick neodymium magnet plate (remanent magnetization of 1.22-1.28 T) and a 2 mm thick steel plate. They are then heated on a hot plate at 100 °C for a certain period of time (30, 60, 90, or 105 minutes) in a dry nitrogen environment, to allow for the diffusion of DCJTb molecules into the NPB film to occur. In each case, one half of the NPB film surface is left without contact with the donor substrate, to be used as reference (this half corresponds to the right part of the substrate depicted in diagrams (ii) and (iii) of Figure 5.1). The donor substrate is then removed, and UV-Vis absorption spectra of the acceptor film are measured.

In addition, similar experiments are performed to investigate dependency on temperatures and materials. In the experiments, while the contact time is fixed at 60 minutes, variable temperatures of 60, 80, 100 and 120 °C and variable host materials of 4,4'-N,N'-dicarbazolebiphenyl (CBP), NPB, TBADN

and Alq₃ are used. The host materials are chosen based on T_g of these materials: CBP ($T_g=60^\circ\text{C}$), NPB ($T_g=99^\circ\text{C}$), TBADN ($T_g=126^\circ\text{C}$), and Alq₃ ($T_g=175^\circ\text{C}$).

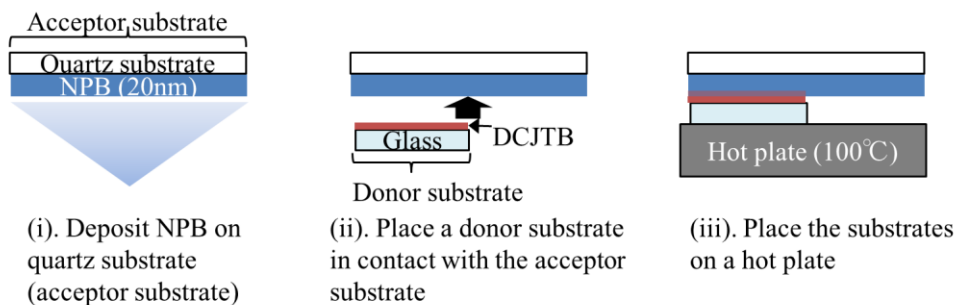


Figure 5.1. A schematic diagram illustrating the steps of the procedure followed for introducing luminescent dopant from a donor substrate to an acceptor substrate.

Results and discussion

Figure 5.2 presents the absorption spectra collected from the acceptor films contacted with the donor substrates for the various periods of contact time. Spectra from the “non-contacted” NPB areas are also included in the figures in each case for comparison. As can be seen, the host films contacted with the donor substrate show higher absorbance in the 450-550 nm range relative to the non-contacted reference films. This increase in absorbance becomes increasingly more significant with longer contact time. As this wavelength range corresponds to an absorption band of DCJTb (with a peak at ~ 510 nm), the increased absorbance clearly points to the presence of DCJTb molecules in the NPB as a result of diffusion from the donor film which, not surprisingly, is more significant with longer contact time. Figure 5.3(a) presents traces that correspond to the mathematical differences between the spectra from the contacted area versus those from the non-contacted areas, verifying that the spectral differences due to the contact indeed correspond to a band with a peak around 510 nm, consistent with DCJTb absorption.

The height of this peak increases linearly with contact time (Fig. 5.3(b)). Since the absorbance is proportional to the number of DCJTb molecules in the film, the linear correlation indicates that the diffusion of DCJTb molecules from the donor substrate to NPB film occurs throughout the contact time

and proceeds at a constant rate in the time frame of our measurements (i.e. during at least the first 105 minutes of contact). Such constant mass transfer rate is not unreasonable considering that the diffusion rate and the change in concentration remain relatively limited. The fact that the amount of DCJTB in the acceptor film increases with contact time verifies that the transfer of molecules from the donor film does not occur in a single mass transfer step that occurs upon contact (e.g. as in the case of contact printing or LITI) but rather the result of continuous molecular diffusion that continues with time. In Figure 5.3 (b), the absorbance at 510 nm of 5 nm NPB films doped with various DCJTB concentrations (from 2-16% by volume) made by co-deposition for comparison is also included (after subtracting absorption from NPB and substrate background). As shown in the figure, the DCJTB absorbance in the films contacted with the donor substrate is equivalent to that of a co-deposited film with a 2-10% DCJTB concentration, indicating that the number of molecules in the two cases is comparable.

Since the typical DCJTB concentration in OLEDs made by co-deposition is 1-2%^[67], it follows from these results that the diffusion process can produce sufficient doping levels. It is worth noting that no significant morphological changes (based on optical microscopy examination) or changes in the optical absorption spectra are observed in the heated NPB films despite heating to a temperature close to the NPB glass transition temperature. This may be attributed to NPB resistance to crystallization even at 100°C^[68]. It is also possible that the substrate temperature remains slightly lower than the hot plate temperature due to heat losses through the magnet and the metal plate.

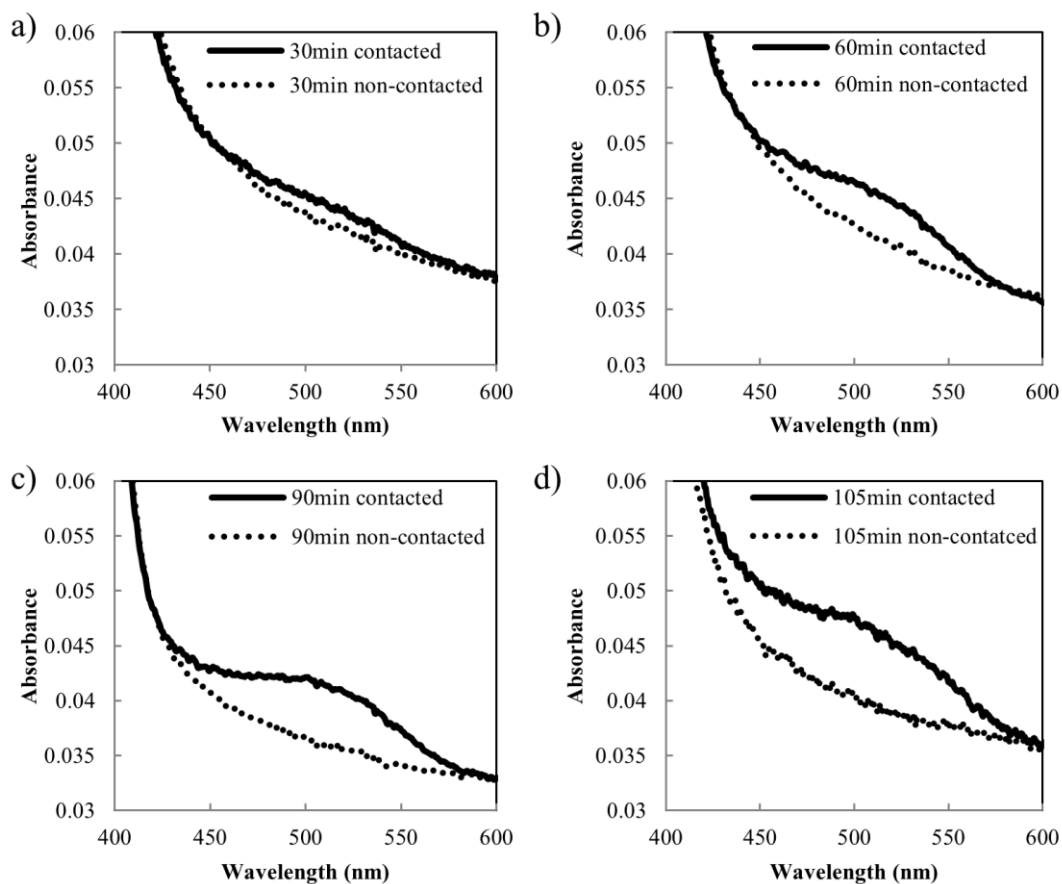


Figure 5.2. UV-Vis absorption spectra of the acceptor host films after contact with the donor substrate for 30min (a), 60min (b), 90min (c) and 105min (d). The dotted traces represent spectra collected from the non-contacted areas for reference.

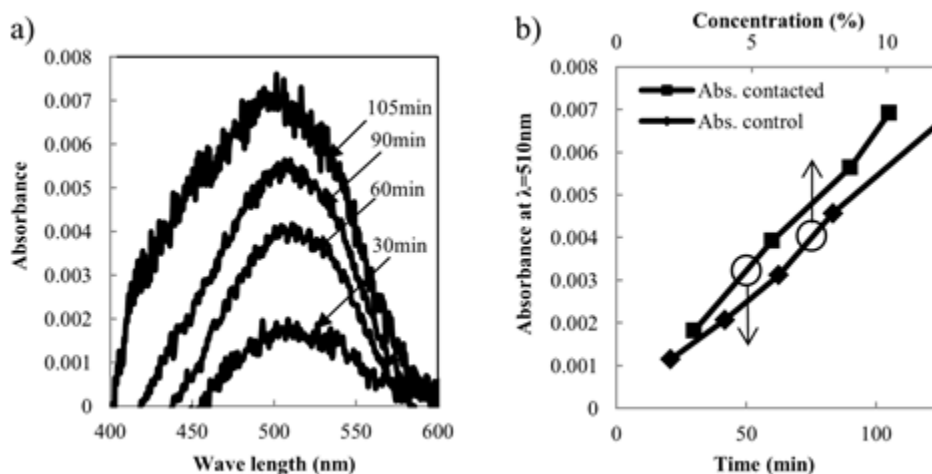
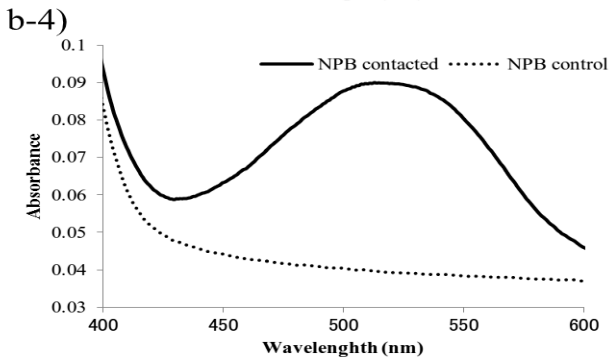
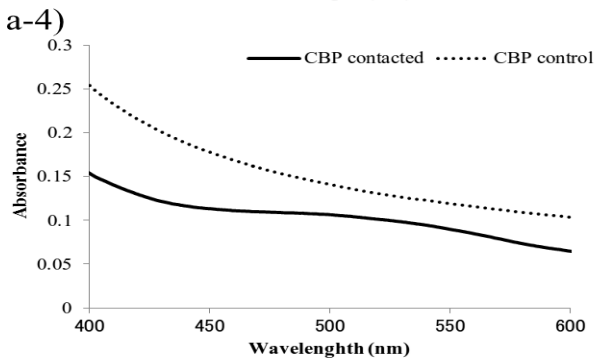
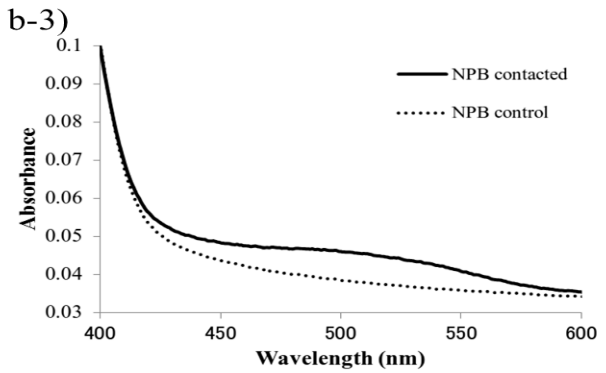
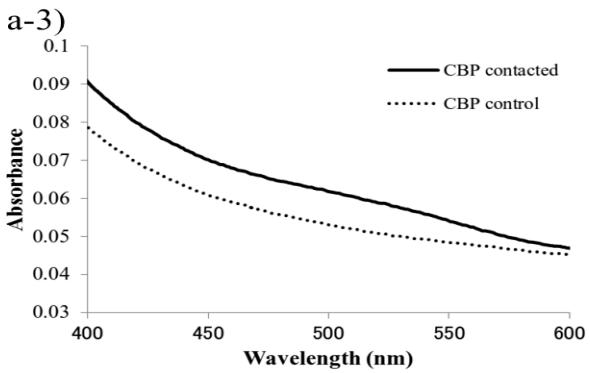
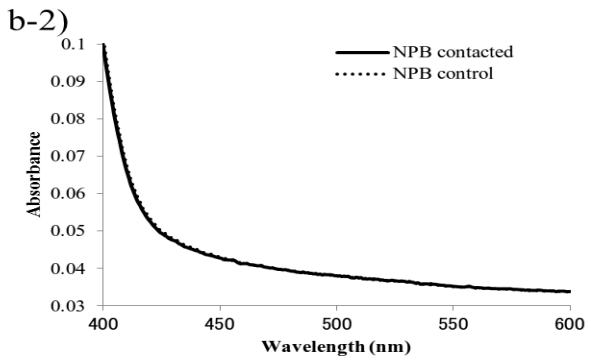
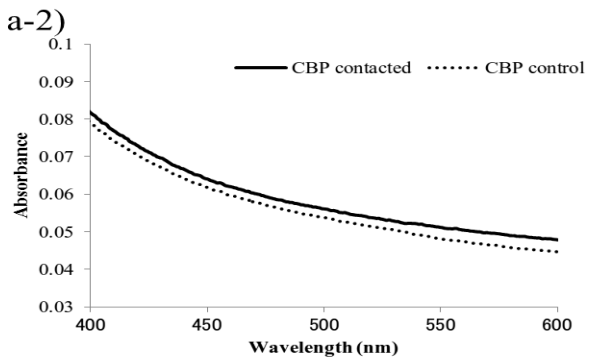
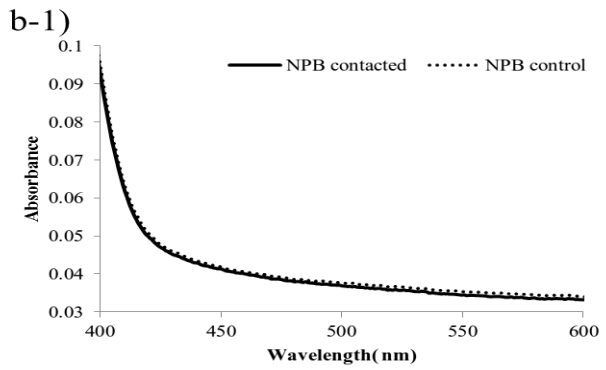
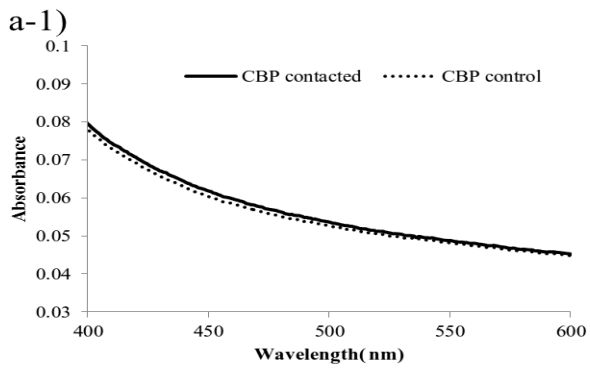


Figure 5.3 (a) UV-Vis absorption spectra of the acceptor host films after contact with the donor substrate for the various times after subtracting the background absorption by NPB and the substrate. (b) The corresponding absorbance at 510 nm vs contact time (bottom axis). The absorbance of 5 nm NPB films doped with various DCJTb concentrations at the same wavelength after subtracting absorption from NPB and substrate background are shown for comparison (top axis).

The absorption spectra collected from the acceptor films contacted with the donor substrates for the various temperatures and materials at the fixed contact time of 60 minutes are presented in Figure 5.4 with those of control films. The absorbance of the acceptor films after subtracting that of the corresponding control films at the DCJTB peak absorption peak wavelength of 510 nm is summarized in Figure 5.5. As can be seen, the absorbance significantly increases from 100°C regardless of materials. Considering that this temperature is fairly close to T_g of the dopant material (DCJTB), this result indicates that the doping level is dominantly dependent on T_g of the dopant. Not surprisingly, doping level also depends on T_g of the acceptor materials: doping level is higher with lower T_g of the acceptor material at the same temperature. For example, the absorbance at 120°C of NPB($T_g=99^\circ\text{C}$), TBADN($T_g=126^\circ\text{C}$), and Alq₃($T_g=175^\circ\text{C}$) is ~0.05, 0.035 and 0.02, respectively. This experimental result indicates that proper combinations of dopant and host materials for this technique can be chosen based on T_g of these materials. Finally, it should be noted that the absorbance of the CBP film contacted with the donor substrate is lower than that of the control film at 120°C, unlike what is seen for other materials. This is because significant crystallization occurs in the neat CBP film, while it is less significant in the CBP film contacted with the donor substrate. Here, the presence of dopant molecules prevents the film from crystallization.



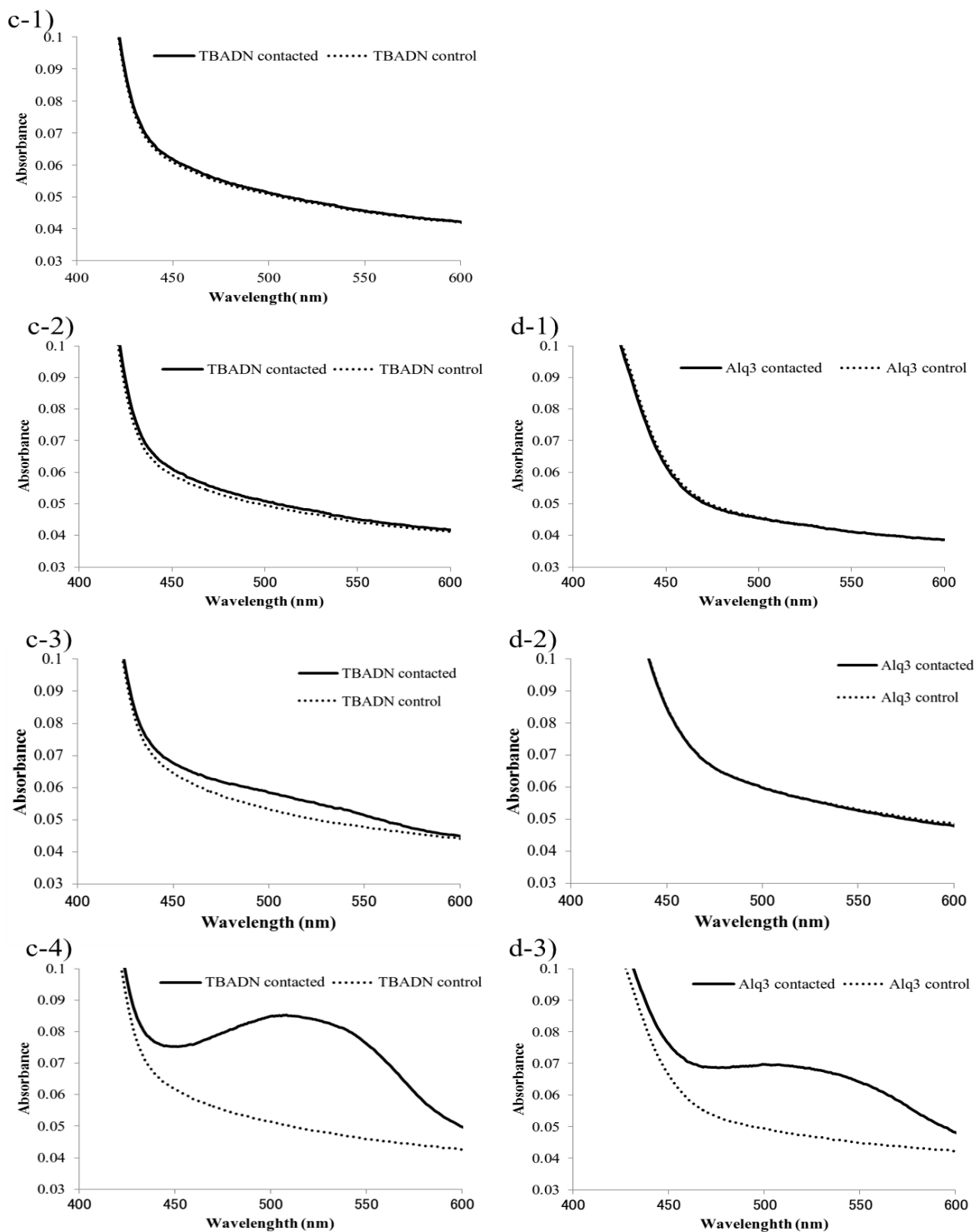


Figure 5.4 UV-Vis absorption spectra of the acceptor host films ((a) CBP, (b) NPB, (c) TBADN and (d) Alq₃) after contact with the donor substrate for 60 min at (1) 60°C, (2) 80°C, (3) 100°C and (4) 120°C. The dotted traces represent spectra collected from the non-contacted areas for reference.

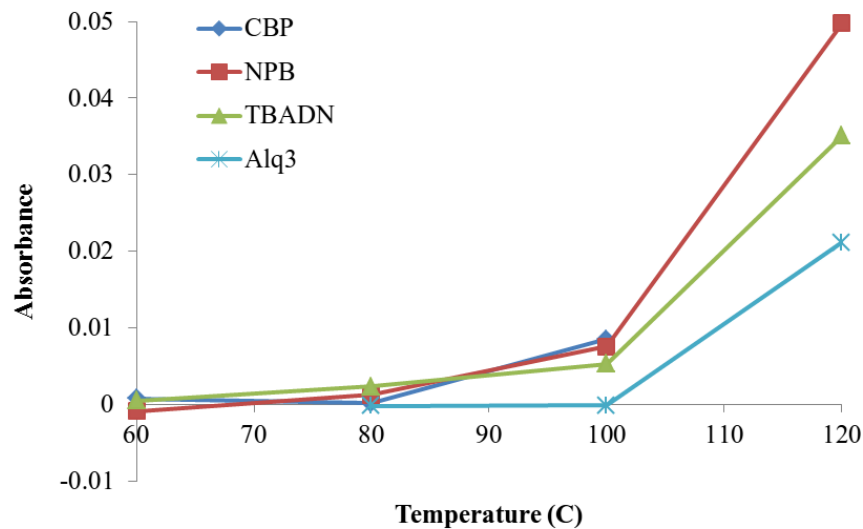


Figure 5.5 Absorbance of the acceptor films (CBP, NPB, TBADN and Alq₃) at the DCJTb peak absorption peak wavelength of 510 nm after contact with the donor substrate for 60min at various temperature from 60°C to 120°C. The absorbance of the corresponding control films is subtracted.

5.2 Examining electroluminescence characteristics of devices fabricated using this technique

Introduction

Although the previous experiments demonstrate that a sufficient amount of luminescent material molecules can be transferred through solid state diffusion from a donor substrate to dope a host film on another substrate, achieving good device performance also having an optimal doping concentration and profile. While dopant concentration can be relatively well controlled in the case of conventional co-deposition methods, controlling the concentration and profile may be more difficult in case of diffusion. For example, if the diffused dopant molecules remain near the host material film surface (due, for example, to a limited diffusivity of the dopant into the host material bulk) one can expect the dopant concentration to be very high at the surface which could lead to concentration quenching effects and, as a result, a lower device efficiency. In contrast, if they diffuse easily across the host layer and penetrate deep into the charge transport layers, a high driving voltage (due to charge trapping by the dopant in the charge transport layers) and/or inefficient host-to-guest energy transfer (due to a lower than desired

dopant concentration in the host) may result. Therefore, the electroluminescence characteristics are compared between devices doped by this technique versus those of devices doped via the conventional co-deposition method.

Experimental Procedure

The “diffused-dopant” devices are fabricated through the steps shown in Figure 5.6. First, a ~3 nm thick MoO₃ HIL, a ~60 nm thick NPB layer that functions as both a HTL and a host are vacuum-deposited on an ITO coated substrate (acceptor substrate). The substrate is then placed in physical contact with a glass “donor substrate”, pre-coated with a ~20 nm thick layer of DCJTJB using the same magnet plate as before, and heated to 100 °C in a dry nitrogen environment for one of various periods of time (15, 30, and 60 minutes). After heating, the donor substrate is removed, the acceptor substrate is placed in the vacuum system, and a ~40 nm thick Alq₃ ETL, followed by a ~0.5 nm thick LiF EIL and a ~70 nm Al cathode are deposited to complete the device.

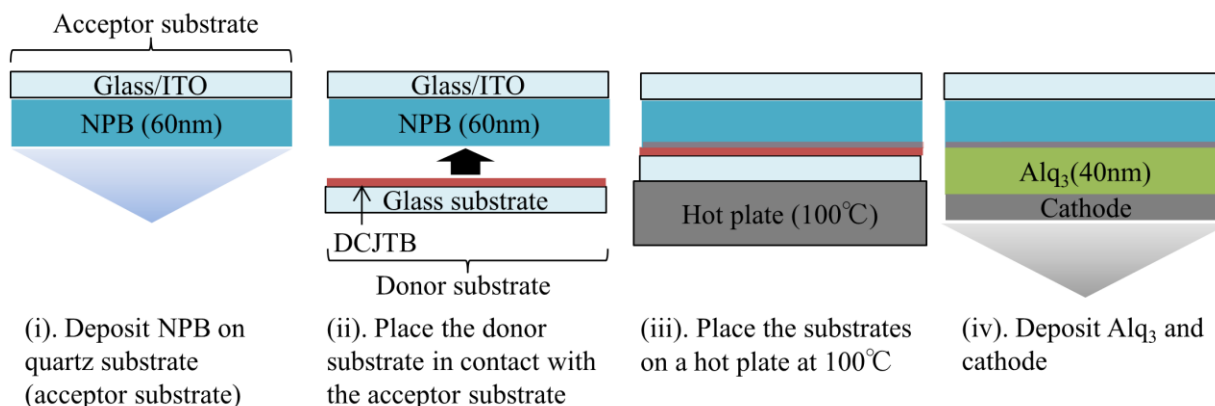


Figure 5.6. A schematic diagram illustrating the steps of the procedure followed for fabricating OLEDs. (ii) and (iii) illustrate the steps of introducing the dopant via diffusion.

Results and discussion

Figure 5.7 presents the EL spectra of the devices produced through the procedure in Figure 5.6. Spectra from reference devices with similar structure (ITO/ MoO₃ (3 nm)/NPB (60-x nm)/NPB:DCJTB (x nm, y%)/Alq₃ (40 nm)/LiF (0.5 nm)/Al (70nm) where x=0, 10, 5, 2.5 or 0.2 nm, and y=0, 2, 4, 8 or 100%), in which the NPB:DCJTB layer is fabricated by the conventional co-deposition of NPB and DCJTB are also included for comparison (the dotted traces). In these reference devices different thicknesses are used for the doped layer in order to obtain comparable overall number of dopant molecules in all devices.

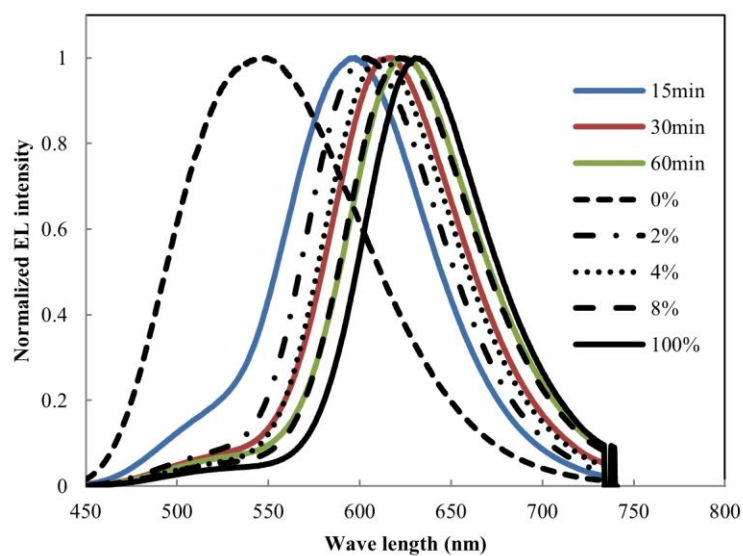
As can be seen, the spectra of the reference devices demonstrate a redshift as the concentration of DCJTB increases. It is worth noting that this redshift is not due to aggregation of DCJTB molecules (based on the insignificant spectral shift in the absorption spectra of NPB films doped with various DCJTB concentrations (see Appendix 2)) but rather is due to a progressive decrease in contribution from Alq₃ as DCJTB concentration increases, which makes energy transfer from the Alq₃ to the DCJTB increasingly more efficient. As shown in Figure 5.7, the spectra of the diffused-dopant devices are equivalent to reference devices with 2-8% DCJTB concentration. For example, in the 30-60 minute diffused-dopant devices, the 540 nm Alq₃ emission band is almost absent and the main DCJTB band has a maximum at ~620 nm, very similar to the spectral features of the 4-8% DCJTB reference devices. This result indicates that the two devices have very similar dopant concentrations, which indicates that diffusion can readily produce very similar doping levels as those produced by co-deposition.

Also, from Figure 5.8 the J-V and L-V characteristics of the two sets of devices are similar. For example, the driving voltage and luminance at 20 mA/cm² of the diffused-dopant devices are ~6.7 V and 200-1000 cd/m² (power efficiency ~ 0.43-2.35 lm/W), comparable to the 2-8% DCJTB control devices. The similar device characteristics indicate that contact with the donor substrate and/or heating does not cause significant damage or defects to devices. However, a close examination reveals that the efficiency of the diffused-dopant device is slightly lower than that of the control device with the similar EL spectrum. For example, while the device contacted with the donor substrate for 60 minutes and the control device doped with 8% DCJTB have the similar EL spectrum, the power efficiency of the

diffused-dopant device of 0.43 lm/W is lower than that of the control device of 0.56 lm/W. This is likely due to non-uniform dopant concentration profile.

Because the luminescent material is transferred to the host through physical contact with the donor substrate, the concentration of DCJTb is likely high at the surface of the NPB layer, causing concentration quenching. This non-uniform concentration profile can be overcome by using a diffusion barrier, which is discussed in the following section. Finally, it should be noted that the effect of thermal stress on the device performance is generally negligible at this temperature. In fact our experiments show that NPB/Alq₃ devices in which the NPB layer is heated to 100 °C for 60 minutes have a luminance of ~800 cd/m² and a driving voltage of ~6.9 V at 20 mA/cm² (power efficiency of ~1.75 lm/W). These are typical values for this device architecture despite the same thermal stress condition used above for deriving the diffusion.

From these results it has been shown that doping an OLED host material by solid state diffusion from a donor substrate can produce optimal device performance, comparable to devices produced through the standard fabrication technique. The results also show that the physical contact does not cause significant damages to devices. The results demonstrate the technical viability and potential of the approach as a maskless color patterning approach.



Device	15min	30min	60min		
CIE	(535 447)	(584 402)	(598 389)		
Device	0%	2%	4%	8%	100%
CIE	(365 526)	(557 427)	(584 404)	(605 382)	(622 366)

Figure 5.7. Red, green and blue colored solid lines: EL spectra of the devices fabricated following the procedure in Fig. 5.6 for various contact times. Black lines: EL spectra of reference devices with 0, 2, 4, 8 and 100% DCJTB fabricated by conventional co-deposition. Corresponding CIE coordinates of these devices are also included.

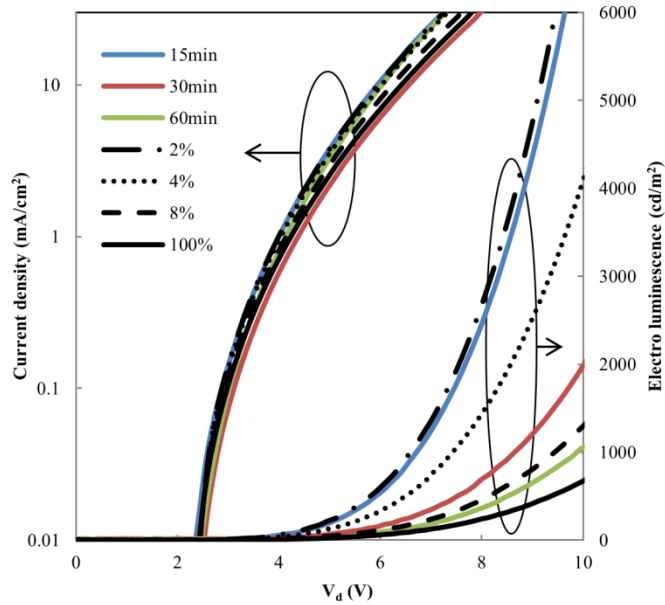


Figure 5.8. Red, green and blue colored solid lines: J-V and L-V characteristics of devices fabricated following the procedure in Fig. 5.6. Black lines: those of reference devices with 2, 4, 8 and 100% DCJTB concentration.

5.3 Demonstrating RGB color patterning by selective diffusion of a luminescent material

Introduction

Next, in order to demonstrate the potential of the approach for OLED RGB color patterning, red, green and blue OLEDs are fabricated side-by-side on one substrate by this approach. For RGB color patterning, the diffusion of the luminescent material from the donor substrate needs to be limited to certain selected areas of the OLED host material on the acceptor substrate. Although this can generally be done by the use of pre-patterned donor substrates (e.g. in the form of micro stamps) or by screen printing that will restrict the physical contact between the two substrates to the desired areas^{[29][30][31][64]}, local Joule heating is employed, using for that purpose the OLED ITO anodes that are already present on the OLED substrate, to achieve this positional selectivity of diffusion^{[28][69]}. Unlike stamping and screen printing where mechanical alignment between the stamp or the print screen and the substrate is required, this technique provides an opportunity to achieve positional selectivity without any mechanical alignment which makes it even simpler and capable of providing higher accuracies. In this

approach, the donor and acceptor substrates are already in physical contact, and heated by passing current through ITO anodes on the OLED backplane. This causes local heating in the desired areas only. Thus, dopant molecules can be selectively diffused to the desired areas of the OLED host layer on the backplane substrate.

Experimental Procedure

In this demonstration, a glass substrate on which three strips of ITO anodes are already patterned is used. The ITO strips will serve as anodes of red, green and blue OLEDs. The OLEDs are fabricated through the procedure shown in Figure 5.9. A ~3 nm MoO₃ and a ~60 nm NPB are deposited on the entire substrate through conventional vacuum deposition (without a shadow mask) to serve as HIL and HTL and host, respectively, for the three devices. For color patterning, DCJTb and C545T are selectively doped from separate donor substrates into the NPB host layer on the acceptor substrate by local Joule heating using the respective ITO strips. For Joule heating, a 13V bias is applied between the two ends of the respective ITO anodes for 60 minutes. After the red and green doping steps are completed, a ~10 nm of TBADN, a ~15 nm of 1,3,5-tris(N-phenylbenzimidazole-2-yl)benzene (TPBi) and a cathode are deposited on the entire substrate (again without a shadow mask). The TBADN layer functions as a blue emission layer (EML) for the blue device, whereas the TPBi layer functions as an ETL for all the three devices.

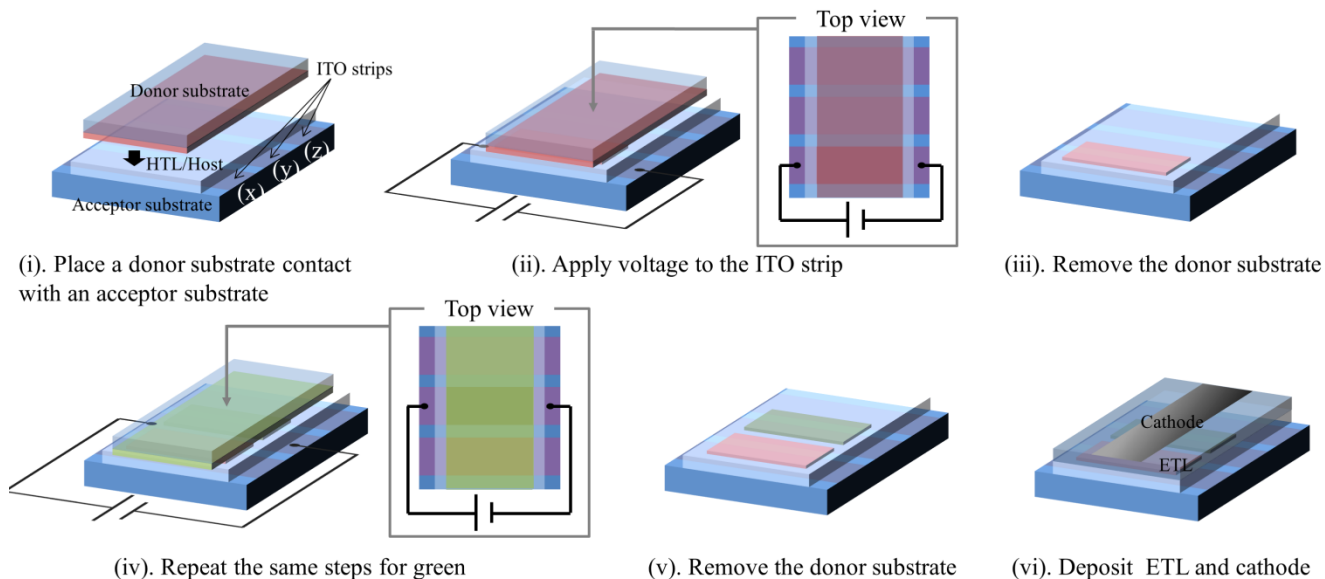
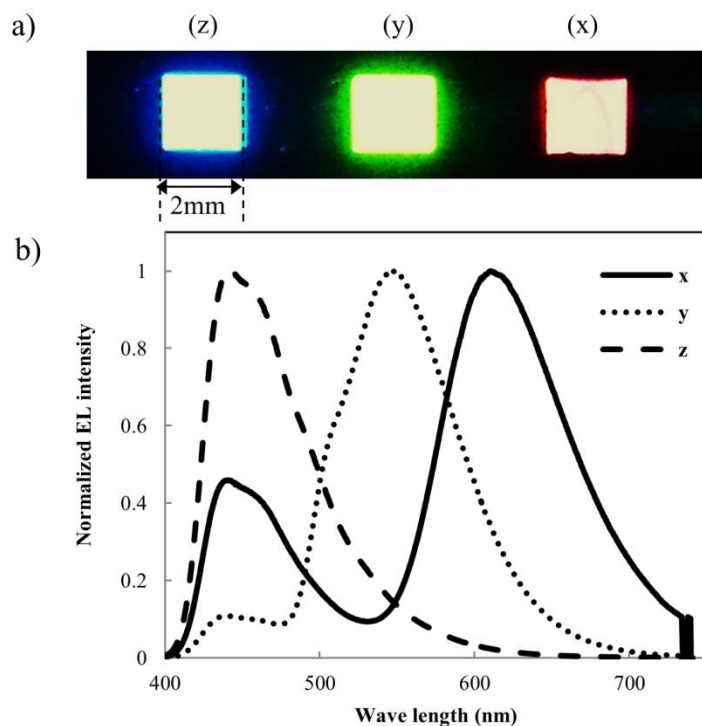


Figure 5.9 A schematic diagram illustrating the steps of the procedure followed for fabricating red, green and blue OLEDs. (ii) and (iv) show the Joule heating steps used to induce the diffusion for introducing the red and green dopants selectively in devices x and y, respectively.

Results and discussion

Figure 5.10 (a) and 10 (b) show an EL image and EL spectra, respectively, of these devices. Clearly, the technique is capable of producing red, green and blue OLEDs side-by-side on the same substrate. It should be emphasized that the different OLED emission colors are obtained without using shadow masks, stamps or any sort of mechanical alignment between the donor substrate and the OLED backplane substrate. Therefore, this diffusion-based technique appears to be capable of realizing maskless RGB OLED color patterning reliably for display fabrication. It should be pointed out that in theory lateral diffusion of the dopant may also occur, causing the dopant to spread outside of the desired area boundaries. Our preliminary investigations reveal that such lateral diffusion is limited to $\sim 5\text{-}10\ \mu\text{m}$. For high resolution displays this lateral diffusion can perhaps be readily prevented through the use of pre-patterned grooves or separators in the OLED substrate.

Finally, it should be pointed out that the EL spectrum of the red device contains some blue emission from TBADN. This residual emission could be reduced by optimizing device structure and the process parameters such as the diffusion time and voltage applied across ITO strips for Joule heating.



Device	B	G	R
CIE	(144 091)	(284 535)	(476 341)

Figure 5.10 (a) EL images and (b) EL spectra of the devices fabricated following the procedure in Fig. 5.9. Corresponding CIE coordinates of these devices are also included.

5.4 Assessing solvent vapor exposure as a method to accelerate solid state diffusion

Introduction

The previous results demonstrate that the use of physical contact between donor and acceptor substrates for introducing dopants is capable of producing OLEDs with typical performance. However, from a manufacturing standpoint, the long diffusion time required for sufficient dopant transfer could be disadvantageous. For instance, the previous experiment shows that in order to obtain a device with EL

spectrum similar to that of a reference device with 4% DCJTB concentration made by conventional co-deposition, 30 minutes of contact are required. Such long diffusion times can limit the value of the technique as it would result in long manufacturing time, low throughput and high production costs. Therefore, in order to reduce the required contact time, the effect of solvent exposure is explored as a method to accelerate diffusion. It is well known that molecular diffusion into an acceptor organic material can be enhanced upon exposing the material to a suitable solvent as a result of the increased free volume that the solvent absorption produces in the material. This approach was utilized for promoting diffusion in polymer OLEDs in the past ^{[64][70][71]}. As a preliminary investigation for testing if this approach can be applied to small molecule OLEDs, the effects of solvent vapor exposure on organic layers and device performance are investigated.

Experimental Procedure

First, in order to test if molecular diffusion in solid state organic films can be enhanced by solvent vapor exposure, changes in the PL spectrum of a vacuum-deposited NPB(60 nm)/DCJTB(10 nm) bilayer stack coated on a glass substrate is monitored. The detailed experimental setup for exposing the sample to solvent vapor is shown in Figure 5.11.

Next, effects of solvent vapor exposure on device performance are investigated. Figure 5.12 depicts the experimental procedure. OLED films are deposited through standard thermal vacuum deposition on an ITO coated glass substrate. The substrate is then placed in a sealed test box filled with toluene vapor to expose the deposited films to toluene vapor, for 30 minutes. This long exposure time is used in order to ensure that any effects on the organic layers from solvent exposure become significant and will well surpass what may occur from the much shorter exposure times during the device fabrication procedure.

After vapor exposure, the substrate is put back in the vacuum system, and the rest of the OLED films and cathode are deposited to complete devices. In this experiment, three different types of OLED layers are exposed to solvent vapor: (1) HTLs, (2) HTL/dopant bilayers and (3) HTL:dopant mixed layers. In test 1, effects of exposing a neat layer of a HTM to solvent vapor on device performance is tested. Two common HTMs, NPB and 4,4',4''-tri(N-carbazolyl) triphenylamine (TcTa), are exposed to

solvent vapor as shown in the step (ii) of Figure 5.12. The complete device structures are shown in Table 5.1. In test 2, effects of intermixing of a HTL/dopant bilayer due to solvent vapor exposure on device performance is investigated. Two different HTL/dopant bilayers, NPB(60 nm)/DCJTb(2.4 nm) and NPB(45 nm)/C545T(2.4 nm) are exposed to solvent vapor (complete structures shown in Table 5.1). In test 3, effects of exposing a host:dopant premixed layer on device performance is investigated. Two different host:dopant premixed layers, NPB:DCJTb and NPB:C545T, are exposed to solvent vapor (complete structures shown in Table 5.1).

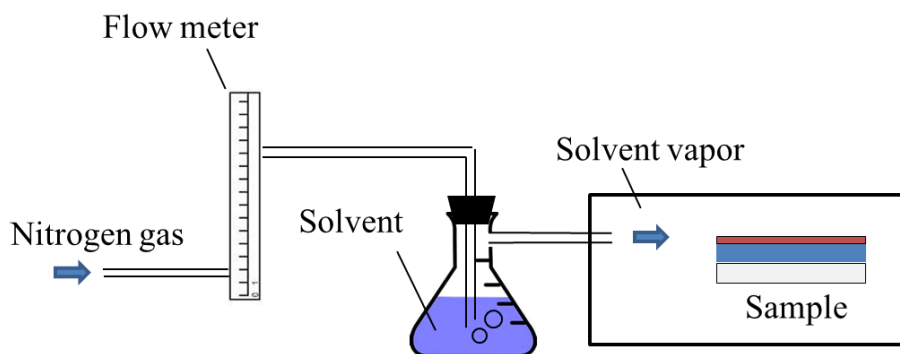


Figure 5.11 Schematic presentation for the experimental setup for exposing the sample to solvent vapor.

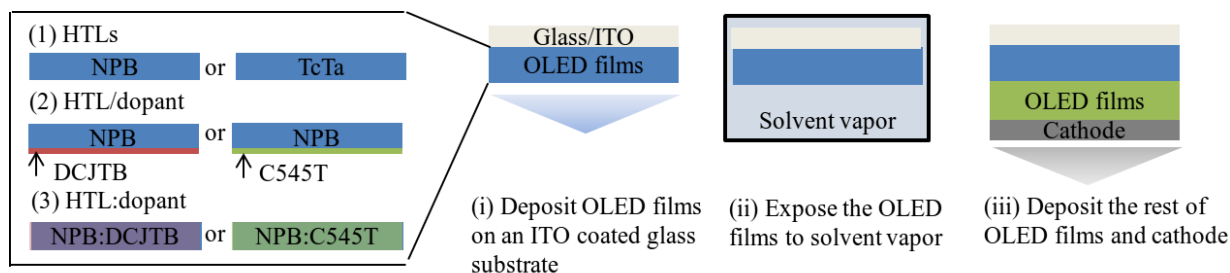


Figure 5.12 A schematic diagram illustrating the steps of the procedure followed for fabricating OLEDs. (ii) illustrate the steps of exposing the sample to solvent vapor.

	Complete structure
Test (1)	NPB(60nm)/(Solvent)/Alq ₃ (40nm)
	TcTa(40nm)/(Solvent)/TPBi(40nm)
Test (2)	NPB(60nm)/DCJTB(2.4nm)/(Solvent)/Alq ₃ (40nm)
	NPB(45nm)/C545T(2.4nm)/(Solvent)/Bphen(40nm)
Test (3)	NPB:DCJTB(4%,60nm)/(Solvent)/Alq ₃ (40nm)
	NPB:C545T(45nm,4%)/(Solvent)/Bphen(40nm)
* All devices have MoO ₃ (3nm) and LiF(0.5nm)/Al(70nm) as HIL and EIL/cathode, respectively.	

Table 5.1 Complete device structures. (Solvent) indicates the solvent vapor exposure step.

Results and discussion

Figure 5.13 shows PL spectra collected from the stack before and after 6 minutes of exposure to the solvent vapor under 360 nm excitation. As can be seen from the figure, the PL spectrum of the unexposed bilayer stack corresponds mostly to NPB emission, with no significant emission from DCJTB. This is due to concentration quenching effects in DCJTB which makes luminescence from a neat layer very weak. However, the PL spectrum becomes drastically different after exposure to solvent vapor for 6 minutes, and emission becomes dominated by 605 nm emission from DCJTB whereas the NPB emission is quenched. The change indicates significant interlayer molecular diffusion between the NPB layer and the DCJTB layer which dilutes the DCJTB, thereby making it capable of efficient luminescence. Simultaneously, NPB is quenched by energy transfer to the DCJTB molecules that now dope the entire NPB layer. Figure 5.14 shows PL images taken under UV excitation of the bilayer before and after the acetone vapor exposure. The result suggests that exposing the acceptor substrate to solvent can result in a significant enhancement in the diffusion rate, making it possible to reduce the time required for introducing dopants via contact with a donor substrate to only a few minutes.

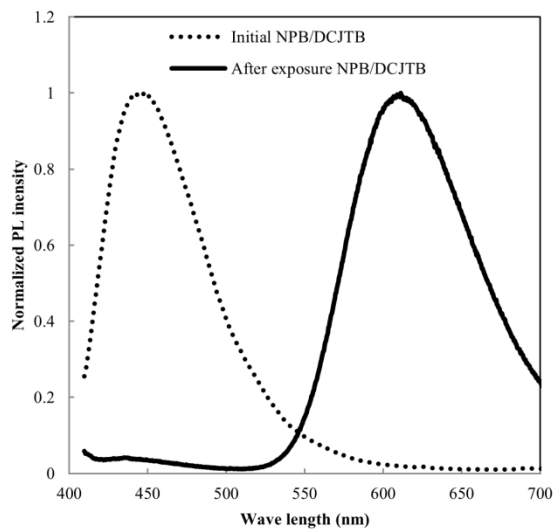


Figure 5.13 PL spectra of the NPB/DCJTb bilayer stack before and after the acetone vapor exposure. The spectra are collected under 360nm excitation.

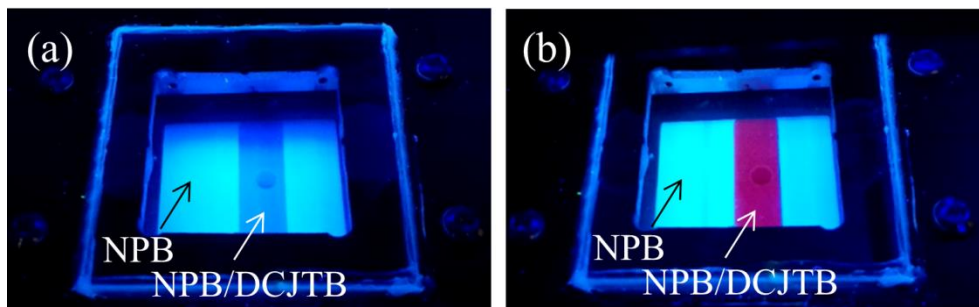


Figure 5.14 PL images of the NPB/DCJTb bilayer stack before (a) and after (b) the acetone vapor exposure.

Figure 5.15 presents the J-V and L-V characteristics of the devices whose HTL is exposed to solvent vapor (test 1). The inset is the current versus luminance (J-L) characteristics, which indicate the current efficiency by its slope. As can be seen, no significant effects on the J-V and L-V characteristics and the current efficiency are observed when the neat layer of the HTLs is exposed to solvent vapor. This result indicates that solvent exposure does not cause detrimental effects on devices such as molecular decomposition or significant morphology changes which could cause electrical shorting short of devices. It should be noted, however, that solvent exposure causes significant crystallization to

organic thin films depending on materials. For example, a thin film of CBP, which is susceptible to crystallization, is crystallized due to solvent vapor exposure in a few minutes.

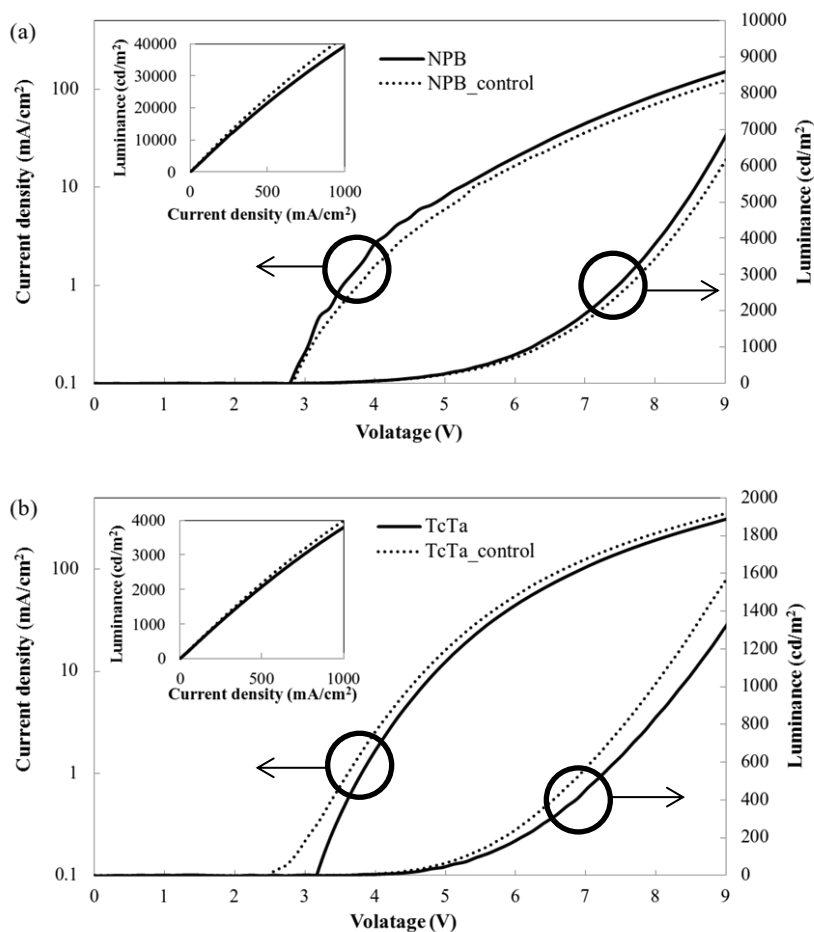


Figure 5.15 J-V and L-V characteristics of the devices whose HTL (NPB (a) and TcTa (b)) is exposed to toluene vapor. The inset is the J-L characteristics.

Figure 5.16 presents the J-V and L-V characteristics of the devices where their HTL/dopant bilayer is exposed to solvent vapor (test 2) with the J-L characteristics in the inset. As can be seen, the current efficiency of those devices is significantly increased due to solvent vapor exposure around 10 times higher than that of the control device. This improvement in efficiency results from molecular diffusion due to solvent vapor exposure. While the efficiency of the control device is low due to concentration quenching in the neat layer of the dopant, the efficiency of the solvent-exposed device is relatively high

because of lower dopant concentration that results from molecular diffusion between the HTL and the dopant layer. The lower dopant concentration of the solvent-exposed devices is also indicated by EL spectrum (Fig. 5.17). As can be seen, the EL spectrum is blue-shifted due to solvent vapor exposure. This spectral shift is likely due to decreased aggregation of dopant molecules because of lower dopant concentration. This result further confirms that solvent vapor exposure causes significant molecular diffusion.

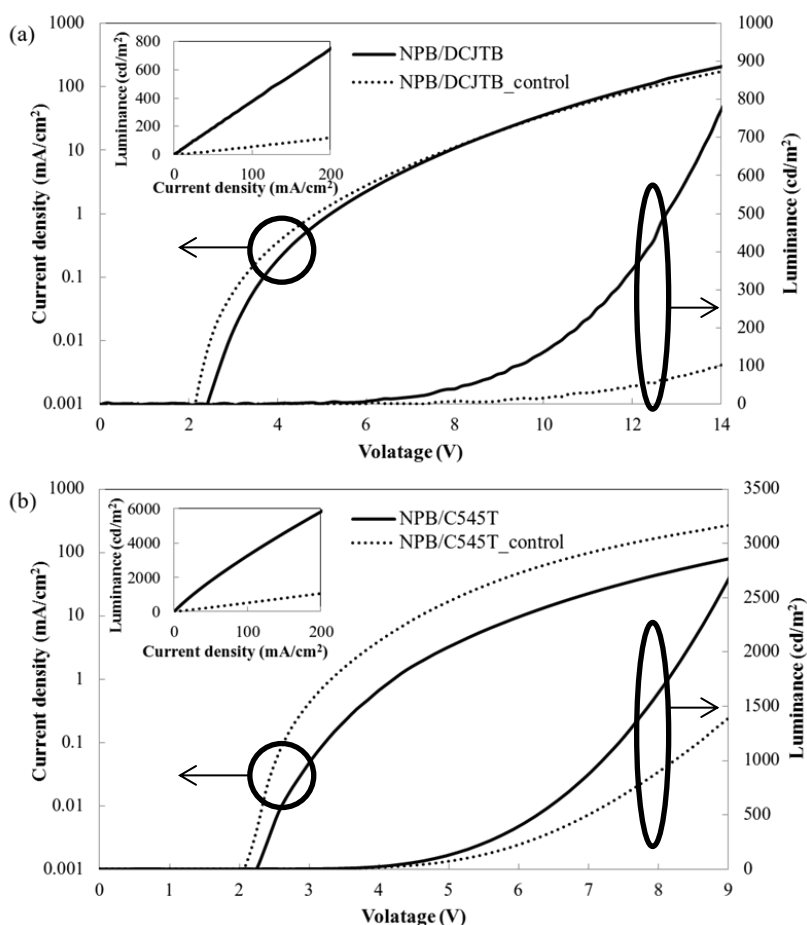


Figure 5.16 J-V and L-V characteristics of the devices where the HTL/dopant bilayer ((a) NPB/DCJTb and (b) NPB/C545T) are exposed to toluene vapor. The inset is the J-L characteristics. The dotted lines represent those of the corresponding control devices.

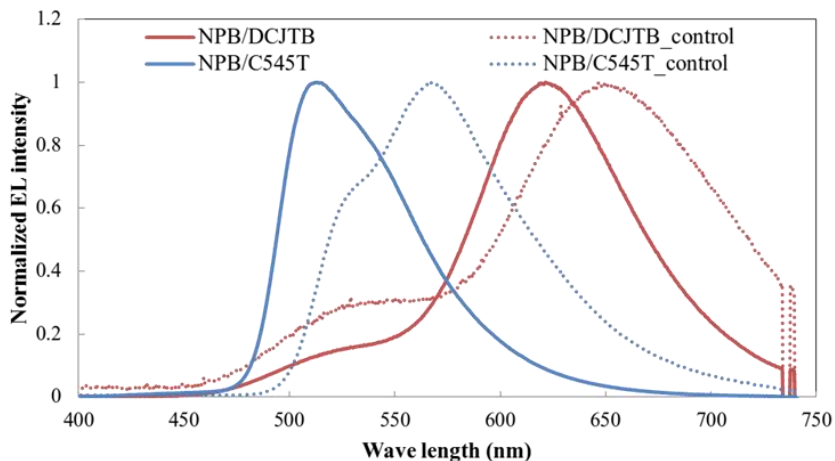


Figure 5.17 EL spectrum of the devices where the HTL/dopant bilayer (NPB/DCJTБ (red) and NPB/C545T (blue)) is exposed to toluene vapor. The dotted lines represent those of the corresponding control devices.

Figure 5.18 presents the J-V and L-V characteristics of the devices where their host:dopant premixed layer is exposed to solvent vapor (test 3) with the J-L characteristics in the inset. As can be seen, while the change in efficiency of the device with C545T is relatively small, the efficiency of the device with DCJTБ is significantly reduced due to solvent exposure. This significant decrease in efficiency of the device with DCJTБ may be explained by aggregation of DCJTБ molecules which occurs during molecular diffusion. The aggregation of DCJTБ molecules is indicated by the EL spectrum of the device which is red-shifted due to solvent vapor exposure (Fig. 5.19).

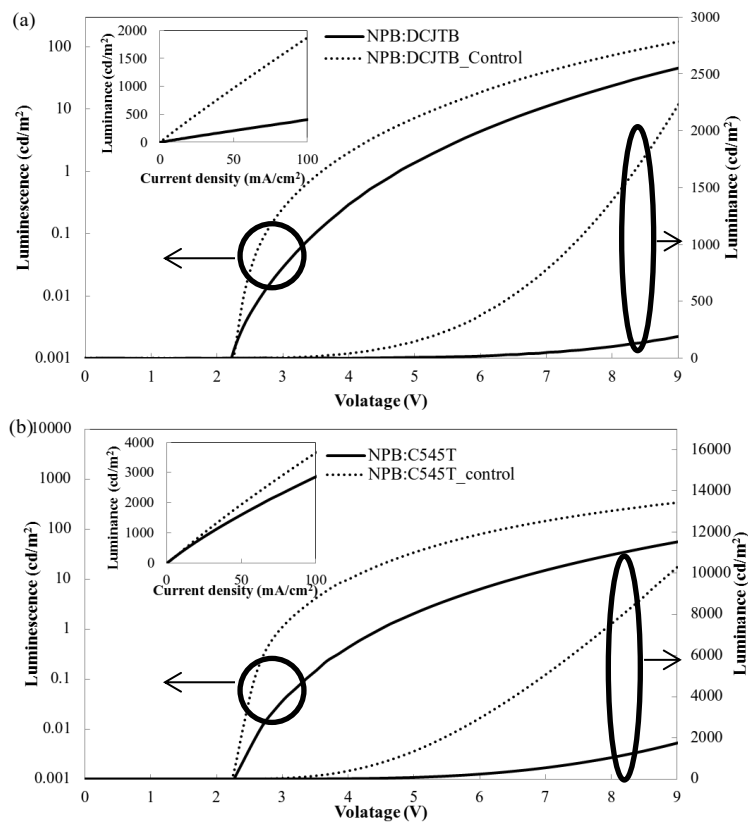


Figure 5.18 J-V and L-V characteristics of the devices where the HTL:dopant bilayer ((a) NPB:DCJTb and (b) NPB:C545T) is exposed to toluene vapor. The inset is the J-L characteristics. The dotted lines represent those of the corresponding control devices.

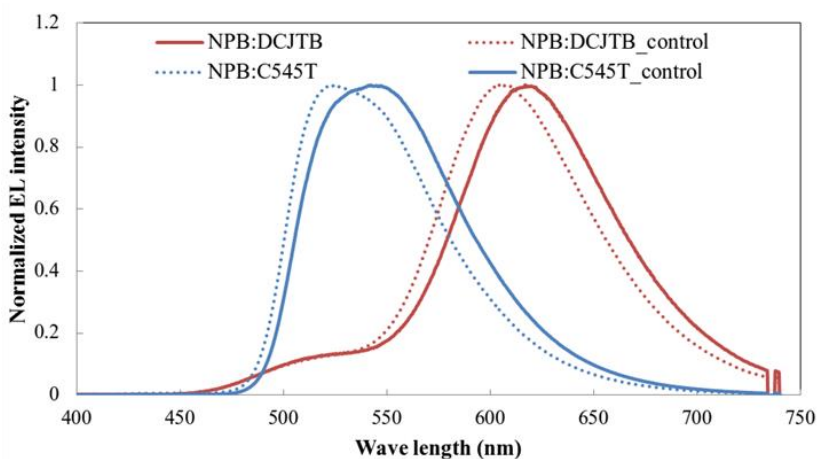


Figure 5.19 EL spectrum of the devices where their HTL:dopant bilayer (NPB:DCJTb (red) and NPB:C545T (blue)) is exposed to toluene vapor. The dotted lines represent those of the corresponding control devices.

In summary, this study shows that the effects of solvent vapor exposure highly depend on materials. For example, while HTL materials such as NPB and TcTa are not affected by solvent vapor exposure, materials which are more susceptible to crystallization such as CBP are significantly crystallized. Also, while the efficiency significantly drops when the NPB:DCJTB premixed layer is exposed to solvent vapor, the efficiency drop is relatively small compared in the case of the NPB:C545T premixed layer. This efficiency drop of the NPB:DCJTB mixed layer due to solvent exposure may be attributed to aggregation of DCJTB molecules during molecular diffusion. While the enhancement of diffusion by solvent vapor exposure has great potential to accelerate diffusion, further systematic investigations are required to clarify effects of solvent exposure and to understand mechanisms.

5.5 Assessing semiconducting diffusion barrier as a method to block undesirable diffusion

Introduction

While the capability of the technique for OLED color patterning is demonstrated, controlling doping levels through diffusion is expected to be difficult, which could limit device performance. For example, the diffusion of the luminescent material molecules may extend beyond the EML into the HTL. The presence of dopant molecules into the HTL may cause them act as charge traps, which could result in higher driving voltage. Additionally, the dopant concentration is likely to be non-uniform across the EML, with higher concentrations near the surface. Such non-uniformity and high dopant concentrations near the surface could decrease device efficiency due to concentration quenching effects.

In order to overcome the aforementioned limitations, the use of semiconducting diffusion barriers made of organic and inorganic material mixtures is proposed for achieving controlled and uniform concentrations of luminescent dopants in the EML. The use of these diffusion barriers allows for controlling the diffusion depth and achieving uniform concentration by means of blocking undesirable dopant diffusion. This is the first time that diffusion barriers are used in the field of organic semiconductors. Figure 5.20 illustrates this idea by comparing diffusion-based doping with and without the diffusion barrier. The barrier effectively blocks the diffusion of the dopant molecules in the

underlying organic layers and thus allows limiting the diffusion to only the desired depth (step (b-ii) of Fig. 5.20). By limiting the diffusion depth, it also allows for obtaining a uniform dopant concentration across the EML (step (b-iv) of Fig. 5.20). For diffusion barriers, MoO₃ mixed with the hole transport material (HTM) used in the HTL is utilized. Due to the relatively high density and small molecular size of MoO₃, the HTM:MoO₃ mixture can be expected to have higher density relative to the neat HTM, thereby blocking the diffusion of the dopant material. At the same time, the relatively high conductivity of HTM:MoO₃ mixtures, caused by the formation of a charge transfer (CT) complex, prevents disruption of charge transport across the device^{[72][73]}.

The effectiveness of the diffusion barrier in the doping method via diffusion is investigated through following three experiments. First, the effectiveness of the HTM:MoO₃ film in substantially reducing the inter-diffusion of luminescent materials present in two layers located on opposite sides of the barrier is tested. In this case, changes in PL are used to detect any inter-mixing that may result from such inter-diffusion. The tests are done for two different scenarios in which either heating (at 100 °C) or exposure to solvents (toluene) is used to drive and accelerate the diffusion process. Next, the diffusion barrier is introduced in OLED devices, and its capability of controlling a dopant concentration is investigated. Finally, OLEDs with the diffusion barrier are fabricated through the doping method via diffusion. The ability of this approach to produce OLEDs with highly controlled device structure and performance when a luminescent material is doped into a host layer via diffusion is demonstrated by this experiment.

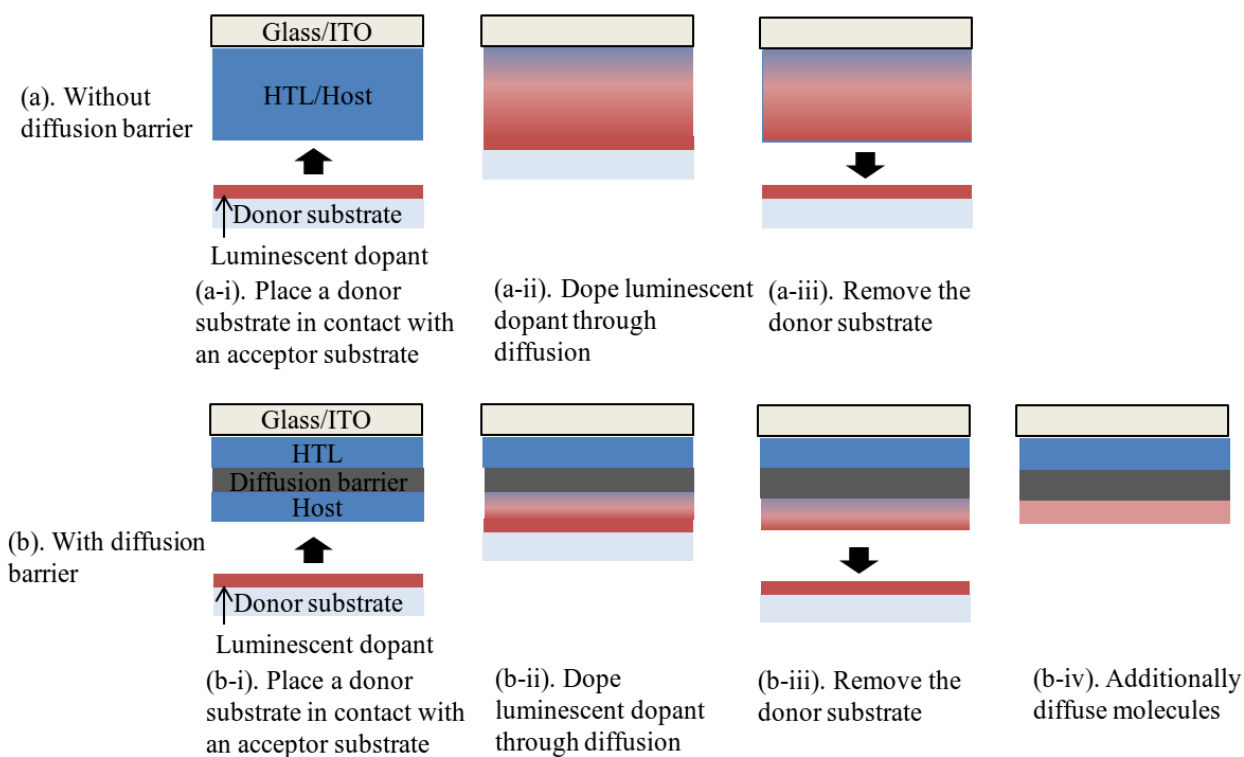


Figure 5.20 Scheme for the diffusion-based doping method without (a), and with (b) the diffusion barrier.

5.5.1 Assessing the effectiveness of using a MoO_3 :HTM film in reducing inter-diffusion of luminescent materials

Experimental Procedure

The effectiveness of using a $\text{HTM}:\text{MoO}_3$ film in reducing inter-diffusion of luminescent materials between two layers located on opposite sides of it is tested. For this purpose, organic stacks in which the $\text{HTM}:\text{MoO}_3$ film is sandwiched between two organic layers containing different luminescent materials are used, and PL measurements are utilized for detecting any inter-mixing that may occur as a result of inter-diffusion. NPB, C545T, and DCJTb are used as a host, green dopant, and red dopant material, respectively. The organic layer stack consists of NPB:C545T(5%, 40 nm)/NPB: MoO_3 (50%, 5 nm)/DCJTb(3 nm) (Fig. 5.21 (b)). Since DCJTb has a lower band gap than that of C545T, any intermixing between the two materials due to diffusion would lead to quenching of C545T luminescence by DCJTb as a result of energy transfer. As such, any changes in PL spectra over time

would correlate with the extent of intermixing between the two layers due to diffusion across the HTM:MoO₃ film. For comparison, stacks of the same structure except with the NPB:MoO₃ layer replaced with a 5 nm thick neat layer of NPB are also fabricated to be used as reference (i.e. represents the case of no diffusion barrier). The complete structure of the reference stacks is therefore NPB:C545T(5%, 40 nm)/NPB(5 nm)/DCJTB(3 nm) (Fig. 5.21 (a)). All stacks are fabricated by the sequential deposition of the organic layers using standard thermal vacuum deposition on glass substrates. After fabrication, the substrates (with the stacks) are placed on a hot plate at 100 °C for driving molecular diffusion.

Results and discussion

Figures 5.21 (b) and (e) show PL spectra collected every 10 minutes from the organic stacks without and with the diffusion barrier, respectively, under 360 nm excitation. As can be seen from the figures, the initial (at t=0 min, i.e. before heating) spectra collected from the two stacks correspond almost entirely to C545T emission, with no significant emission from DCJTB. The absence of DCJTB emission can be attributed to concentration quenching effects which make luminescence from a neat layer of DCJTB very weak. Upon heating, the PL spectra of the organic stack without the diffusion barrier start exhibiting a red shift, and after 50 minutes, the emission becomes dominated by 605 nm DCJTB emission (Fig. 5.21 (b)). This spectral change clearly points to the diffusion of DCJTB molecules into the NPB:C545T layer, resulting in quenching of C545T and efficient luminescence from DCJTB that now dopes the layer. In contrast, the spectra from the stack with the diffusion barrier exhibits very little change and remain dominated by ~530 nm emission from C545T even after heating for 50 minutes (Fig. 5.21 (e)). The differences between the PL changes in the two samples are also evident in the PL images taken under UV excitation (Fig. 5.21 (e) and (f)). These results clearly demonstrate that the NPB:MoO₃ film is indeed capable of preventing DCJTB molecules from diffusing to the opposite side.

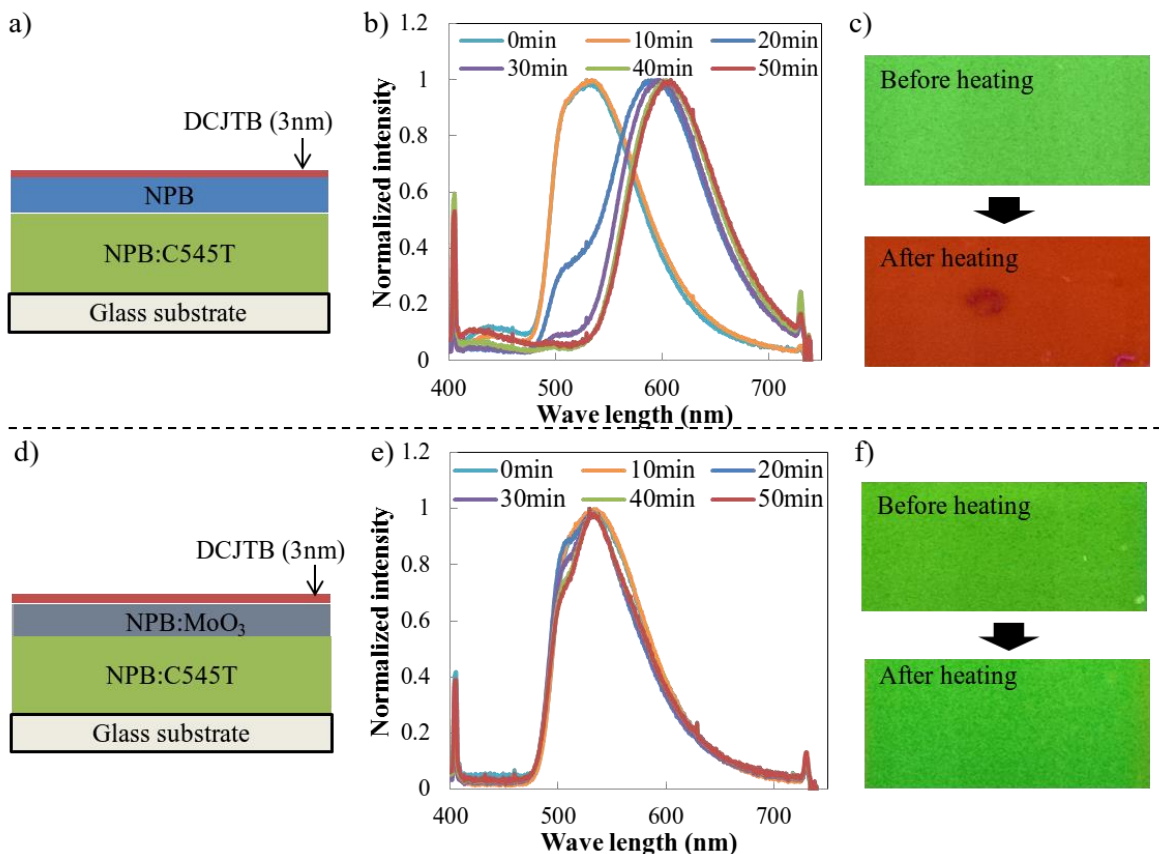


Figure 5.21 (a) and (d) the structure of the organic layer stacks without and with the diffusion barrier film, respectively; (b) and (e) spectra collected every 10 minutes from the organic stacks; and (c) and (f) PL images of the stacks before and after heating.

In the experiment for the other scenario (in the case of diffusion driven by solvent vapor), the same experiment is performed whereby another set of organic stacks are exposed to toluene vapor for 2 minutes instead of heating to 100 °C. Figure 5.22 (b) and (e) show the PL spectra from the stacks without and with the NPB:MoO₃ barrier film respectively for this experiment. The same phenomenon is also observed here, where again the PL spectra of the organic layer stack without the diffusion barrier exhibit a change from green to red emission upon solvent exposure pointing to the diffusion of the DCJTJTB into the NPB:C545T layer whereas the PL spectra from the stack containing the diffusion barrier layer remain unchanged. These results confirm that the HTM:MoO₃ film functions as an effective diffusion barrier that can be used with both heat-assisted and solvent vapor-assisted diffusion-based doping processes.

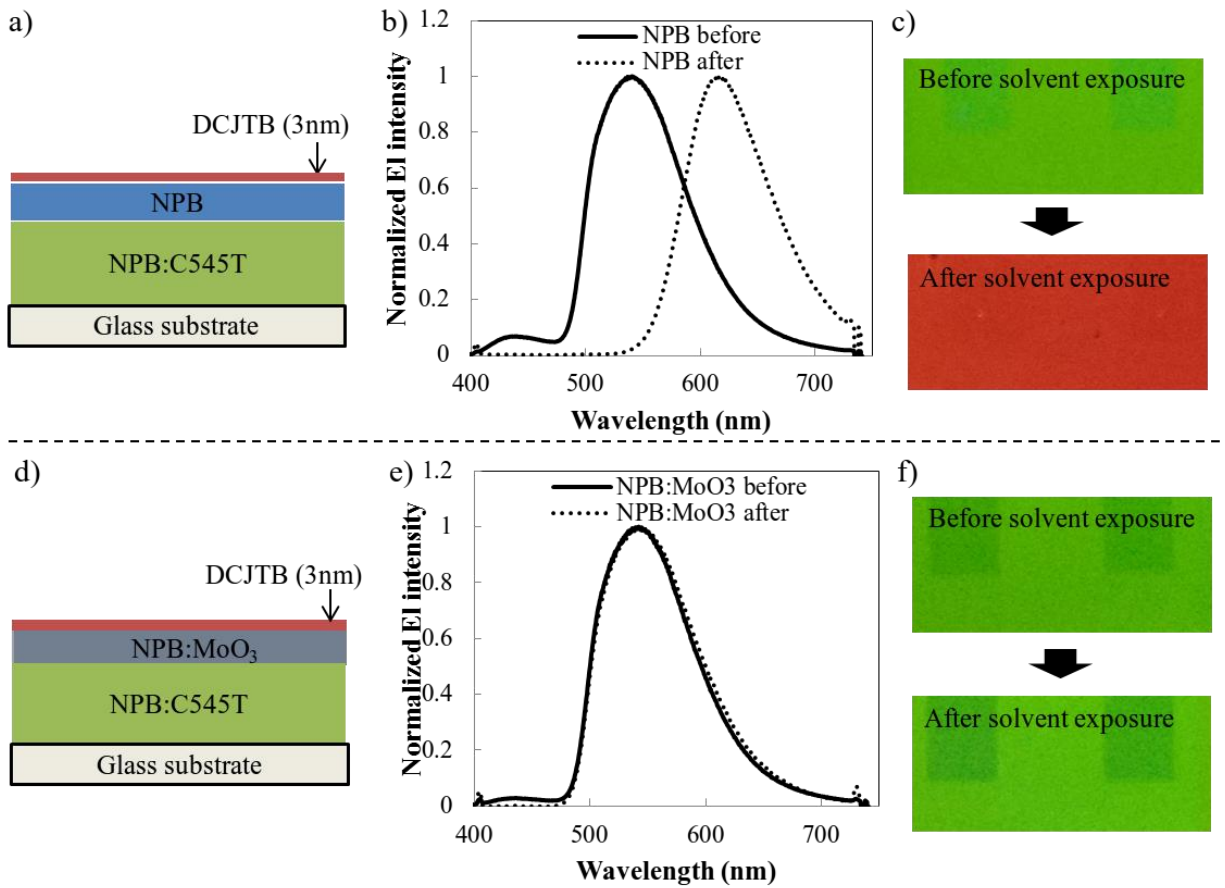


Figure 5.22 (a) and (d) the structure of the organic layer stacks without and with the diffusion barrier film, respectively; (b) and (e) spectra collected from the organic stacks before and after solvent vapor exposure; and (c) and (f) PL images of the stacks before and after solvent vapor exposure.

5.5.2 Investigating capability of the diffusion barrier for controlling a dopant concentration

Experimental Procedure

Next, the diffusion barrier is introduced in OLED devices, and its capability of blocking molecular diffusion and limiting diffusion depth is assessed. In this experiment, OLED devices with the diffusion barrier are fabricated through standard thermal vacuum deposition, and changes in performance due to thermal diffusion are monitored. The device structure used in this experiment consists of a ~3 nm MoO₃ HIL, a 60-x nm thick NPB doped with 50% MoO₃ layer, a x nm thick NPB neat layer, a 0.6 nm thick

DCJTB neat layer, a ~40 nm thick Alq₃ ETL layer, a ~0.5 nm thick LiF EIL, and a ~70 nm Al cathode (device A). In one device x is 10nm whereas in the other device x is 15nm. The complete structure of the device is therefore ITO/MoO₃(3 nm)/NPB:MoO₃(60-x nm, 50%)/NPB(x nm)/DCJTB(0.6 nm)/Alq₃(40 nm)/LiF(0.5 nm)/Al(70 nm) where x=10 or 15 nm (Fig. 5.23 (a)). The NPB:MoO₃ layer in this device functions as both a HTL and diffusion barrier. The completed devices are then heated to 100 °C for one hour in order to drive diffusion of the DCJTB molecules into the NPB layer. During that time the device EL spectrum and current efficiency are measured regularly every 10 or 15 minutes. In addition to the device with the neat layer of DCJTB (device A), a control device with the same structure is also fabricated. However, in this case NPB and DCJTB are premixed by co-deposition while the volume ratio between NPB and DCJTB remains constant. The complete structure of the control device (device B) is therefore ITO/MoO₃(3 nm)/NPB:MoO₃(60-x nm)/NPB:DCJTB(x nm, y%)/Alq₃(40 nm)/LiF(0.5 nm)/Al(70 nm) (Fig. 5.23 (b)). In one device x is 10 nm and y is 6% whereas in the other device x is 15 nm and y is 4%. Note that the volume ratio between DCJTB and NPB of the device with the neat layer of DCJTB (device A) is the same as that of the corresponding control device (device B): 10 nm NPB to 0.6 nm DCJTB is ~6% and 15 nm NPB to 0.6 nm DCJTB is ~4%. This means that these devices with the neat DCJTB layer would have the same structure as the control devices after heating if DCJTB molecules uniformly diffused in the NPB layer without diffusing into the adjacent diffusion barrier and Alq₃ layer.

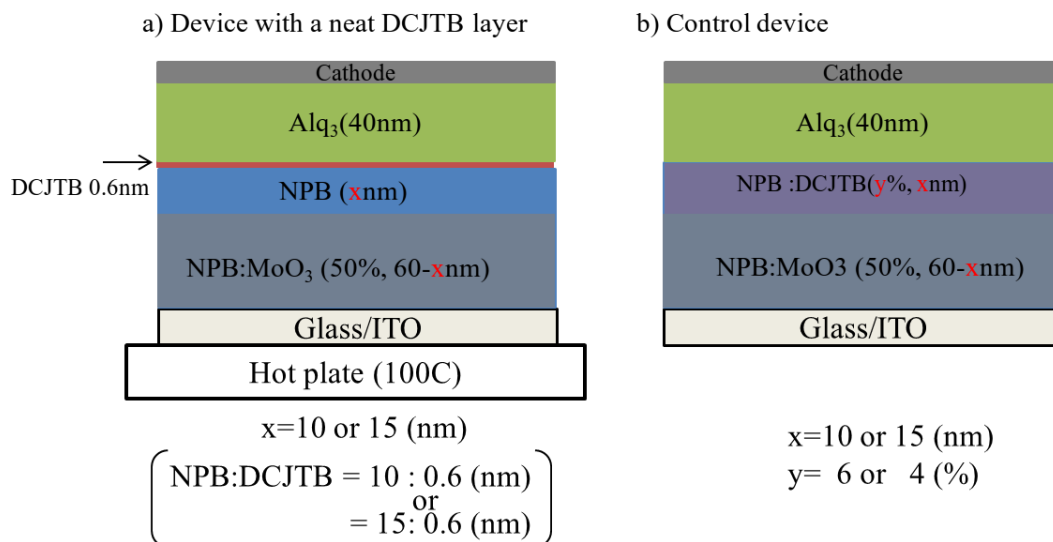


Figure 5.23 Schematic presentation for the device structure of (a) device A and (b) device B.

Results and discussion

Figure 5.24 shows the EL spectra from the two devices with the neat DCJTb layer collected periodically while at 100 °C. As can be seen, the EL spectra show a significant blue-shift with time. This spectral shift reflects a decrease in DCJTb concentration that occurs as a result of its diffusion into the NPB layer, and thus becomes uniformly mixed with the NPB molecules. (It should be noted that the diffusion of DCJTb into the adjacent Alq₃ layer is generally limited because of the high glass transition temperature of Alq₃ (~176 °C) which well exceeds the temperatures used here^[66]).

As DCJTb molecules spread across the NPB layer, their aggregation gradually diminishes, resulting in the observed blue-shift in the spectra. An examination of the un-normalized EL spectra (not shown here) shows that the DCJTb luminescence intensity also increases with time as expected, consistent with an associated decrease in concentration quenching effects. The spectral shift slows down with time and stops almost completely after about 40 minutes of heating at this temperature. This indicates the ending of the DCJTb net mass transfer and redistribution process, signaling that a uniform concentration level of DCJTb across the entire NPB layer has been reached.

The same trend can be observed in the current efficiency trend, where again efficiency increases are initially observed, but then the trend plateaus almost completely after ~40 minutes (Fig. 5.25). Clearly,

the efficiency trend follows the change in DCJTB concentration. Quite remarkably, the final EL spectrum of the device with the neat DCJTB layer (device A) is very similar to that of the corresponding control device (device B). This shows that the DCJTB concentration in the devices with the neat DCJTB layer is similar to the concentration in the corresponding control devices, indicating that the inclusion of the NPB:MoO₃ diffusion barrier limits the diffusion of the DCJTB to the top 10 or 15 nm NPB host layer. Note that the final efficiency of the heated devices is higher than that of the control devices. This could be attributed to improved interface structure between layers due to diffusion and/or optimized carrier balance due to heating^[74].

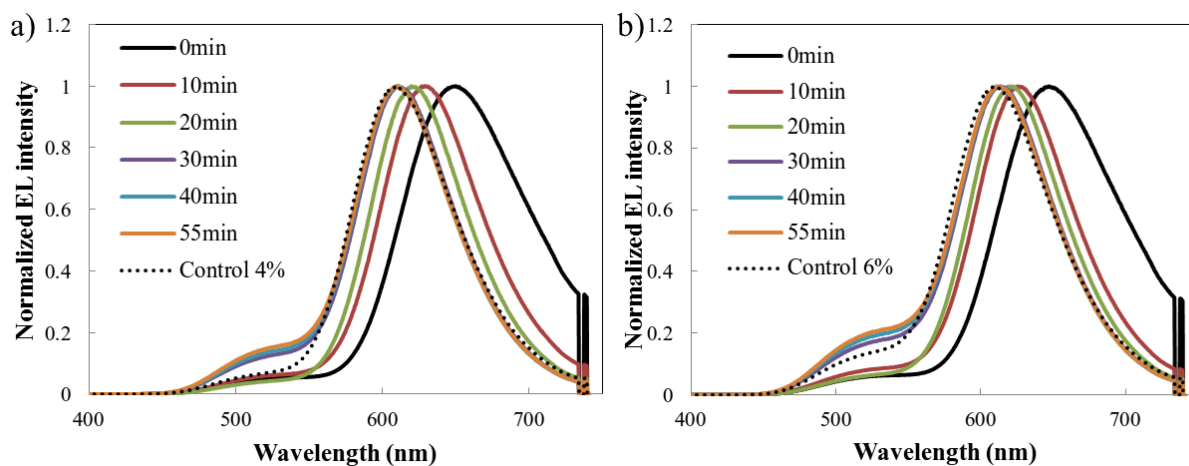


Figure 5.24 EL spectra from the devices (with 15nm NPB (a) and 10nm NPB (b)) with the neat DCJTB layer collected periodically while at 100 °C. The dotted lines represent the EL spectra of the corresponding control devices.

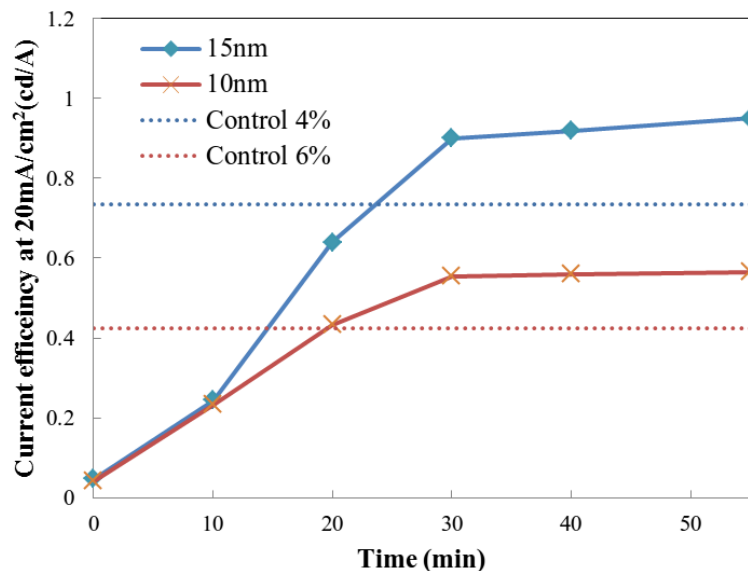


Figure 5.25 Current efficiencies collected every few minutes from the devices with the neat DCJTb layer during the heating step for the device with the 15nm host NPB layer (the blue solid line); and the device with the 10nm host NPB layer (the red solid line). The dotted lines represent the current efficiency of the corresponding control devices.

5.5.3 Demonstrating the ability of the diffusion barrier to produce OLEDs with highly controlled device structure and performance

Experimental Procedure

The use of HTM:MoO₃ diffusion barriers in OLEDs is demonstrated for obtaining controlled doping levels when a luminescent material is introduced in a host via diffusion. In the previous experiment, the neat DCJTb layer is deposited on the host NPB layer through standard thermal vacuum deposition. In this experiment, however, a luminescent material is introduced into a host material layer via diffusion by contact with a donor substrate, and both the diffusion depth and dopant concentration are controlled by utilizing the diffusion barrier.

Device fabrication steps including the diffusion-based doping step are depicted in Figure 5.26. First, a ~3 nm thick MoO₃ hole injection layer (HIL), a 60-x nm thick NPB doped with 50% MoO₃ layer, and a x nm thick NPB neat layer are vacuum-deposited on an ITO coated glass substrate (acceptor substrate).

In one device x is 10nm whereas in the other device x is 15nm. The MoO_3 -doped NPB layer in this device functions as both a HTL and diffusion barrier whereas the neat NPB layer functions as host to be doped by DCJTB via diffusion. The acceptor substrate is then placed in physical contact with a glass “donor substrate” pre-coated with a ~ 20 nm thick layer of DCJTB by holding them together using a 5 mm thick neodymium magnet plate (remanent magnetization of 1.22-1.28 T) and a 2 mm thick steel plate. Still in contact, the substrates are heated for 100 minutes on a hot plate at 100°C in a dry nitrogen environment in order to drive the diffusion of DCJTB from the donor substrate into the NPB layer on the acceptor substrate. After heating, the donor substrate is removed, the acceptor substrate is put back in the vacuum system, and a ~ 40 nm thick Alq_3 ETL followed by a ~ 0.5 nm thick LiF EIL and a ~ 70 nm aluminum cathode are deposited to complete the device. The schematic presentation for the dopant-diffused device is shown in Figure 5.27 (a). Finally, in order to drive the DCJTB deeper into the NPB layer and achieve a more uniform dopant concentration, the completed devices are heated to 100°C for one hour. During that time the device EL spectrum and current efficiency are measured periodically every few minutes.

For reference, the device used in the previous experiment is used again in this experiment. The structure of the control device is therefore $\text{ITO}/\text{MoO}_3(3\text{ nm})/\text{NPB}:\text{MoO}_3(60-x\text{ nm})/\text{NPB}:\text{DCJTB}(x\text{ nm}, y\%)/\text{Alq}_3(40\text{ nm})/\text{LiF}(0.5\text{ nm})/\text{Al}(70\text{ nm})$, where x is 10 nm and y is 6% whereas in the other device x is 15 nm and y is 4% (Fig. 5.27 (b)). The amount of DCJTB in the control device would correspond to the amount in the “diffused-dopant” device for the 100 minute contact duration used above. This DCJTB amount was estimated based on the experimental results in Section 5.1 where diffusion of molecules from the donor to the acceptor substrates proceeds at a constant rate for at least the initial 100 minutes. Given this linear correlation between the number of DCJTB molecules and time, the amount of DCJTB that gets diffused from the donor substrate into the host during any given contact duration (in this case 100 minutes) can be accurately estimated.

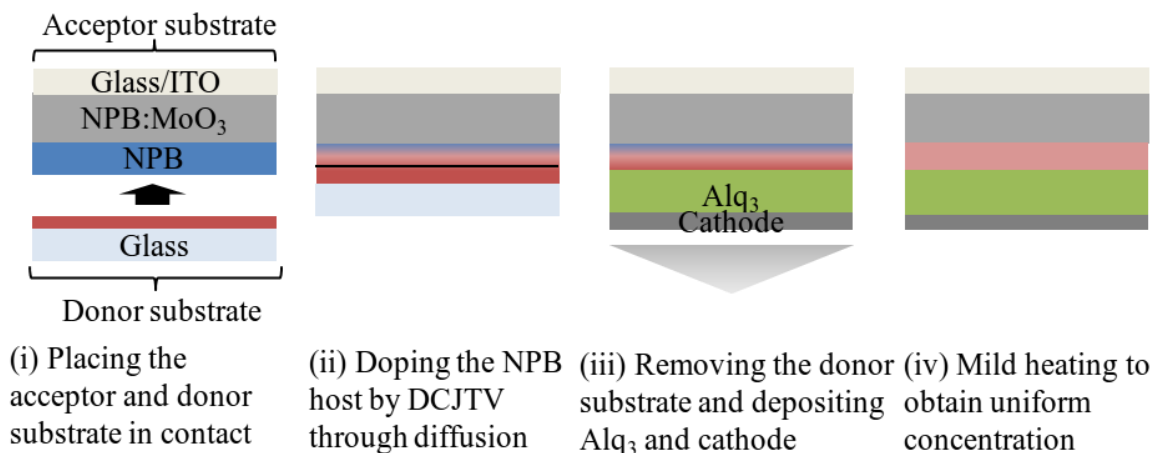


Figure 5.26 A schematic diagram illustrating the steps of the procedure followed for the diffused-dopant OLEDs. (i)-(iii) illustrates the steps of introducing the dopant via diffusion and (iv) illustrates the subsequent heating step used for making the DCJTB concentration uniform across the layer.

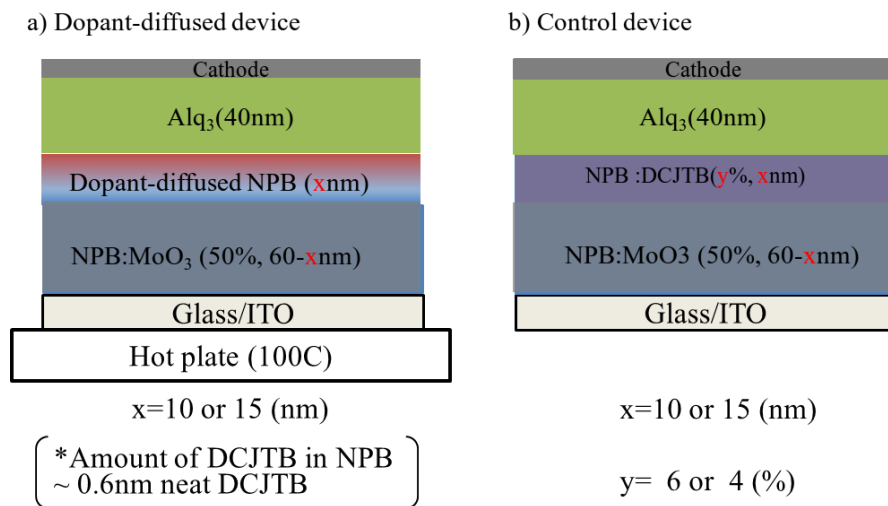


Figure 5.27 Schematic presentation for the device structure of (a) the dopant-diffused device and (b) the control device. The concentration of DCJTB in NPB is supposed to be graded as shown in the figure since DCJTB is transferred to the host through physical contact. The structure with the graded DCJTB concentration appears in the step (iii) of Fig. 5.26.

Results and discussion

Figures 5.28 and 5.29 show the EL spectra and current efficiency, respectively, of the two “diffused-dopant” devices collected periodically at 100 °C. Similar to the previous experiment,

significant blue-shift of the EL spectrum and efficiency increases are initially observed, and then slow with time. This is again due to the DCJTB redistribution process, indicating a uniform concentration level of DCJTB across the entire NPB layer. The final EL spectrum and efficiency of each of the two dopant-diffused devices are similar to those of the corresponding control devices. This shows that the DCJTB concentration in the “diffused-dopant” devices is very similar to that in the corresponding control devices, indicating that earlier estimation of the amount of DCJTB diffused into the NPB in a given period of contact time was accurate. This indicates that highly controlled doping levels can indeed be achieved when using this doping method. It also shows that the NPB:MoO₃ diffusion barrier is still effective when a luminescent material is introduced via diffusion, and makes it possible to use diffusion followed by a simple heating step to reach uniform and predictable dopant concentration levels in OLEDs.

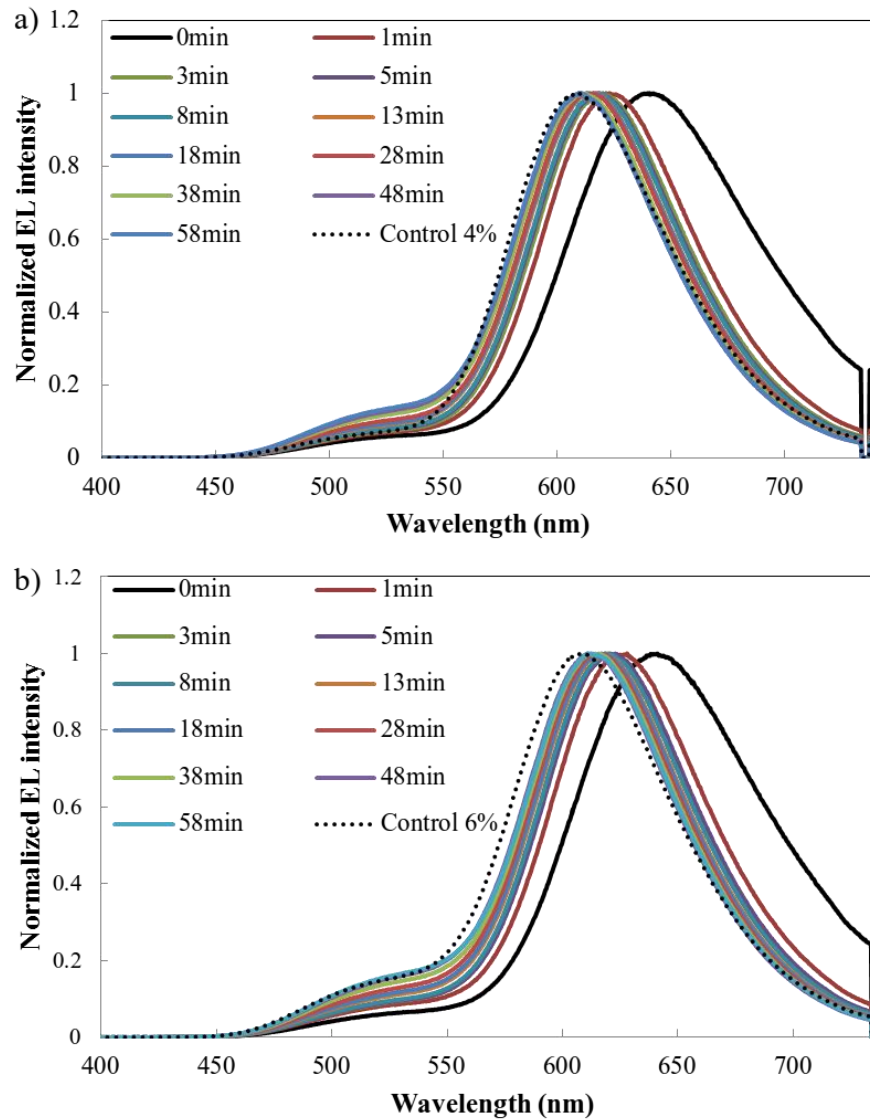


Figure 5.28 EL spectra collected every few minutes from the “diffused-dopant” devices during the heating step (of Fig.5.26 (iv)) for the device with the 15nm host NPB layer (a); and the device with the 10nm host NPB layer (b). The dotted lines represent the EL spectra of the corresponding control devices.

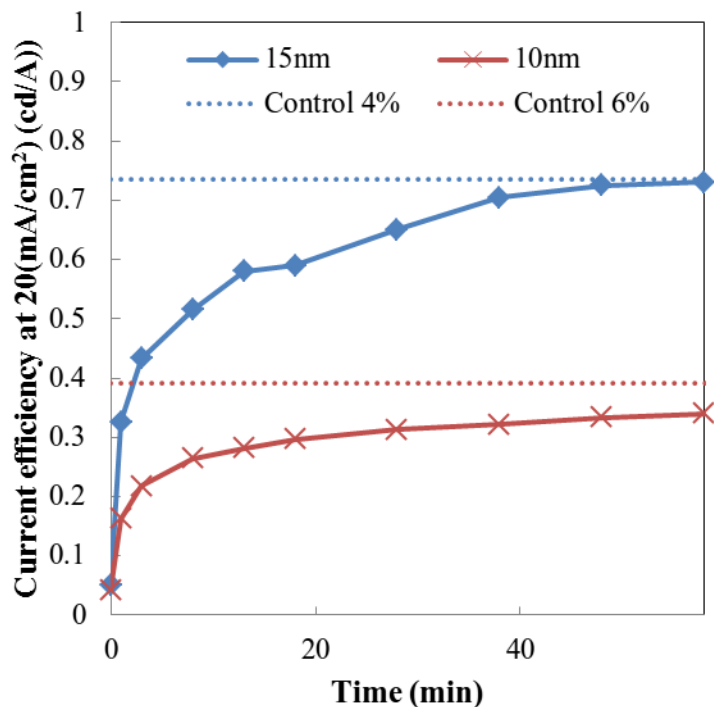


Figure 5.29 Current efficiencies collected every few minutes from the “diffused-dopant” devices during the heating step (of Fig.5.26 (iv)) for the device with the 15 nm host NPB layer (the blue solid line); and the device with the 10 nm host NPB layer (the red solid line). The dotted lines represent the current efficiency of the corresponding control devices.

5.6 Theoretical analysis of dopant concentration profile

Introduction

The transient dopant concentration profiles of the OLED devices produced by thermal diffusion (“diffused-dopant” devices), which corresponds to the devices fabricated in Section 5.2, are estimated based on the Fick’s diffusion theory. Although dopant concentration profiles of the devices can be roughly inferred from the experimental results, actual dopant concentration profiles have not been confirmed. The theoretical analysis helps estimate actual dopant concentration profiles in the “diffused-dopant” devices. In addition, the theoretical analysis allows us to roughly estimate the time required to obtain desirable dopant concentration.

Two parameters including the diffusion coefficient of the organic film “ D ” and the mass transfer coefficient “ h ” are required for the theoretical analysis. These two parameters are determined from the other two experimental observations. The diffusion coefficient “ D ” is obtained from the experimental observation in Subsection 5.5.2. In this experiment, OLED devices with the diffusion barrier are fabricated, and efficiency changes due to thermal diffusion with heating time are monitored. The mass transfer coefficient “ h ” is introduced for the molecular mass transfer between the donor film and the host film which are physically contacted. The mass transfer coefficient is obtained from the experimental observation in Section 5.2. In this experiment, the luminescent material is transferred through solid state diffusion from a donor substrate to dope the host film on another substrate, and the amount of the luminescent material in the host film with contact time is monitored. By comparing the experimental observations with theoretical fits, the diffusion coefficient and the mass transfer coefficient are determined. After determining the two parameters, the transient dopant concentration profiles of the OLED devices produced by thermal diffusion are theoretically obtained.

This section consists of three subsections. First, the diffusion coefficient D and the mass transfer coefficient h are determined in Subsections 5.6.1 and 5.6.2, respectively. Then, the transient dopant concentration profiles of the “diffused-dopant” devices are then theoretically estimated in Subsection 5.6.3.

5.6.1 Determining the Diffusion Coefficient

Model and Equations

The diffusion coefficient of the organic film “ D ” is obtained from the experimental observation in Subsection 5.5.2. The model considered here is adjacent NPB and DCJTB layers sandwiched by impermeable layers (Fig. 5.30). This model corresponds to the experiment performed in Subsection 5.5.2. In the actual device, the impermeable layers correspond to the Alq₃ layer and the NPB:MoO₃ diffusion barrier (Fig. 5.31). Assuming that molecular diffusion is directional perpendicular to the plane of the layers, molecular diffusion obeys Fick’s diffusion theory, and the layers sandwiching the organic

layers are completely impermeable, the transient dopant concentration $C(x,t)$ is given by infinite sum of error function:

$$C(x,t) = \frac{1}{2}C_0 \sum_{n=0}^{\infty} \left\{ \operatorname{erf}\left(\frac{-(x-d_s) - 2n(d_s+d_a)}{2\sqrt{Dt}}\right) + \operatorname{erf}\left(\frac{(x-d_s) + 2d_s + 2n(d_s+d_a)}{2\sqrt{Dt}}\right) \right\} \\ + \frac{1}{2}C_0 \sum_{n=1}^{\infty} \left\{ \operatorname{erf}\left(\frac{-(x-d_s) + 2n(d_s+d_a)}{2\sqrt{Dt}}\right) + \operatorname{erf}\left(\frac{(x-d_s) + 2d_s - 2n(d_s+d_a)}{2\sqrt{Dt}}\right) \right\} \quad \text{----- (eq. 5.1)}$$

*erf(z): Error function $\operatorname{erf}(z) = \frac{2}{\pi^{1/2}} \int_0^z \exp(-\eta^2) d\eta$

where x represents the distance from the impermeable/DCJTB interface, C_0 the initial concentration of the DCJTB layer, d_s and d_a the thickness of the DCJTB and the NPB layers, and D denotes the diffusion coefficient of DCJTB molecules in the matrix. In addition, in order to evaluate uniformity of dopant concentration profile across the host layer, a uniformity parameter $U(t)$ is introduced. This parameter corresponds to the difference between the maximum dopant concentration ($C_{Max}(t)$) and the minimum dopant concentration ($C_{Min}(t)$) within the two organic layers divided by the sum of them:

$$U(t) = -(C_{Max}(t) - C_{Min}(t))/(C_{Max}(t) + C_{Min}(t)) \quad \text{----- (eq. 5.2)}$$

Note that $C_{Max}(t)$ corresponds to the dopant concentration at the interface between the impermeable layer and the DCJTB layer ($x=0$), and $C_{Min}(t)$ corresponds to the one at the interface between the NPB layer and the impermeable layer ($x = d_s + d_a$) at time t in this model.

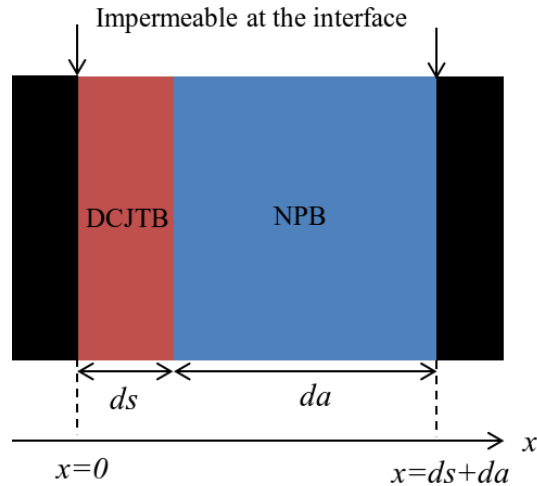


Figure 5.30 Schematic representation for the theoretical model. Adjacent NPB and DCJTJ layers are sandwiched by impermeable layers in this model.

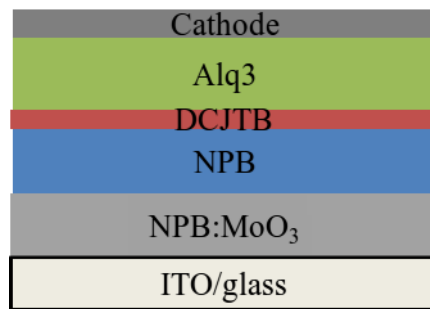


Figure 5.31 The actual device structure for the model in Fig. 5.30.

Results and discussion

Figure 5.32 shows the change in the uniformity parameter of dopant concentration ($U(t)$) with time for various diffusion coefficients. The experimental result of the change in luminescent efficiency due to heating with time is also shown. As discussed, the efficiency increases initially but then the trend plateaus almost completely after ~40 minutes. Since the efficiency change stops following the end of the dopant redistribution process, the efficiency and uniformity reach the plateau at the same time. The diffusion coefficient D is therefore extracted by fitting the uniformity parameter $U(t)$ to the efficiency change. As shown in the figure, the uniformity parameter with the diffusion coefficient of $D = 4 \times$

10^{-20} (m^2/s) reaches the plateau after ~ 40 minutes. This allows us to determine the diffusion coefficient of the organic film as $D = 4 \times 10^{-20}$ (m^2/s). It would be interesting to estimate the transient dopant concentration profile across the organic layers using the extracted diffusion coefficient D (Fig. 5.33). It is clearly demonstrated that the concentration of DCJTb significantly decreases with time at the boundary with the Alq_3 layer ($x=0$) where the recombination zone exists. The decrease in dopant concentration at the recombination zone with time is consistent with the experimental observation which shows the increase in efficiency with heating time.

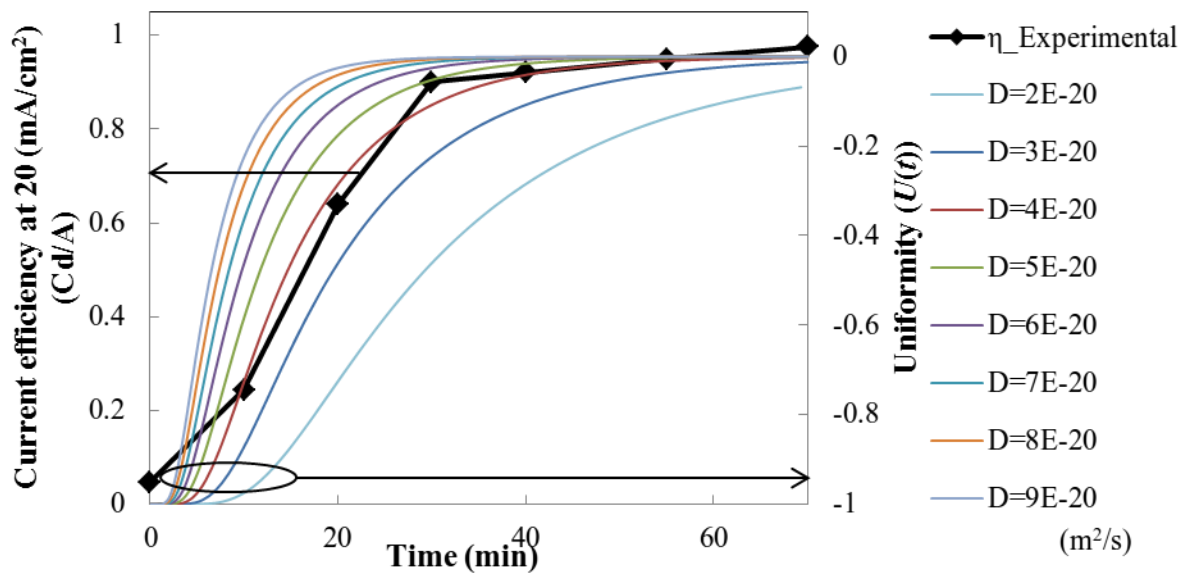


Figure 5.32 The change in the uniformity of dopant concentration ($U(t)$) with time for various diffusion coefficients (right axis). The experimental result of the change in luminescent efficiency due to heating with time is also shown (left axis).

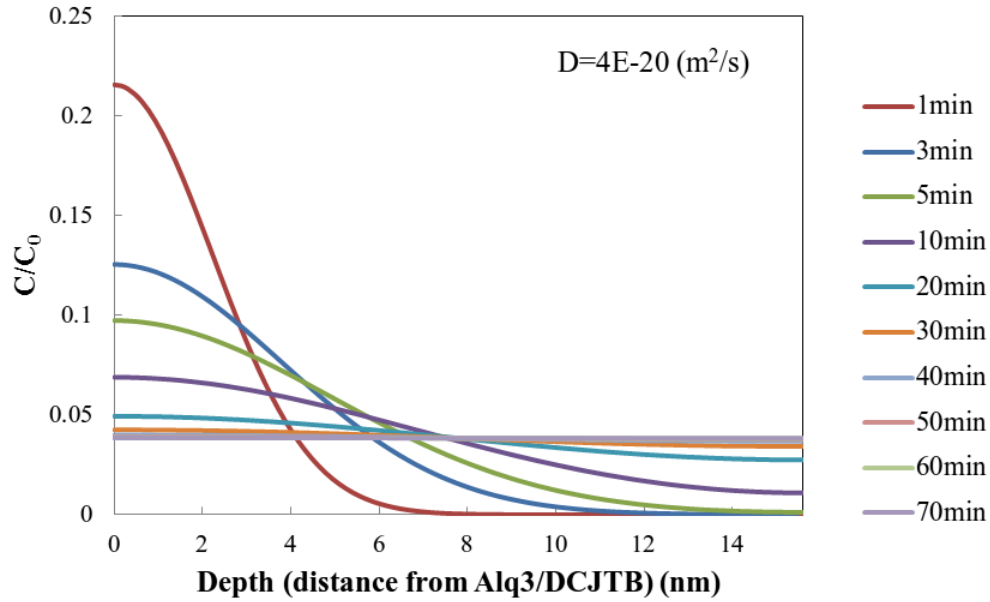


Figure 5.33 The transient dopant concentration distribution across the NPB layer.

5.6.2 Determining the Mass Transfer Coefficient

Model and Equations

The mass transfer coefficient between the donor film and the host film when in physical contact is obtained from the experimental observation in Section 5.1. Here, DCJTB molecules are transferred to the host NPB film via diffusion by physical contact between the DCJTB donor film and the host NPB film (Fig. 5.34). In this model shown in Figure 5.35, in addition to the assumptions used in the previous model, an infinite source is assumed for the donor DCJTB film. Also, since the DCJTB molecules are transferred through physical contact in this case, a diffusion resistance exists between the DCJTB film and the NPB film. The mass transfer rate between the donor film and the host film is assumed to be proportional to the difference in concentrations at the interface. Based on these assumptions, the diffusion equation can be solved as follows:

$$C(x, t) = C_0 - \sum_{n=1}^{\infty} A_n \cos(\lambda_n x) \exp(-\lambda_n^2 Dt) \quad \text{----- (eq. 5.3)}$$

$$A_n = \frac{2C_0 \sin \lambda_n L}{\lambda_n L + \sin \lambda_n L \cos \lambda_n L}$$

$$\left(\lambda_n \text{ satisfies: } \cot \lambda_n L = \frac{\lambda_n L}{(hL/D)} \right)$$

where L represents the thickness of the host film.

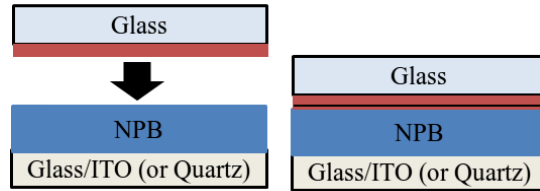


Figure 5.34 Schematic representation for the actual experiment considered in this model.

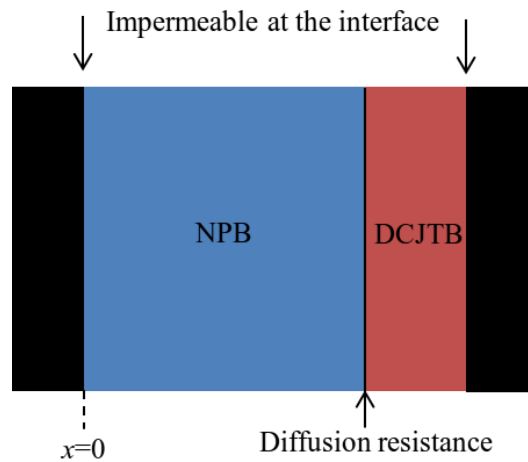


Figure 5.35 Schematic representation for the theoretical model based on the actual experiment in Fig. 5.34. DCJTb molecules are transferred to the host NPB film via diffusion by physical contact in this model.

Results and discussion

The total amount of the dopant in the host film over time for various mass transfer coefficients is shown in Figure 5.36 with the experimental result obtained in Section 5.1. The total amount of the dopant across the entire host film is given by the integration with respect to $C(x,t)$ from 0 to L . Diffusion coefficient D is assumed to be the same as the diffusion coefficient determined in the

previous model since the same host film and temperature are used in this experiment. The mass transfer coefficient h is determined as $h = 2.16 \times 10^{-21}$ by fitting the theoretical result to the experimental result.

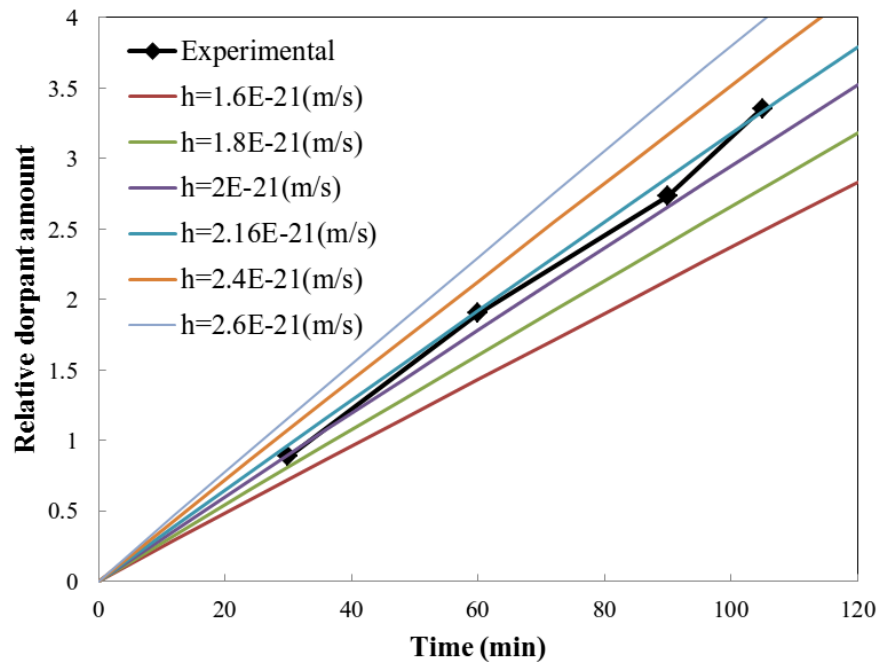


Figure 5.36 The total amount of the dopant in the host film with time for various mass transfer coefficients. The total amount is shown as the relative amount to the amount of DCJTb in 5nm NPB doped with 4% DCJTb by volume.

5.6.3 Estimating the Transient Dopant Concentration Profile

Finally, by using the diffusion coefficient and the mass transfer coefficient that are determined in the previous models, the transient dopant profile of the “diffused-dopant” device, which corresponds to the device fabricated in Section 5.2, is obtained (Fig. 5.37). The same equation (eq. 5.3) used in the previous model is applied since the molecular diffusion process via contact is the same in both experiments (experiments in Sections 5.1 and 5.2). From this result, it has been shown that the concentration distribution tends to be non-uniform across the host film as expected. This result justifies

the use of the diffusion barrier to achieve uniform dopant concentration in the diffusion-based technique. This theoretical analysis also allows us to obtain the mass transfer rate as shown in Subsection 5.6.2. From the estimated mass transfer rate, the time required to transfer the desirable amount of a dopant can be roughly estimated.

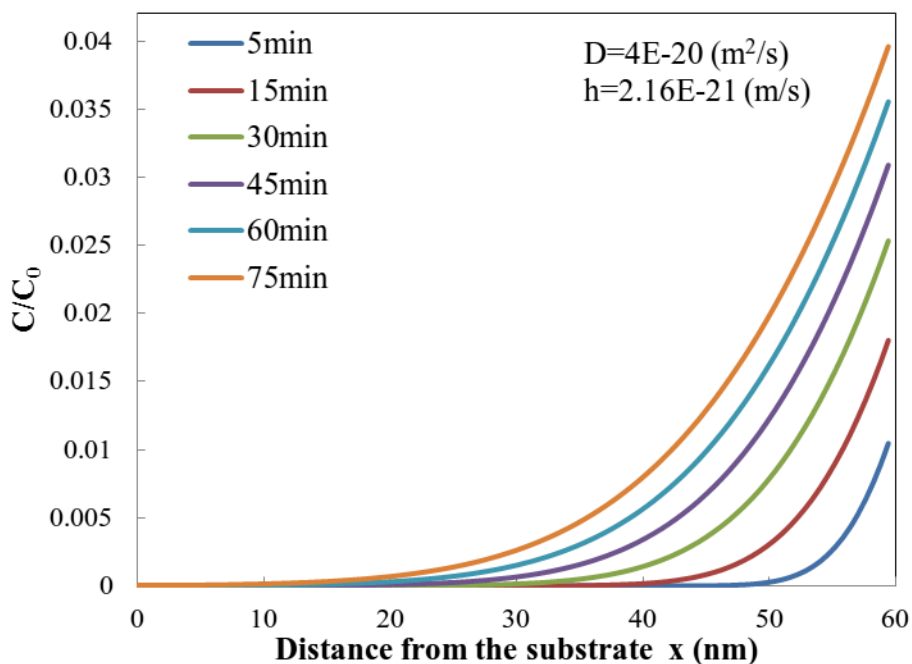


Figure 5.37 The transient dopant profile of the “diffused-dopant” device.

5.7 Conclusions

In this chapter, the potential of the diffusion of a luminescent material from a donor substrate placed in physical contact with the OLED substrate is assessed as an approach for maskless RGB color patterning of small molecule OLED displays. Also, the use of solvent vapor exposure is explored as a method to reduce diffusion time. In addition, the potential of a semiconducting diffusion barrier as a method to block undesirable diffusion is assessed. Finally, the transient dopant concentration of the dopant-diffused device is theoretically estimated. The result shows that the dopant concentration of the

devices is graded as expected. This justifies the use of the diffusion barrier to achieve uniform dopant concentration in the diffusion-based technique. In addition, the result allows us to estimate the time required to obtain the desirable amount of dopant in the host film via diffusion. The conclusions of a series of these studies are summarized as follows:

- ❑ Doping levels typical for those used in OLEDs can be achieved through solid state diffusion between donor and host films which are placed in physical contact
- ❑ Devices produced by the technique demonstrate performance similar to those produced by standard co-deposition
- ❑ Red, green and blue OLEDs can be fabricated side-by-side on one substrate without the use of shadow masks by selective diffusion of a luminescent material using local ITO Joule heating
- ❑ Diffusion time can be significantly reduced by solvent vapor exposure
- ❑ Exposing a neat layer of a HTM to solvent vapor does not affect device performance while efficiency is reduced when a HTM:dopant premixed layer is exposed
- ❑ The use of the semiconducting diffusion barriers allows controlling the diffusion depth and achieving uniform concentration of luminescent dopants in OLEDs when using diffusion-based fabrication processes
- ❑ The graded dopant concentration of the diffused-dopant devices is confirmed by theoretical analysis, which justifies the use of the diffusion barrier in the diffusion-based technique
- ❑ A simple model for estimating the time required to transfer amount of dopant from a donor film to a host film via diffusion is provided

Chapter 6

Summary and Future Work

In this work, two novel RGB color patterning techniques for OLED display fabrication are proposed as alternatives to the FMM technique. The potential and technical feasibility of these approaches are investigated. The summary of results and the conclusions for the investigations on each technique are shown in parallel as follows.

6.1 Technique 1: Color patterning using the laser-patterned PI shadow masks

Summary of research results

The first technique is color patterning using the laser-patterned PI sheet as a contact shadow mask. First, the capability of the laser-patterned PI sheet as a shadow mask and the effect of contact of organic layers with the PI sheet on device performance are investigated. The results of these investigations verify that the laser-patterned PI sheets have strong capability to deposit OLED materials with high line edge uniformity and limited shadow effects without compromising device performance. Furthermore, RGB OLEDs have been successfully fabricated by standard thermal vacuum deposition utilizing the laser-patterned PI shadow masks. The results show that this technique has strong potential for achieving high performance displays with high pixel density (>330 ppi) and high aperture ratio ($\sim 100\%$) without compromising device performance. In addition, as a variant of this technique, the *in-situ* shadow mask patterning technique is also proposed. For this technique, the protective layer is introduced to avoid contamination of the underlying substrates. By using the protective layer, the OLED device with the size of $16\ \mu\text{m}$ -by- $130\ \mu\text{m}$ sub-pixel size is fabricated through the *in-situ* shadow mask patterning technique without affecting device performance. Finally, the RGB OLEDs with small feature sizes less than $25\ \mu\text{m}$ are successfully fabricated on one substrate using this technique. The research results are summarized below.

Conclusions and future work

The successful fabrication of RGB OLEDs with small feature sizes and high aperture ratio indicates that the laser-patterned PI mask technique is reliable enough to be put into practical use. In fact, test samples of the laser-patterned PI shadow masks have been fabricated and the practical applicability in actual display production is currently being tested. In contrast, further investigations and improvement are required for the *in-situ* shadow mask patterning technique. In particular, defects are observed in the emissive areas of the devices fabricated through this technique. This is perhaps due to ablation debris from some limited unintentional ablation of the bottom protective PI sheet which is left on the back side of the patterned PI sheet. The contamination issue could be addressed, for example, by replacing the bottom protective PI sheet with any other thin sheet which is resistant to laser ablation, such as a thin glass sheet. Alternatively, the contamination may be also be reduced by utilizing dry etching when the PI sheet is penetrated to create apertures. Investigations on these alternative approaches are required to use this technique in a practical manner.

6.2 Technique 2: Color patterning via diffusion of a luminescent material

Summary of research results

The other technique proposed here is color patterning via selective diffusion of a luminescent material from a donor substrate to an acceptor substrate. First, doping levels of a luminescent material achieved via diffusion and effects on device performance are studied. The results show that doping levels typical for those used in OLEDs can be achieved through solid state diffusion between donor and host films which are placed in physical contact. The investigations on device performance reveal that devices produced by this technique demonstrate performance comparable to those produced by standard co-deposition. Furthermore, using the maskless color patterning technique, RGB OLEDs are successfully fabricated side-by-side on one substrate. In this demonstration, positional selectivity of diffusion is achieved through local Joule heating using the OLED ITO anodes for that purpose. Shadow masks, microstamps or any mechanical alignment for color patterning is therefore not employed to

obtain the different OLED emission colors in this case, which offers significant advantage in color patterning processes.

From these results, it has been demonstrated that the diffusion-based maskless color patterning technique is technically feasible and potentially provides us an opportunity to achieve OLED display fabrication with higher reliability. In addition, it is demonstrated that diffusion time can be significantly reduced by solvent vapor exposure. The reduction of diffusion time enhances the technical value of this technique. However, the preliminary results show that exposing a premixed HTM:dopant layer to solvent exposure can reduce device efficiency depending on materials. Further investigations are required to clarify effects on device performance. Also, the use of the semiconducting diffusion barrier is introduced as a method to control diffusion depth and dopant concentrations. OLED devices doped via diffusion are fabricated with highly controlled diffusion depth and dopant concentration utilizing the diffusion barrier. The result demonstrates that the use of the diffusion barrier is helpful to control diffusion depth and dopant concentrations when a luminescent material is doped via diffusion. Finally, a simple model for predicting the dopant concentration profile and the approximate time needed to obtain a certain desired dopant concentration level is provided.

Conclusions and future work

Although RGB OLEDs have been successfully fabricated by using the diffusion-based maskless color patterning technique, the development of this technique is still in the early stages. Further investigations are required for practical use. For example, the resolution limitation needs to be investigated. The resolution is likely limited due to lateral diffusion of the dopant in the host layer, which causes the dopant to spread outside of the desired area boundaries. Preliminary investigations reveal that such lateral diffusion is limited to ~5-10 μm . For high resolution displays, this lateral diffusion can perhaps be readily prevented through the use of pre-patterned grooves or separators in the OLED substrate. Also, compatibility of this technique with wide variety of materials needs to be tested. The results have shown that the diffusion property depends on T_g of organic materials. However, the diffusion property could also depend on other factors such as molecular structure and density of films. In order to demonstrate applicability of this technique to a wide variety of materials, further systematic

studies are required. In addition, while the enhancement of diffusion by solvent vapor exposure has been confirmed, the effects on devices have not been clarified. The preliminary investigation indicates that device efficiency can be significantly reduced when a HTM:dopant premixed layer is exposed to solvent vapor depending on materials. In order to clarify the mechanism and to discover methods to reduce the adverse effects, further investigation is necessary. Such investigations may include effects of solvent vapor exposure on morphology and optical properties of organic films in addition to investigations on the effects on device performance.

Bibliography

- [1] C. W. Tang and S. A. VanSlyke, "Organic electroluminescent diodes," *Appl. Phys. Lett.*, vol. 51, no. 12, p. 913, 1987.
- [2] S. Forrest, P. Burrows, and T. Mark, "The dawn of organic electronics," *Spectrum, IEEE*, vol. 37, no. 8, pp. 29–34, 2000.
- [3] J. K. Borchart, "Developments in organic displays," *Mater. Today*, vol. 7, no. 9, pp. 42–46, 2004.
- [4] B. Geffroy, P. le Roy, and C. Prat, "Organic light-emitting diode (OLED) technology: materials, devices and display technologies," *Polym. Int.*, vol. 55, no. 6, pp. 572–582, Jun. 2006.
- [5] J. H. Kwon, R. Pode, and H. D. Kim, "High-Performance Organic Light-Emitting Diode Displays," *Springer US*, pp. 57–81, 2013.
- [6] L. . Hung and C. . Chen, "Recent progress of molecular organic electroluminescent materials and devices," *Mater. Sci. Eng. R Reports*, vol. 39, no. 5–6, pp. 143–222, Dec. 2002.
- [7] H. Sasabe and J. Kido, "Recent Progress in Phosphorescent Organic Light-Emitting Devices," *European J. Org. Chem.*, vol. 2013, no. 34, pp. 7653–7663, Dec. 2013.
- [8] NPD DisplaySearch, "LCD TV Shipment Growth to Improve in 2012 , Driven by 40 " and Larger Sizes," 2012. [Online]. Available: http://www.displaysearch.com/cps/rde/xchg/displaysearch/hs.xsl/120103_lcd_tv_shipment_growth_to_improve_in_2012_driven_by_40_and_larger_sizes.asp.
- [9] P. E. Burrows, G. Gu, V. Bulovi, Z. Shen, S. R. Forrest, and M. E. Thompson, "Achieving Full-Color Organic Light-Emitting Devices for Lightweight , Flat-Panel Displays," *Electron Devices, IEEE Trans.*, vol. 44, no. 8, pp. 1188–1203, 1997.
- [10] T. Tsujimura, *OLED Displays Fundamentals and Applications*. A John Wiley & Sons, Inc., Publication, 2012.
- [11] Y. Kajiyama, Q. Wang, K. Kajiyama, S. Kudo, and H. Aziz, "Vacuum Deposition of OLEDs with Feature Size $s \leq 20\mu\text{m}$ Using a Contact Shadow Mask Patterned In-situ by Laser Ablation," *Dig. Tech. Pap.-Soc. Inf. Disp. Int. Symp.*, vol. 43, no. 1, p. 1544 1547, 2012.

- [12] Y. Kajiyama, K. Joseph, K. Kajiyama, S. Kudo, and H. Aziz, "Recent progress on the vacuum deposition of OLEDs with feature sizes $\leq 20 \mu\text{m}$ using a contact shadow mask patterned in-situ by laser ablation," *Proc. SPIE*, vol. 8829, p. 882919, Sep. 2013.
- [13] Y. Kajiyama, K. Joseph, K. Kajiyama, S. Kudo, and H. Aziz, "Small feature sizes and high aperture ratio organic light-emitting diodes by using laser-patterned polyimide shadow masks," *Appl. Phys. Lett.*, vol. 104, no. 5, p. 053303, Feb. 2014.
- [14] J. H. Brannon, J. R. Lankard, a. I. Baise, F. Burns, and J. Kaufman, "Excimer laser etching of polyimide," *J. Appl. Phys.*, vol. 58, no. 5, p. 2036, 1985.
- [15] H. M. Phillips, D. L. Callahan, R. Sauerbrey, G. Szabó, and Z. Bor, "Sub-100 nm lines produced by direct laser ablation in polyimide," *Appl. Phys. Lett.*, vol. 58, no. 24, p. 2761, 1991.
- [16] B. M. T. Bernius, M. Inbasekaran, J. O. Brien, and W. Wu, "Progress with Light-Emitting Polymers," no. 23, pp. 1737–1750, 2000.
- [17] C. Sekine, Y. Tsubata, T. Yamada, M. Kitano, and S. Doi, "Recent progress of high performance polymer OLED and OPV materials for organic printed electronics," *Sci. Technol. Adv. Mater.*, vol. 15, no. 3, p. 034203, Jun. 2014.
- [18] J. Kido, M. Kimura, and K. Nagai, "Multilayer white light-emitting organic electroluminescent device.," *Science*, vol. 267, no. 5202, pp. 1332–4, Mar. 1995.
- [19] H. Sasabe and J. Kido, "Development of high performance OLEDs for general lighting," *J. Mater. Chem. C*, vol. 1, no. 9, p. 1699, 2013.
- [20] S. N. Kumar, R. John, S. Lauer, W. Little, and B. Daul, "Electroforming Technology for Manufacturing Thin Metal Masks with Very Small Apertures for OLED Display Manufacturing," pp. 211–214, 2015.
- [21] M. M. Ling and Z. Bao, "Thin Film Deposition , Patterning , and Printing in Organic Thin Film Transistors," *Chem. Mater.*, vol. 16, no. 23, pp. 4824–4840, 2004.
- [22] R. A. O. Light-emitting, S. Hong, J. Sim, I. Seo, K. Kim, S. Bae, H. Lee, N. Lee, and J. Jang, "New Pixel Design on Emitting Area for High Diode Displays," *J. Disp. Technol.*, vol. 6, no. 12, pp. 601–606, 2010.
- [23] H. Jin and J. C. Sturm, "Super-High Resolution Transfer Printing for Full-Color OLED Display Patterning," *SID Symp Dig. Tech Pap*, vol. 40, pp. 597–599, 2009.

- [24] J. Choi, K.-H. Kim, S.-J. Choi, and H. H. Lee, "Whole device printing for full colour displays with organic light emitting diodes," *Nanotechnology*, vol. 17, no. 9, pp. 2246–2249, May 2006.
- [25] M. B. Wolk, J. P. Baetzold, E. Bellmann, T. R. Hoffend, Jr., S. Lamansky, Y. Li, R. R. Roberts, V. Savvateev, J. S. Staral, and W. a. Tolbert, "Laser Thermal Patterning of OLED Materials," *Opt. Sci. Technol. SPIE 49th Annu. Meet. Int. Soc. Opt. Photonics*, vol. 5519, pp. 12–23, Nov. 2004.
- [26] S. Lamansky, T. R. Hoffend, Jr., H. Le, V. Jones, M. B. Wolk, and W. a. Tolbert, "Laser induced thermal imaging of vacuum-coated OLED materials," *Opt. Photonics 2005. Int. Soc. Opt. Photonics*, vol. 5937, p. 593702, Aug. 2005.
- [27] S. H. Ko, H. Pan, S. G. Ryu, N. Misra, C. P. Grigoropoulos, and H. K. Park, "Nanomaterial enabled laser transfer for organic light emitting material direct writing," *Appl. Phys. Lett.*, vol. 93, no. 15, p. 151110, 2008.
- [28] T. Tada and A. Nakamura, "Three-Color Polymer Light-Emitting Devices Patterned by Maskless Dye Diffusion onto Prepatterned Electrode," *Jpn. J. Appl. Phys., Part 2*, vol. 38, pp. 1143–1145, 1999.
- [29] F. Pschenitzka and J. C. Sturm, "Three-color organic light-emitting diodes patterned by masked dye diffusion," *Appl. Phys. Lett.*, vol. 74, no. 13, p. 1913, 1999.
- [30] C. Wu, C. Yang, H. Chang, C.-W. Chen, and C.-C. Lee, "Finite-source dye-diffusion thermal transfer for doping and color integration of organic light-emitting devices," *Appl. Phys. Lett.*, vol. 77, no. 6, p. 794, 2000.
- [31] A. Nakamura, T. Tada, M. Mizukami, S. Hirose, and S. Yagyu, "Three-color polymer light-emitting diodes by stamped dye diffusion," *Appl. Phys. Lett.*, vol. 80, no. 12, p. 2189, 2002.
- [32] H. Ohshima, "Past, Present and Future of Mobile Displays," *Twent. Int. Work. on. IEEE*, pp. 13–16, 2013.
- [33] J. Pollack, "Displays of a different stripes," *Spectrum, IEEE*, vol. 43, no. 8, p. 40 44, 2006.
- [34] L. Fang, O. C. Au, and N. Cheung, "Subpixel Rendering: From Font Rendering to Image Subsampling," *IEEE Signal Process. Mag.*, vol. 30, no. 3, pp. 177–183, 2013.
- [35] S. H. Cho, S. M. Lee, and M. C. Suh, "Enhanced efficiency of organic light emitting devices (OLEDs) by control of laser imaging condition," *Org. Electron.*, vol. 13, no. 5, pp. 833–839, May 2012.

- [36] S. H. Ko and C. P. Grigoropoulos, "Unconventional , Laser Based OLED Material Direct Patterning and Transfer Method," *InTech*, 2011.
- [37] A. a. Zakhidov, J.-K. Lee, H. H. Fong, J. a. DeFranco, M. Chatzichristidi, P. G. Taylor, C. K. Ober, and G. G. Malliaras, "Hydrofluoroethers as Orthogonal Solvents for the Chemical Processing of Organic Electronic Materials," *Adv. Mater.*, vol. 20, no. 18, pp. 3481–3484, Jul. 2008.
- [38] P. G. Taylor, J.-K. Lee, A. a. Zakhidov, M. Chatzichristidi, H. H. Fong, J. a. DeFranco, G. G. Malliaras, and C. K. Ober, "Orthogonal Patterning of PEDOT:PSS for Organic Electronics using Hydrofluoroether Solvents," *Adv. Mater.*, vol. 21, no. 22, pp. 2314–2317, Jun. 2009.
- [39] N. Reckefuss, M. Rojahn, C. D. Mu, P. Rudati, H. Frohne, O. Nuyken, H. Becker, and K. Meerholz, "Multi-colour organic light-emitting displays by solution processing," *Nature*, vol. 421, no. 6925, pp. 829–833, 2004.
- [40] M. C. Gather, a. Köhnen, a. Falcou, H. Becker, and K. Meerholz, "Solution-Processed Full-Color Polymer Organic Light-Emitting Diode Displays Fabricated by Direct Photolithography," *Adv. Funct. Mater.*, vol. 17, no. 2, pp. 191–200, Jan. 2007.
- [41] P. E. Malinowski, T. Ke, A. Nakamura, and T. Chang, "True-Color 640 ppi OLED Arrays Patterned by CA i-line Photolithography bottom patterning (a) (a) full patterning 800 μm ECL (c) ITO 800 μm ECL ITO," pp. 215–218, 2015.
- [42] M. A. Baldo and S. R. Forrest, "Highly efficient phosphorescent emission from organic electroluminescent devices," *Nature*, vol. 395, no. 6698, pp. 151–154, 1998.
- [43] C. Adachi, M. a. Baldo, M. E. Thompson, and S. R. Forrest, "Nearly 100% internal phosphorescence efficiency in an organic light-emitting device," *J. Appl. Phys.*, vol. 90, no. 10, p. 5048, 2001.
- [44] H. Aziz and Z. D. Popovic, "Degradation Phenomena in Small-Molecule Organic Light-Emitting Devices," *Chem. Mater.*, vol. 16, no. 23, pp. 4522–4532, Nov. 2004.
- [45] F. So and D. Kondakov, "Degradation mechanisms in small-molecule and polymer organic light-emitting diodes.," *Adv. Mater.*, vol. 22, no. 34, pp. 3762–77, Sep. 2010.
- [46] J. McElvain, H. Antoniadis, M. R. Hueschen, J. N. Miller, D. M. Roitman, J. R. Sheats, and R. L. Moon, "Formation and growth of black spots in organic light-emitting diodes," *J. Appl. Phys.*, vol. 80, no. 10, p. 6002, 1996.

- [47] H. Aziz, Z. Popovic, S. Xie, A.-M. Hor, N.-X. Hu, C. Tripp, and G. Xu, "Humidity-induced crystallization of tris (8-hydroxyquinoline) aluminum layers in organic light-emitting devices," *Appl. Phys. Lett.*, vol. 72, no. 7, p. 756, 1998.
- [48] Y.-F. Liew, H. Aziz, N.-X. Hu, H. S.-O. Chan, G. Xu, and Z. Popovic, "Investigation of the sites of dark spots in organic light-emitting devices," *Appl. Phys. Lett.*, vol. 77, no. 17, p. 2650, 2000.
- [49] Y. Kim, D. Choi, H. Lim, and C.-S. Ha, "Accelerated pre-oxidation method for healing progressive electrical short in organic light-emitting devices," *Appl. Phys. Lett.*, vol. 82, no. 14, p. 2200, 2003.
- [50] P. E. Burrows, V. Bulovic, S. R. Forrest, L. S. Sapochak, D. M. McCarty, and M. E. Thompson, "Reliability and degradation of organic light emitting devices," *Appl. Phys. Lett.*, vol. 65, no. 23, p. 2922, 1994.
- [51] a. P. Ghosh, L. J. Gerenser, C. M. Jarman, and J. E. Fornalik, "Thin-film encapsulation of organic light-emitting devices," *Appl. Phys. Lett.*, vol. 86, no. 22, p. 223503, 2005.
- [52] D. Y. Kondakov, W. C. Lenhart, and W. F. Nichols, "Operational degradation of organic light-emitting diodes: Mechanism and identification of chemical products," *J. Appl. Phys.*, vol. 101, no. 2, p. 024512, 2007.
- [53] Q. Wang and H. Aziz, "Poor photo-stability of the organic/LiF/Al contact in organic optoelectronic devices," *Org. Electron.*, vol. 12, no. 9, pp. 1571–1575, Sep. 2011.
- [54] Q. Wang, G. Williams, and H. Aziz, "Photo-degradation of the indium tin oxide (ITO)/organic interface in organic optoelectronic devices and a new outlook on the role of ITO surface treatments and interfacial layers in improving device stability," *Org. Electron.*, vol. 13, no. 10, pp. 2075–2082, Oct. 2012.
- [55] OLED-info, "77,000 OLED TVs were sold in 2014, generating \$280 million in revenue," 2014. [Online]. Available: <http://www.oled-info.com/displaysearch-says-77000-oled-tvs-were-sold-2014-generating-280-million-revenue>.
- [56] NPD DisplaySearch, "Small and Medium Display Active Matrix OLED Penetration to More Than Double by 2015," 2012. [Online]. Available: http://www.displaysearch.com/cps/rde/xchg/displaysearch/hs.xsl/121217_small_and_medium_display_active_matrix_oled_penetration_to_more_than_double.asp.
- [57] NPD DisplaySearch, "LTPS TFT LCDs Growing to Half of All Mobile Phone Display Revenue in 2020," 2014. [Online]. Available:

http://www.displaysearch.com/cps/rde/xchg/displaysearch/hs.xsl/140121_ltps_tft_lcds_growing_to_half_of_all_mobile_phone_display_revenue.asp.

- [58] NPD DisplaySearch, “New AMOLED TV Costs Ten Times More than LCD TV to Produce,” 2012. [Online]. Available: http://www.displaysearch.com/cps/rde/xchg/displaysearch/hs.xsl/120808_new_amoled_tv_costs_ten_times_more_than_lcd_tv_to_produce.asp.
- [59] M. Cryst, L. Cryst, A. M. Kini, J. M. W. K. D. Carlson, J. R. Whitworth, B. D. Gates, B. D. C. Duffy, R. J. Jackman, K. M. Vaeth, K. F. Jensen, and G. M. Whitesides, “Patterning Electroluminescent Materials with Feature Sizes as Small as 5 m m Using Elastomeric Membranes as Masks for Dry Lift-Off,” *Adv. Mater.*, vol. 11, no. 7, pp. 546–552, 1999.
- [60] D. V. Muyres, P. F. Baude, S. Theiss, M. Haase, T. W. Kelley, and P. Fleming, “Polymeric aperture masks for high performance organic integrated circuits,” *J. Vac. Sci. Technol. A Vacuum, Surfaces, Film.*, vol. 22, no. 4, p. 1892, 2004.
- [61] F. Papadimitrakopoulos, X.-M. Zhang, D. L. Thomsen, and K. a. Higginson, “A Chemical Failure Mechanism for Aluminum(III) 8-Hydroxyquinoline Light-Emitting Devices,” *Chem. Mater.*, vol. 8, no. 7, pp. 1363–1365, Jan. 1996.
- [62] a. B. Djurišić, T. W. Lau, L. S. M. Lam, and W. K. Chan, “Influence of atmospheric exposure of tris (8-hydroxyquinoline) aluminum (Alq3): a photoluminescence and absorption study,” *Appl. Phys. A*, vol. 78, no. 3, pp. 375–380, Nov. 2002.
- [63] J. E. Knox, M. D. Halls, H. P. Hratchian, and H. B. Schlegel, “Chemical failure modes of AlQ3-based OLEDs: AlQ3 hydrolysis.,” *Phys. Chem. Chem. Phys.*, vol. 8, no. 12, pp. 1371–7, Mar. 2006.
- [64] K. Long, F. Pschenitzka, M. H. Lu, and J. C. Sturm, “Full-Color OLEDs Integrated by Dry Dye Printing,” *IEEE Trans. Electron Devices*, vol. 53, no. 9, pp. 2250–2258, 2006.
- [65] B. J. Chen, X. W. Sun, T. K. S. Wong, X. Hu, and a. Uddin, “Organic light-emitting devices with in situ postgrowth annealed organic layers,” *Appl. Phys. Lett.*, vol. 87, no. 6, p. 063505, 2005.
- [66] S. Ninomiya, K. Ichiki, H. Yamada, Y. Nakata, T. Seki, T. Aoki, and J. Matsuo, “Molecular depth profiling of multilayer structures of organic semiconductor materials by secondary ion mass spectrometry with large argon cluster ion beams,” *Rapid Commun. Mass Spectrom.*, vol. 23, no. 20, pp. 3264–3268, 2009.
- [67] C. H. Chen, C. W. Tang, J. Shi, and K. P. Klubek, “Recent developments in the synthesis of red dopants for Alq 3 hosted electroluminescence,” vol. 363, pp. 327–331, 2000.

- [68] M. S. Xu, J. B. Xu, and J. An, "Visualization of thermally activated morphology evolution of N, N'-di(naphthalene-1-yl)-N, N'-dipthalbenzidine films on ITO/copper phthalocyanine underlying layer," *Appl. Phys. A*, vol. 81, no. 6, pp. 1151–1156, Nov. 2004.
- [69] K. Tada and M. Onoda, "Color Tuning of Poly(N-vinylcarbazole)-Based Light-Emitting Devices through Maskless Dye-Diffusion Technique Using Phosphorescent Dyes," *Jpn. J. Appl. Phys.*, vol. 47, no. 2, pp. 1290–1292, Feb. 2008.
- [70] T. Graves-Abe, F. Pschenitzka, H. Z. Jin, B. Bollman, J. C. Sturm, and R. A. Register, "Solvent-enhanced dye diffusion in polymer thin films for polymer light-emitting diode application," *J. Appl. Phys.*, vol. 96, no. 12, p. 7154, 2004.
- [71] F. Pschenitzka and J. C. Sturm, "Solvent-enhanced dye diffusion in polymer thin films for color tuning of organic light-emitting diodes," *Appl. Phys. Lett.*, vol. 78, no. 17, p. 2584, 2001.
- [72] W.-J. Shin, J.-Y. Lee, J. C. Kim, T.-H. Yoon, T.-S. Kim, and O.-K. Song, "Bulk and interface properties of molybdenum trioxide-doped hole transporting layer in organic light-emitting diodes," *Org. Electron.*, vol. 9, no. 3, pp. 333–338, Jun. 2008.
- [73] C.-H. Gao, X.-Z. Zhu, L. Zhang, D.-Y. Zhou, Z.-K. Wang, and L.-S. Liao, "Comparative studies on the inorganic and organic p-type dopants in organic light-emitting diodes with enhanced hole injection," *Appl. Phys. Lett.*, vol. 102, no. 15, p. 153301, 2013.
- [74] B. J. Chen, X. W. Sun, T. K. S. Wong, X. Hu, and a. Uddin, "Organic light-emitting devices with in situ postgrowth annealed organic layers," *Appl. Phys. Lett.*, vol. 87, no. 6, p. 063505, 2005.
- [75] H. M. Grandin, H. Aziz, S. Gardner, C. Jennings, a. J. Paine, P. R. Norton, and Z. D. Popovic, "Light-Absorption Phenomena in Novel Low-Reflectance Cathodes for Organic Light-Emitting Devices Utilizing Metal–Organic Mixtures," *Adv. Mater.*, vol. 15, no. 23, pp. 2021–2024, Dec. 2003.

Appendix 1 Selective Diffusion Using Laser Local Heating

In this work, selective diffusion is achieved by utilizing local ITO Joule heating as demonstrated in Section 5.3. Alternatively, selective diffusion can also be achieved by utilizing local laser heating. This appendix describes the proposed procedure of this approach and shows the very first result of a preliminary investigation to assess its technical feasibility.

Introduction

As demonstrated in Section 5.3, local ITO Joule heating can be utilized to selectively dope a host layer with a luminescent material. Instead of local Joule heating, this approach utilizes local laser heating (Fig. 0.1). The advantage of this approach is that existing TFT backplanes can be used, while an additional circuit needs to be built to pass current through the ITO anodes in the case of the local Joule heating method. This approach is also similar to the LITI process, but the required temperature is relatively lower, which reduces the risk of compromising device performance^[26]. In this preliminary investigation, it is determined whether a luminescent material can be transferred via diffusion from a donor to an acceptor film on separate substrate placed in physical contact by laser local heating.

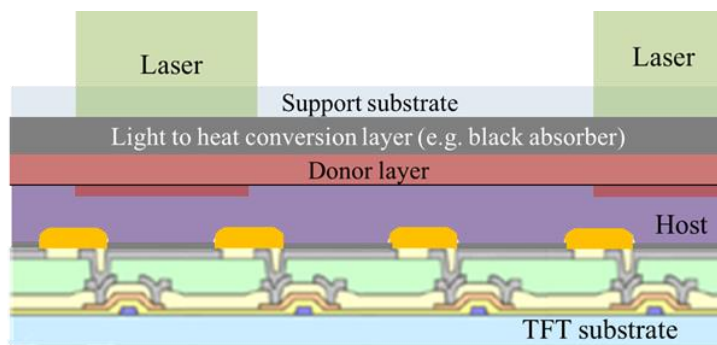


Figure 0.1 General scheme for the selective diffusion of a luminescent material through local heating via laser

Experimental Procedure

In this experiment, the host NPB layer is selectively doped with DCJTB via diffusion by local laser heating. Figure 0.2 presents the procedure for fabricating the OLED that is doped via laser local heating. First, a ~ 3 nm MoO_3 and a ~ 60 nm NPB are deposited on an ITO coated glass substrate to serve as the HIL and HTL and host, respectively (acceptor substrate). DCJTB are then selectively doped from a separate donor substrate into the NPB host layer on the acceptor substrate by local laser heating. The donor substrate is a quartz substrate where the layer stack of a ~ 150 nm Alq_3 :Silver(Ag) mixture, a ~ 100 nm Ag and a ~ 20 nm DCJTB is deposited. The Alq_3 :Ag mixture layer serves as a light to heat conversion (LTHC) layer due to high light absorption^[75]. The Ag layer between the LTCH and DCJTB layers serves as a light reflective layer and also a protective layer to prevent the DCJTB layer from mixing with the LTCH layer. The acceptor and donor substrates are placed in physical contact, and the donor substrate is locally heated by laser exposure in a dry nitrogen environment for 30 minutes with a laser power of 15 W/cm^2 , a beam diameter of 1.2 mm, and a laser wavelength of 532 nm. After that, the donor substrate is removed, the acceptor substrate is put back in the vacuum system, and a ~ 40 nm thick Alq_3 ETL followed by a ~ 0.5 nm thick LiF EIL and a ~ 70 nm Al cathode are deposited to complete the device. The EL image of the device is then captured by optical microscope.

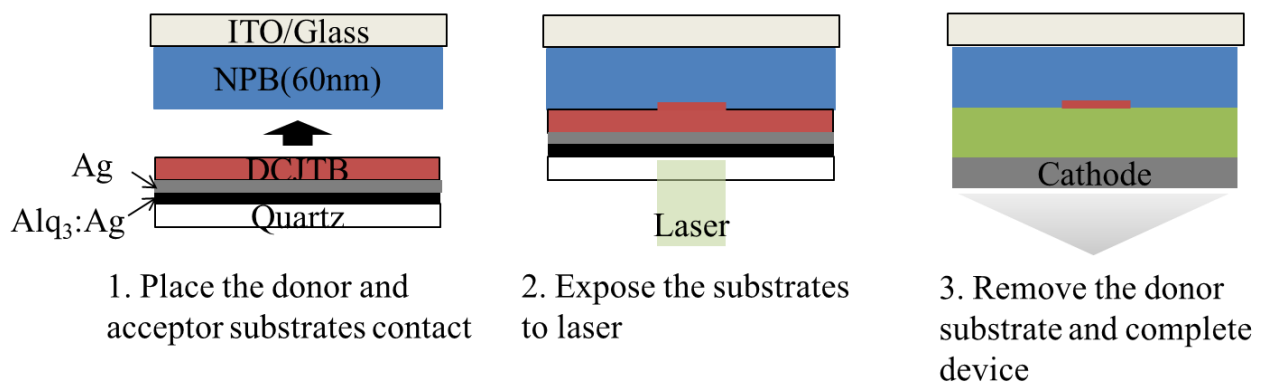


Figure 0.2 A schematic diagram illustrating the steps of the procedure followed for fabricating OLEDs selectively doped via diffusion by local laser heating.

Results and discussion

Figure 0.3 shows the EL image of the OLED fabricated through the procedure in Figure 0.2. As can be seen, red emission is partially observed on the green background. The red emission is emitted from the DCJTb transferred via diffusion from the donor substrate to the NPB host layer by laser heating. This result indicates that a luminescent dopant can be selectively transferred via diffusion by laser local heating without causing significant detrimental effects on devices.

This approach is still in the first stage of investigation. Further studies need to be performed for practical application. For example, a potential critical issue of this technique is the non-uniformity of spatial doping level. As shown in the figure, it seems that the doping level is higher in the middle of the laser-exposed area and lower around the periphery, which likely reflects the non-uniformity of the temperature profile. A method needs to be developed to achieve more uniform spatial doping levels. Also, further investigations on device performance including quantitative device characteristics need to be conducted.

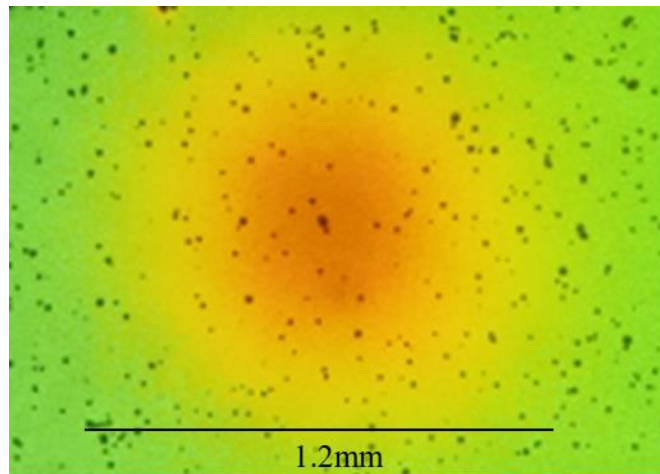


Figure 0.3 EL image of the OLED fabricated through the procedure in Fig. 0.2

Appendix 2 Absorption Spectrum of NPB Doped with DCJTB

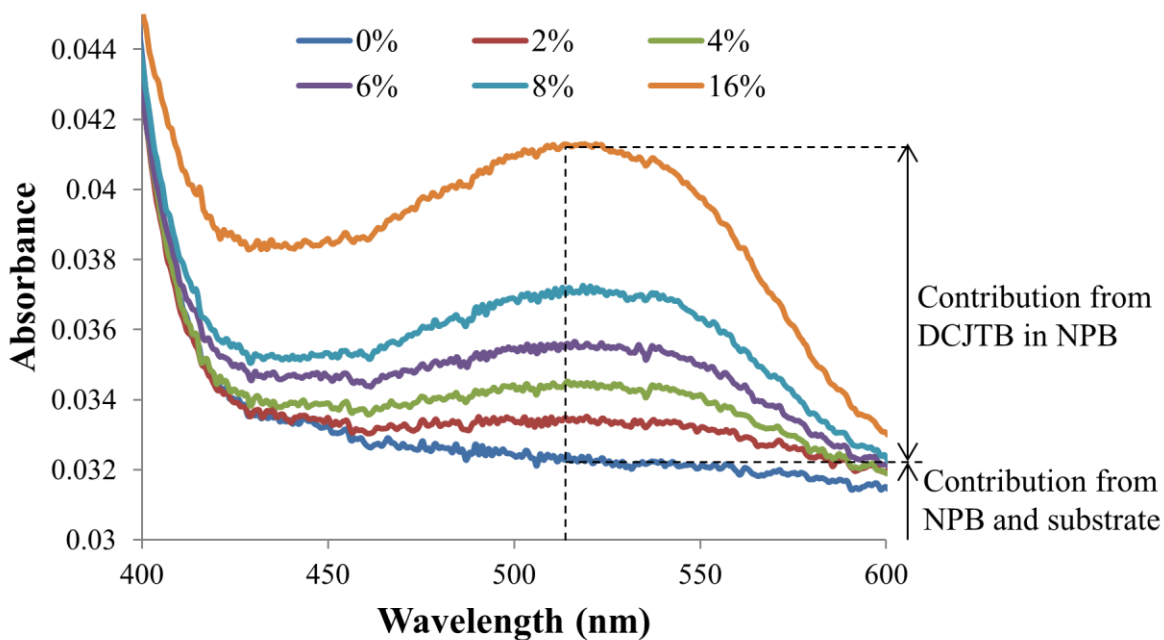


Figure 0.4 The absorption spectra of 5nm of NPB films doped with various DCJTB concentrations (0-16%).

Supplementary Figure 0.4 presents the absorption spectra of 5 nm NPB films doped with various DCJTB concentrations (from 0-16% by volume) made by co-deposition, which are served as reference data for the results in Figure 5.3 (b) (background absorption by NPB and the substrate is subtracted in Figure 5.3 (b)). As can be seen, the peak wavelength does not significantly change with DCJTB concentration, suggesting that molecular aggregation does not significantly increase with concentration in this range. It is therefore possible to use UV-vis optical absorption spectra to estimate the relative amount of DCJTB molecules in the host films (as done in Section 5.1).

Appendix 3 ITO Temperature vs Bias Voltage

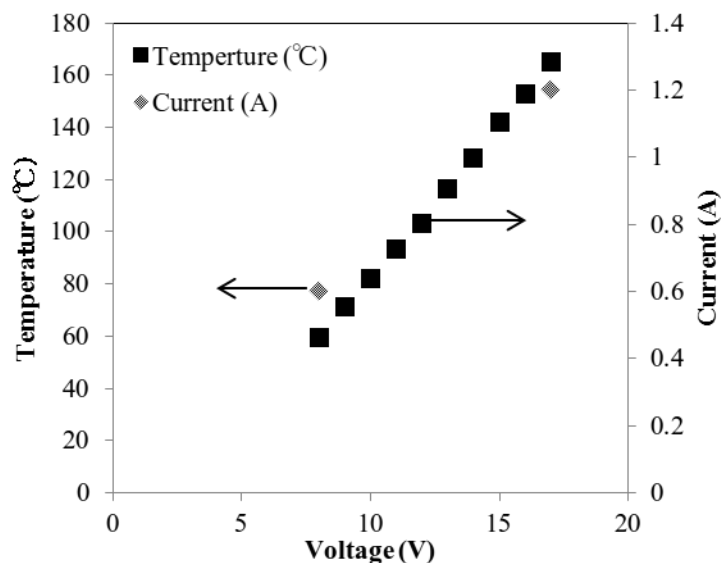


Figure 0.5 Temperature vs bias voltage of the ITO strip

Figure 0.5 presents the temperature vs bias voltage of the ITO strip used in this work. The temperature of the ITO strip is measured by thermocouples. The sheet resistance of the ITO film is 15Ω , which provides the ITO strip with the resistance of $\sim 100 \Omega$. In the experiment shown in section 5.3, 13 V is applied to the ITO strip. According to this result, the temperature of the ITO strip reaches $\sim 120 \text{ }^\circ\text{C}$ at this bias voltage. However, the actual temperature of the ITO film should be lower than $\sim 120 \text{ }^\circ\text{C}$ because of heat dissipation via the donor substrate which is placed in physical contact with the acceptor substrate. Therefore, significant thermal damage does not occur to the NPB film ($T_g = 99 \text{ }^\circ\text{C}$) even though the organic film is deposited on the ITO film.